July 6, 2020

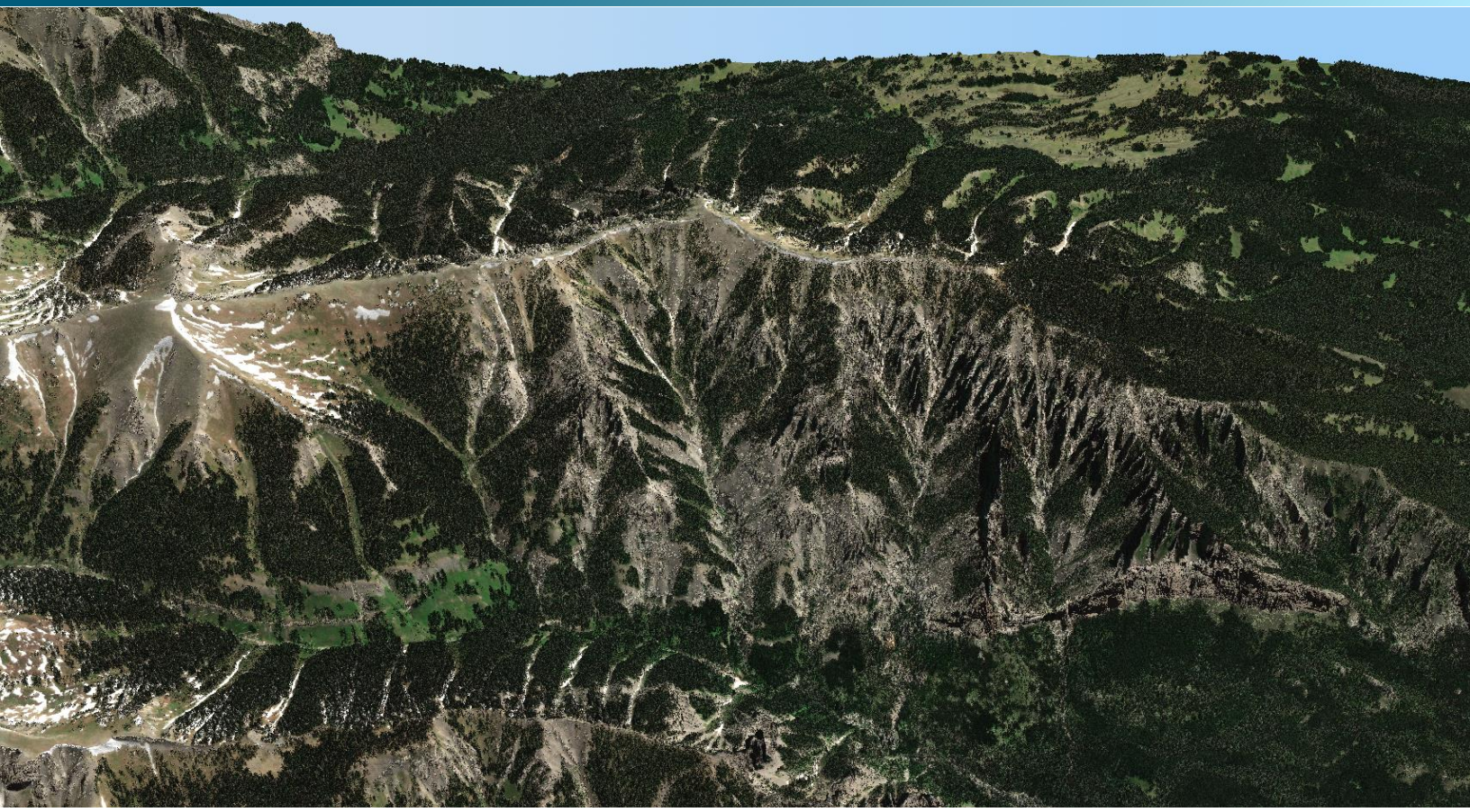

SnowEx 2020 Snow-On, Colorado and Idaho NIR Lidar Technical Data Report

Prepared For:

BOISE STATE UNIVERSITY

H.P. Marshall
Boise State University
6563 W. Summer Hill Dr.
Boise, ID 83714
PH: 303-859-3106

Prepared By:

QSI Corvallis
1100 NE Circle Blvd, Ste. 126
Corvallis, OR 97330
PH: 541-752-1204

Table of Contents

Cover Photo: A view looking across the East River, Colorado area of interest. The image was created from the lidar bare earth model overlaid with the above ground point cloud and colored by orthoimagery.

INTRODUCTION

This photo taken by QSI acquisition staff shows a view of one of the SnowEx 2020 sites in Idaho.

In December 2019, Quantum Spatial (QSI) was contracted by ATA Aerospace (ATA), the National Aeronautics and Space Administration (NASA) and Boise State University (BSU) to collect Light Detection and Ranging (lidar) data and hyperspectral imagery in the winter of 2020 for the SnowEx program sites in Colorado and Idaho. The goal of the SnowEx program is to support snow remote sensing research while assessing the viability of various remote sensing technologies. Data were acquired during a time window where the landscape was covered in winter snowpack to aid BSU in association with NASA in assessing the snow water equivalence (SWE) within study areas.

This report accompanies the delivered lidar data and hyperspectral imagery, and documents contract specifications, data acquisition procedures, processing methods, and analysis of the final dataset including lidar accuracy and density. Acquisition dates and acreage are shown in Table 1, a complete list of contracted deliverables provided to BSU is shown in Table 2, and the project extent is shown in Figure 1.

Table 1: Acquisition dates, acreage, and data types collected on the SnowEx 2020 site

Project Site	Contracted Acres	Buffered Acres	Acquisition Dates	Data Type
SnowEx 2020, Colorado and Idaho	612,904	626,550	02/01/2020, 02/02/2020, 02/09/2020, 02/10/20, 02/11/2020, 02/13/20, 02/14/2020, 02/18/2020, 02/19/2020, 02/20/2020	NIR - Lidar
				VNIR Imaging Spectroscopy

Deliverable Products

Table 2: Products delivered to BSU for the SnowEx 2020 Colorado and Idaho Sites

SnowEx 2020 Snow-On Lidar Products Projection: UTM Zone 11 North , UTM Zone 12 North, UTM Zone 13 North Horizontal Datum: NAD83 (2011) Vertical Datum: NAVD88 (GEOID12B) Units: Meters	
Points	LAS v 1.2 • All Classified Returns • Raw Swaths as Pulsewaves
Lidar Rasters	0.5 Meter ESRI Grids (all Idaho AOIs, Grand Mesa, CO & Fraser Creek, CO) • Bare Earth Digital Elevation Model (DEM) • Highest Hit Digital Surface Model (DSM) 0.5 Meter GeoTiffs (all Idaho AOIs, Grand Mesa, CO & Fraser Creek, CO) • Normalized Intensity Images 3.0 Meter ESRI Grids (East River, CO) • Bare Earth Digital Elevation Model (DEM) • Highest Hit Digital Surface Model (DSM) 3.0 Meter GeoTiffs (East River, CO) • Normalized Intensity Images
Vectors	Shapefiles (*.shp) • Area of Interest • Lidar Tile Index • Flight lines • Smoothed Best Estimate Trajectory (SBETs) • Areas of Potential Cloud Interference
Hyperspectral Imagery	0.5 Meter ENVI Standard BIP Format (all Idaho AOIs, Grand Mesa, CO & Fraser Creek, CO) • Orthorectified Radiance Flight lines (.pix) 3 Meter ENVI Standard BIP Format (East River, CO) • Orthorectified Radiance Flight lines (.pix)

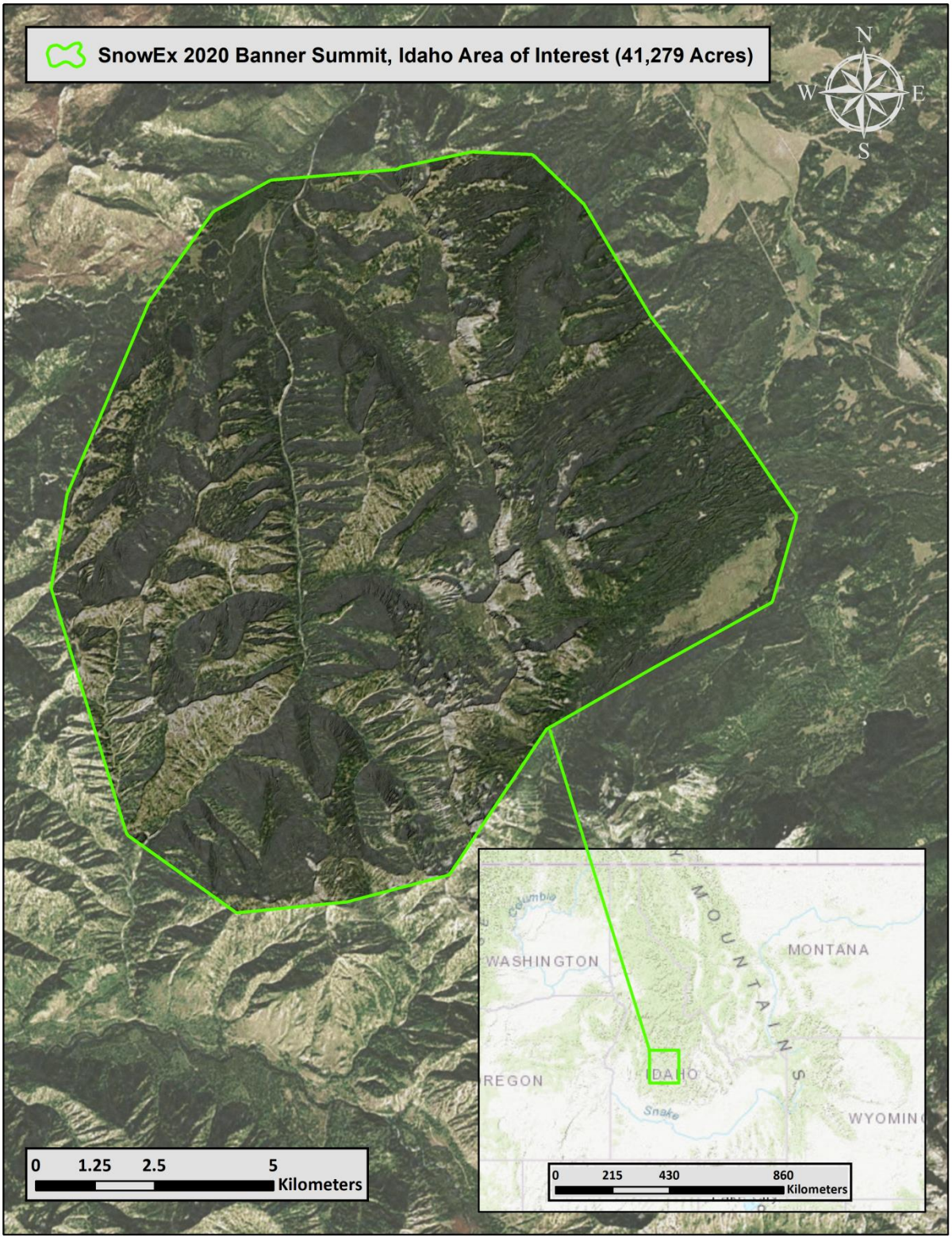

Figure 1: Location map of the SnowEx 2020 Banner Summit site in Idaho

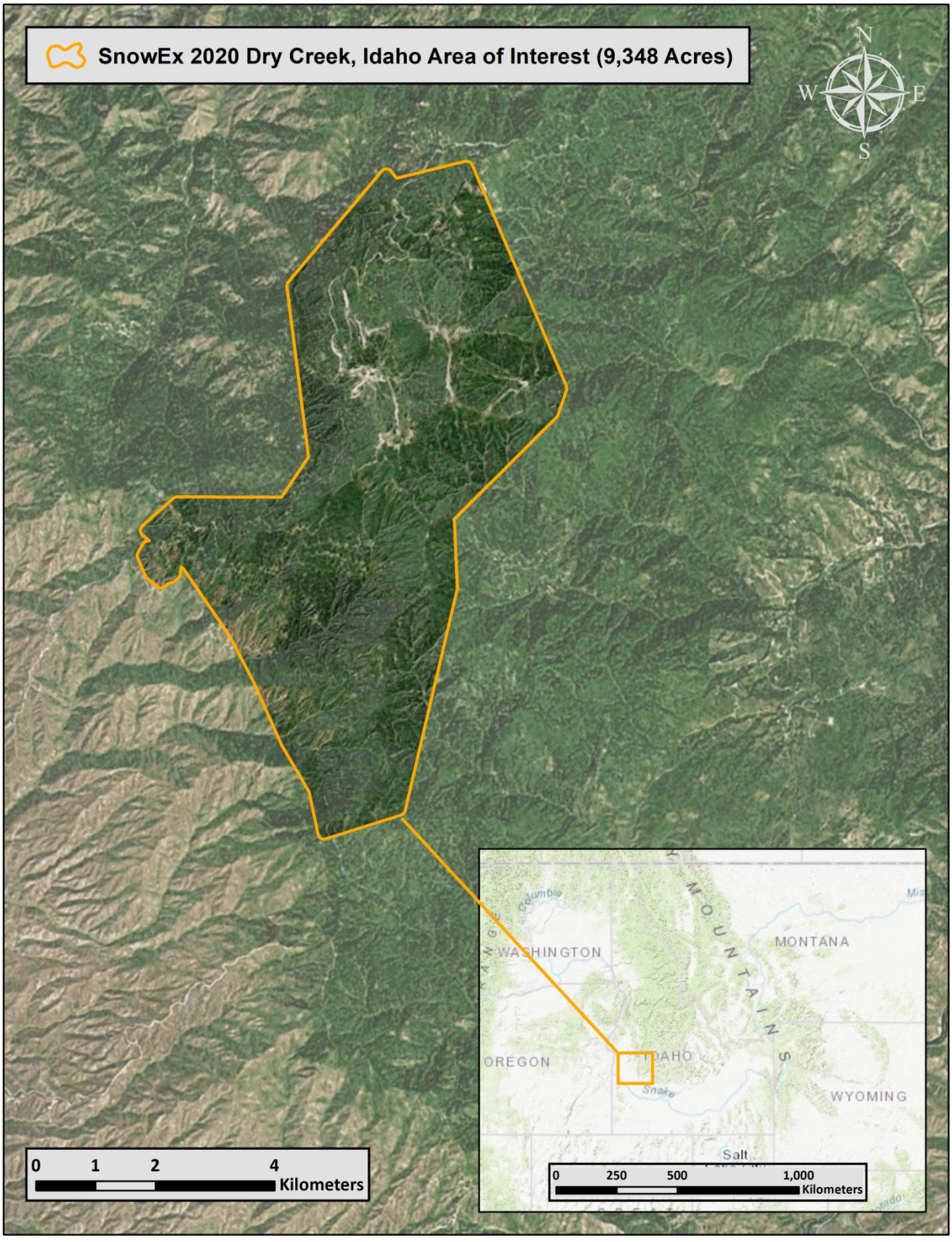

Figure 2: Location map of the SnowEx 2020 Dry Creek site in Idaho

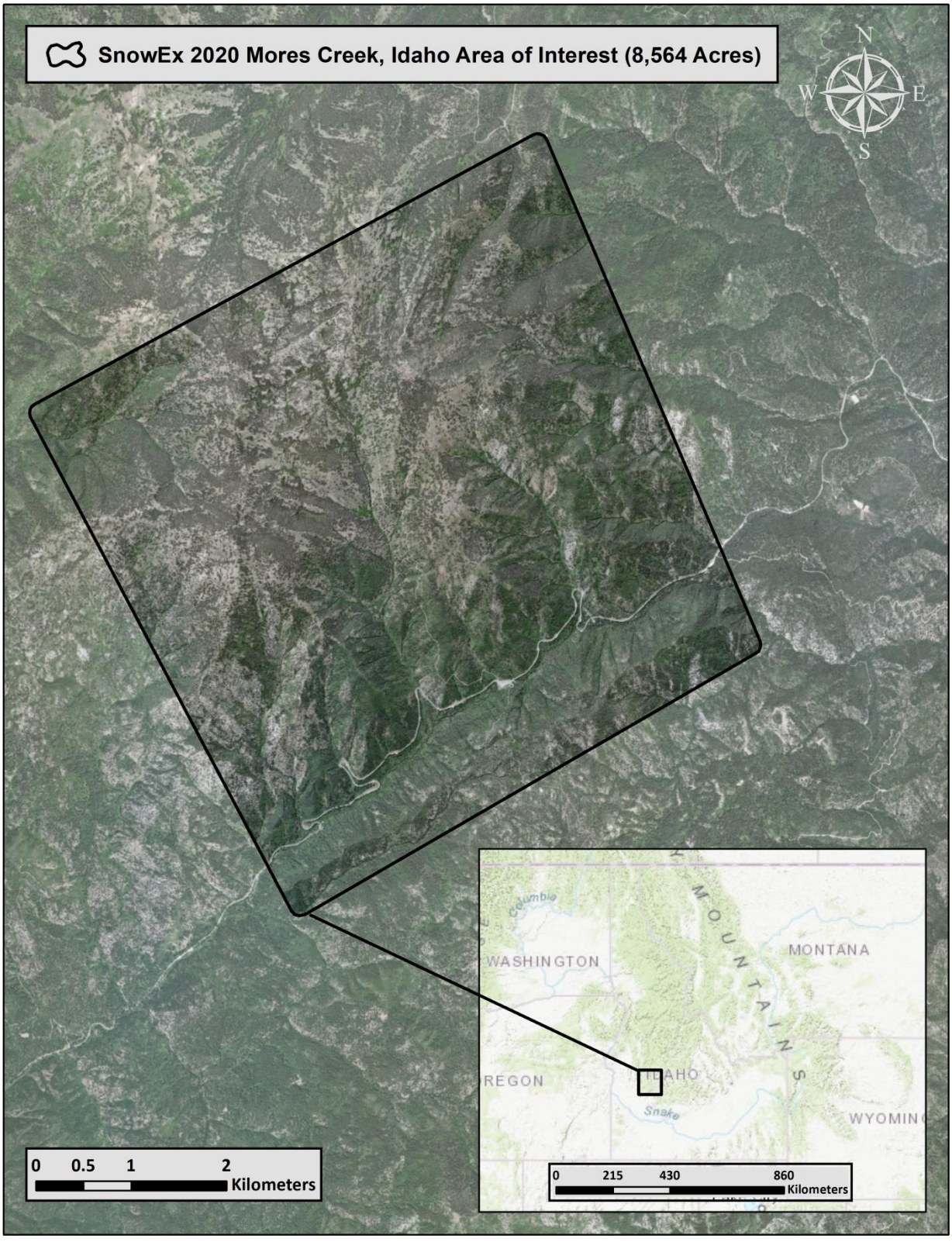

Figure 3: Location map of the SnowEx 2020 Mores Creek site in Idaho

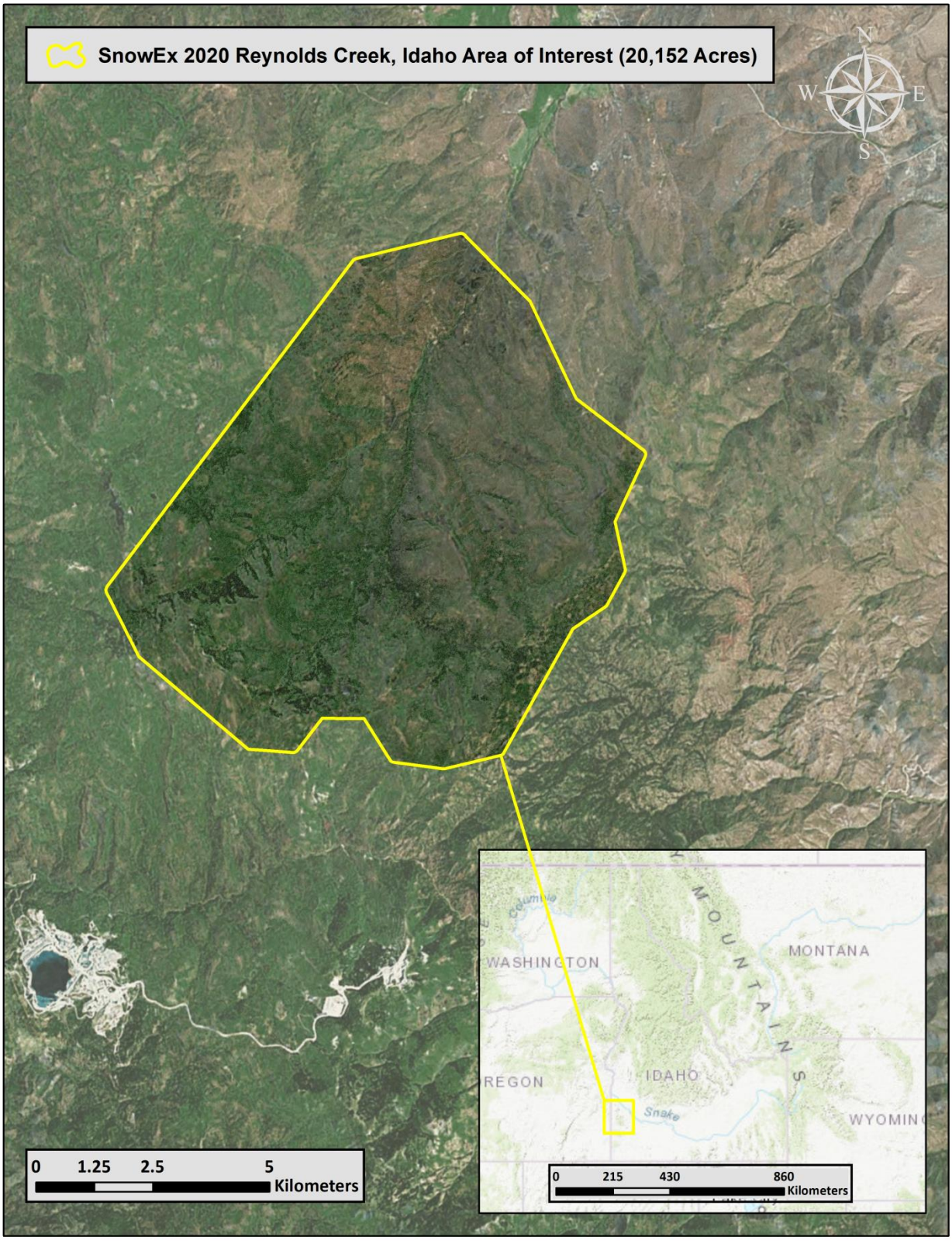

Figure 4: Location map of the SnowEx 2020 Reynolds Creek site in Idaho

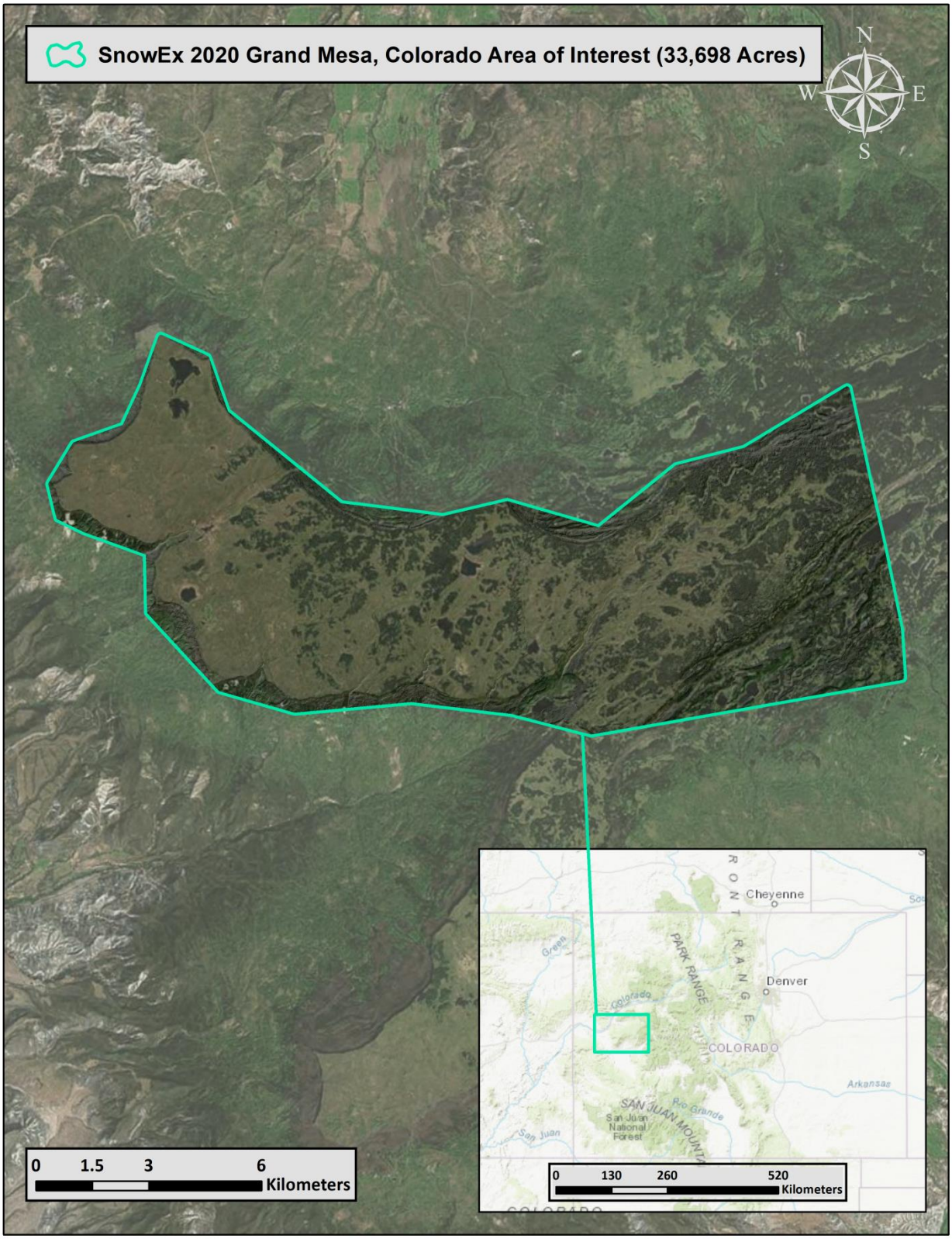

Figure 5: Location map of the SnowEx 2020 Grand Mesa site in Colorado

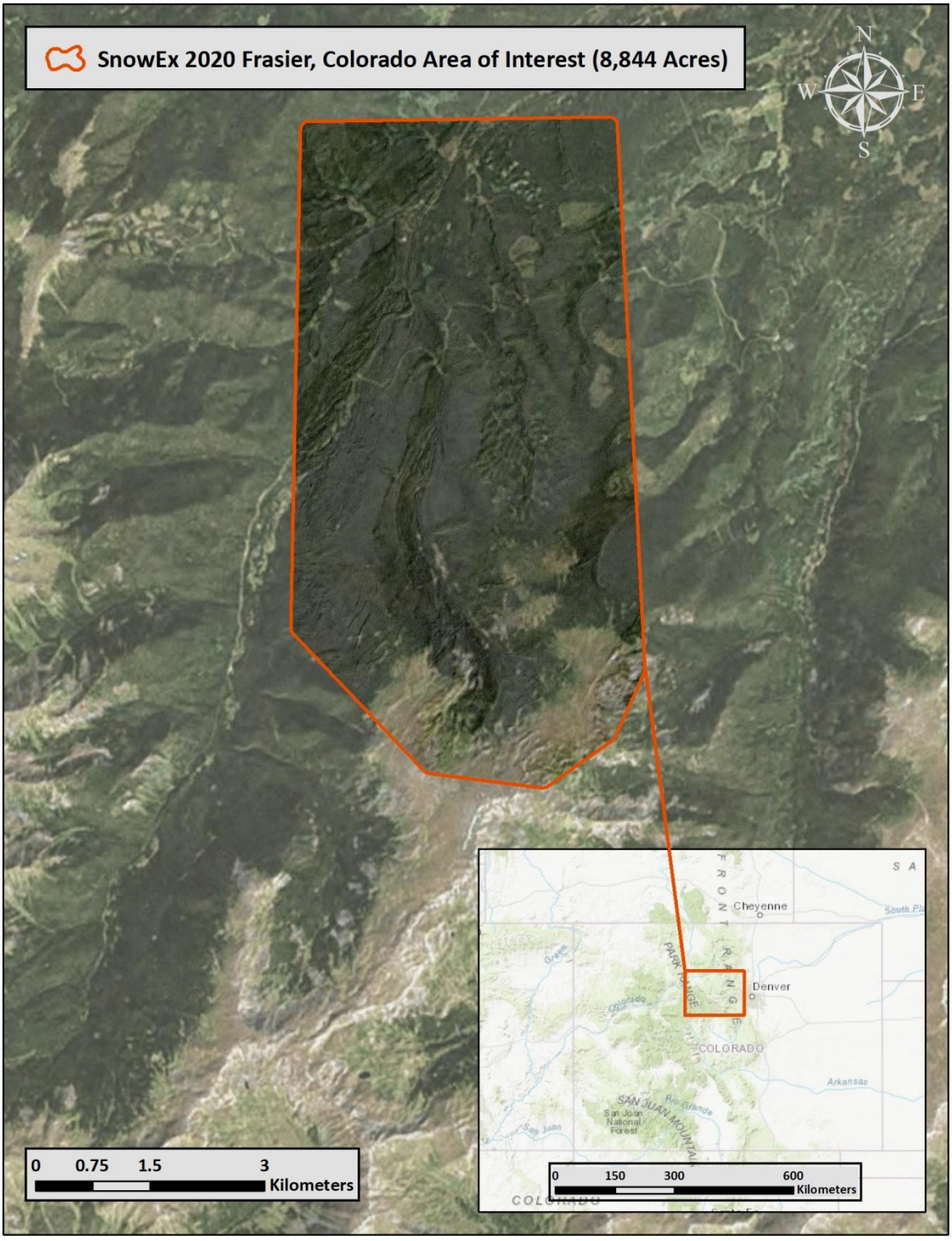

Figure 6: Location map of the SnowEx Frasier site in Colorado

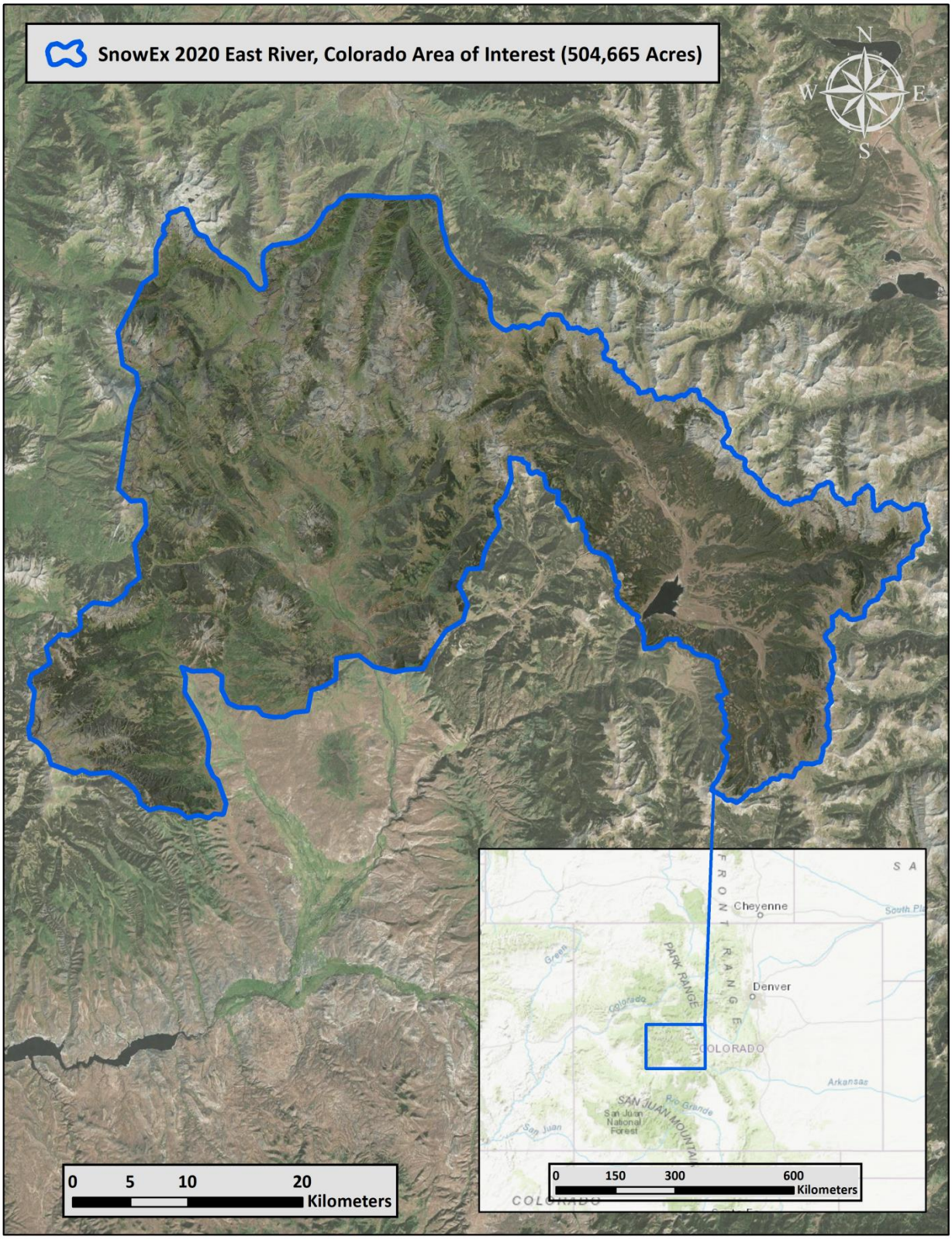

Figure 7: Location map of the SnowEx East River site in Colorado

Planning

In preparation for data collection, QSI reviewed the project area and developed a specialized flight plan to ensure complete coverage of the SnowEx 2020 lidar study area at the target point density of ≥20.0 points/m^2 for the Fraser, Grand Mesa, Banner Summit, Mores Creek, Fry Creek and Reynolds Creek project areas. The East River project area was acquired at a target point density of ≥1.0 points/m^2. Acquisition parameters including orientation relative to terrain, flight altitude, pulse rate, scan angle, and ground speed were adapted to optimize flight paths and flight times while meeting all contract specifications.

Factors such as satellite constellation availability and weather windows must be considered during the planning stage. Any weather hazards or conditions affecting the flight were continuously monitored due to their potential impact on the daily success of airborne and ground operations. In addition, logistical considerations including private property access and potential air space restrictions were reviewed. All flights were conducted during snow on conditions within the project areas to support the research goals being pursued with the acquired data.

Airborne Survey - Lidar

The lidar survey was accomplished using a Riegl VQ-1560i system mounted in a Beechcraft King Air. Table 3 summarizes the settings used to yield an average pulse density of ≥20 pulses/m^2 over the SnowEx Fraser, Grand Mesa, Dry Creek, Mores Creek, Reynolds Creek and Banner Summit project areas and ≥1 pulses/m^2 for the East River project area. The Riegl laser system can record unlimited range measurements (returns) per pulse. It is not uncommon for some types of surfaces (e.g., dense vegetation or water) to return fewer pulses to the lidar sensor than the laser originally emitted. The discrepancy between first return and overall delivered density will vary depending on terrain, land cover, and the prevalence of water bodies. All discernible laser returns were processed for the output dataset.

Table 3: Lidar specifications and survey settings

Lidar Survey Settings & Specifications		
AOI	Fraser, Grand Mesa, Banner Summit, Dry Creek, Reynolds Creek, Mores Creek	East River
Acquisition Dates	02/01/2020 – 02/19/2020	02/14/2020 & 02/20/2020
Aircraft Used	Beechcraft King Air	Beechcraft King Air
Sensor	Riegl	Riegl
Laser	VQ-1560i	VQ-1560i
Maximum Returns	15	15
Resolution/Density	Average 20 pulses/m^2	Average 1.0 pulses/m^2
Nominal Pulse Spacing	0.22	1.0
Survey Altitude (AGL)	1,578 m	6,096 m
Survey speed	125 knots	190 knots
Field of View	58.5°	58.5°
Mirror Scan Rate	153 Lines Per Second	37 Lines Per Second
Target Pulse Rate	1,000 kHz	150 kHz
Pulse Length	3 ns	3 ns
Laser Pulse Footprint Diameter	28 cm	38 cm
Central Wavelength	1064 nm	1064 nm
Pulse Mode	Multiple Times Around (MTA)	Multiple Times Around (MTA)
Beam Divergence	0.18 mrad	0.18 mrad
Swath Width	1767.4 m	2,350 m
Swath Overlap	60%	60%
Intensity	16-bit	16-bit
Accuracy	$RMSE_Z$ (Non-Vegetated) ≤25 cm	$RMSE_Z$ (Non-Vegetated) ≤25 cm

All areas were surveyed with an opposing flight line side-lap of ≥50% (≥100% overlap) in order to reduce laser shadowing and increase surface laser painting. To accurately solve for laser point position (geographic coordinates x, y and z), the positional coordinates of the airborne sensor and the attitude of the aircraft were recorded continuously throughout the lidar data collection mission. Position of the aircraft was measured twice per second (2 Hz) by an onboard differential GPS unit, and aircraft attitude was measured 200 times per second (200 Hz) as pitch, roll and yaw (heading) from an onboard inertial measurement unit (IMU). To allow for post-processing correction and calibration, aircraft and sensor position and attitude data are indexed by GPS time.

This photo taken by QSI acquisition staff shows the snow pack within one of the SnowEx 2020 areas of interest.

VNIR Imaging Spectroscopy

Visible to near infrared (VNIR) hyperspectral imagery was acquired from a Cessna 208 Caravan. In order to ensure consistent illumination, QSI only acquired data when skies were clear over the areas of interest and the solar elevation angle was greater than 30 degrees above the horizon (≈1000 to 1600 PDT). Compared to traditional broadband multispectral (3 or 4 band) imagery surveys, QSI utilized a narrow-band hyperspectral imaging spectrometer which recorded reflected energy from 400 to 1000 nm across 72 narrow bands.

Table 4: Camera manufacturer's specifications

Itres CASI 1500h	
Sensor Type	VNIR Pushbroom Sensor
Sensor Array	Scientific CMOS
Wavelength Range (nm)	380-1050
Across – Track Pixels	1500
FOV	40°
Targeted AGL	1,578 m
Resolution (VNIR)	0.5 m
Spectral Bands (VNIR)	72
Horizontal Accuracy (VNIR)	+/- 3 pixels (1.5m)

Ground Survey

Ground control surveys, including monumentation, aerial targets, and ground survey points (GSPs) were conducted to support the airborne acquisition. Ground control data were used to geospatially correct the aircraft positional coordinate data and to perform quality assurance checks on final lidar data and hyperspectral imagery products.

Base Stations

Base stations were utilized for collection of ground survey points using real time kinematic (RTK) survey techniques. RTK positioning is a relative-positioning method that improves the accuracy of GPS signals, which enhances the precision of location data obtained from satellite-based systems; because RTK positioning allows one to obtain centimeter-level positioning in real time, it remains the procedure of choice for applications that demand high-precision mapping.

Base Station locations were selected with consideration for satellite visibility, field crew safety, and optimal location for GSP coverage. QSI utilized six existing permanent active CORS stations and established one permanent survey monument for the SnowEx 2020 lidar project (Table 5, Figure 8). QSI's professional land surveyor, Steven J. Hyde (IDPLS#L-10235, COPLS#PLSC0038558) oversaw and certified the occupation of all monuments.

Table 5: Base Station positions for the SnowEx 2020 acquisition. Coordinates are on the NAD83 (2011) datum, epoch 2010.00

Base Station ID	Network	Latitude	Longitude	Ellipsoid (meters)
SNOWEX20_RTK_01B	LJR	44° 19' 19.40353"	-115° 14' 03.53681"	2099.277
GC01	MESA COUNTY	38° 32' 42.43685"	-106° 55' 42.18974"	2343.08
MC01	MESA COUNTY	39° 05' 28.39169"	-108° 31' 41.26997"	1438.003
MC02	MESA COUNTY	39° 00' 52.89684"	-108° 29' 24.11206"	1491.258
MC07	MESA COUNTY	39° 19' 03.98036"	-108° 12' 46.31299"	1489.015
MC08	MESA COUNTY	39° 14' 08.55922"	-107° 58' 39.51405"	1835.775
TOCB	MESA COUNTY	38° 52' 15.28871"	-106° 58' 55.31892"	2709.019
COWI	SMARTNET	39° 55' 01.76819"	-105° 47' 09.99273"	2683.303
IDBO	SMARTNET	43° 36' 42.02397"	-116° 19' 06.81563"	800.697
IDHD	SMARTNET	43° 54' 31.07778"	-116° 12' 07.01624"	786.922
IDNR	SMARTNET	43° 12' 19.58301"	-116° 45' 00.40227"	1191.547

QSI utilized static Global Navigation Satellite System (GNSS) data collected at 1 Hz recording frequency for each base station. During post-processing, the static GNSS data were triangulated with nearby Continuously Operating Reference Stations (CORS) using the Online Positioning User Service (OPUS[1]) for precise positioning. Multiple independent sessions over the same monument were processed to confirm antenna height measurements and to refine position accuracy.

Monuments were established according to the national standard for geodetic control networks, as specified in the Federal Geographic Data Committee (FGDC) Geospatial Positioning Accuracy Standards for geodetic networks.[2] This standard provides guidelines for classification of monument quality at the 95% confidence interval as a basis for comparing the quality of one control network to another. The monument rating for this project is shown in Table 6.

Table 6: Federal Geographic Data Committee monument rating for network accuracy

Direction	Rating
1.96 * St Dev $_{NE}$:	0.050 m
1.96 * St Dev $_{z}$:	0.050 m

For the SnowEx 2020 Lidar project, the monument coordinates contributed no more than 5.6 cm of positional error to the geolocation of the final ground survey points and lidar, with 95% confidence.

Ground Survey Points (GSPs)

Ground survey points were collected using real time kinematic (RTK) survey techniques. For RTK surveys, a roving receiver receives corrections from a nearby base station or Real-Time Network (RTN) via radio or cellular network, enabling rapid collection of points with relative errors less than 1.5 cm horizontal and 2.0 cm vertical. All GSP measurements were made during periods with a Position Dilution of Precision (PDOP) of ≤ 3.0 with at least six satellites in view of the stationary and roving receivers. See Table 7 for Trimble unit specifications.

GSPs were collected in areas where good satellite visibility was achieved on paved roads and other hard surfaces such as gravel or packed dirt roads. GSP measurements were not taken on highly reflective surfaces such as center line stripes or lane markings on roads due to the increased noise seen in the laser returns over these surfaces. GSPs were collected within as many flight lines as possible; however, the distribution of GSPs depended on ground access constraints and monument locations and may not be equitably distributed throughout the study area (Figure 8-11).

Table 7: QSI ground survey equipment identification

Receiver Model	Antenna	OPUS Antenna ID	Use
Trimble R8	Integrated Antenna	TRM_R8_GNSS	Static / Rover

[1] OPUS is a free service provided by the National Geodetic Survey to process corrected monument positions. http://www.ngs.noaa.gov/OPUS.

[2] Federal Geographic Data Committee, Geospatial Positioning Accuracy Standards (FGDC-STD-007.2-1998). Part 2: Standards for Geodetic Networks, Table 2.1, page 2-3. http://www.fgdc.gov/standards/projects/FGDC-standards-projects/accuracy/part2/chapter2

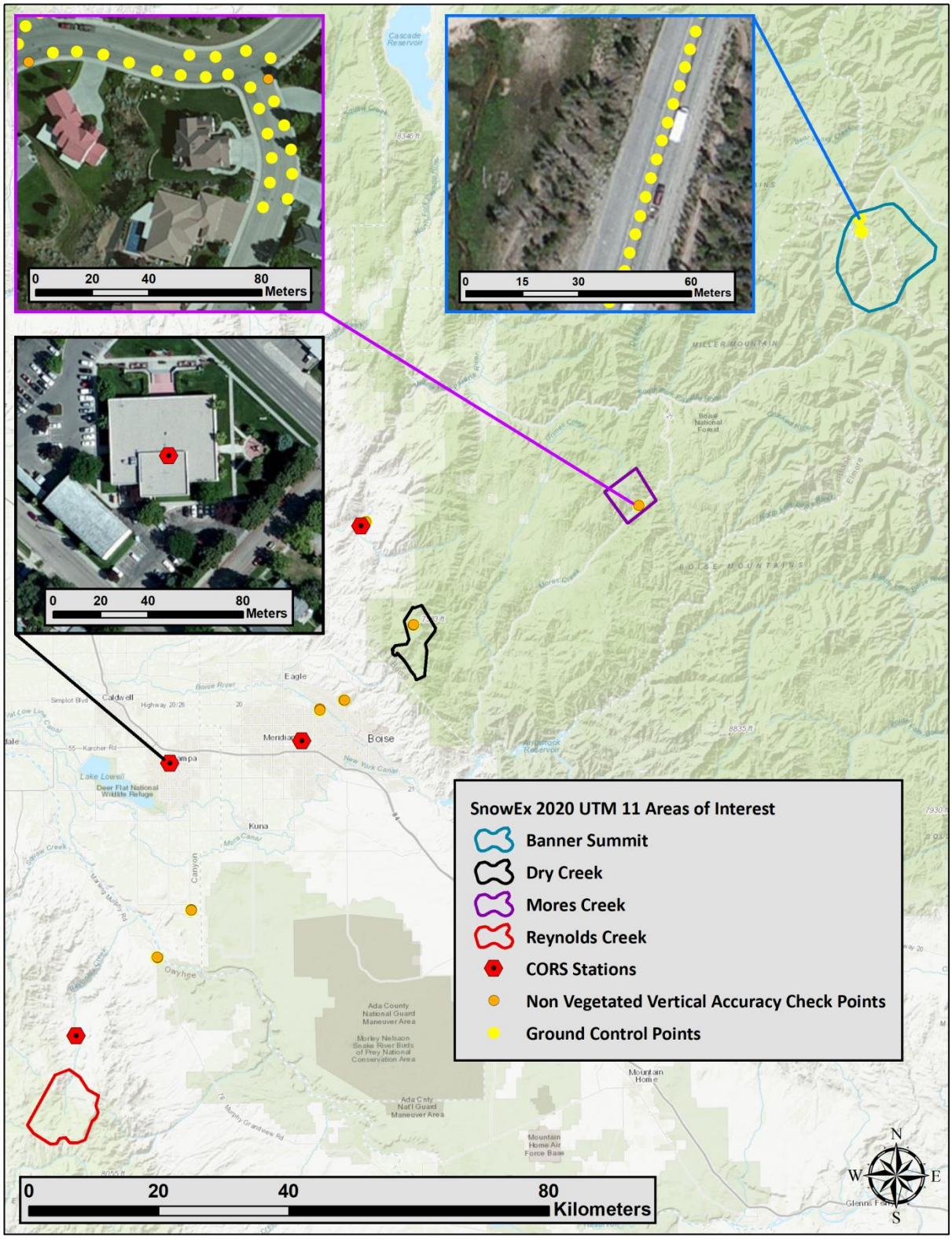

Figure 8: Ground survey location map, UTM 11

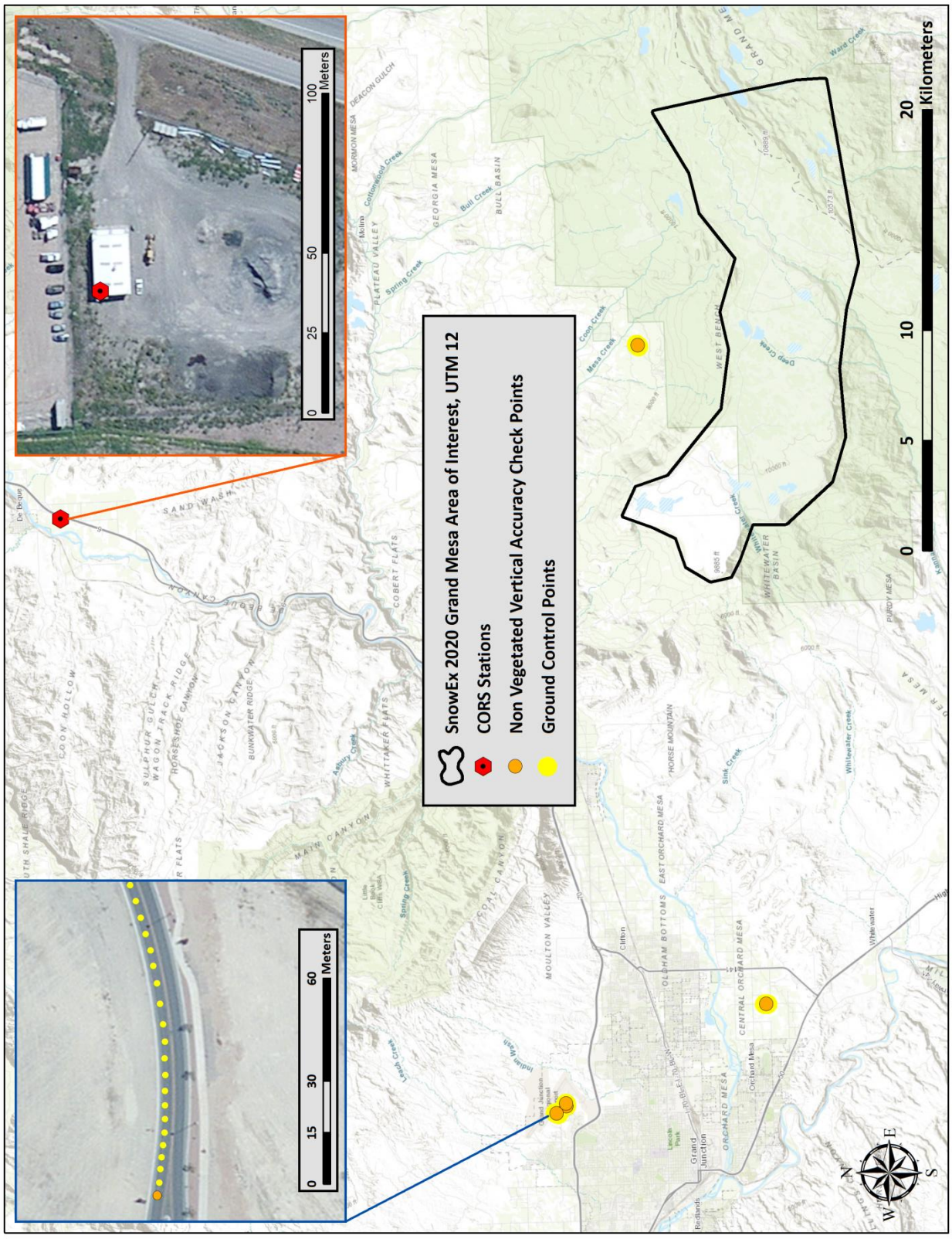

Figure 9: Ground survey location map, UTM 12

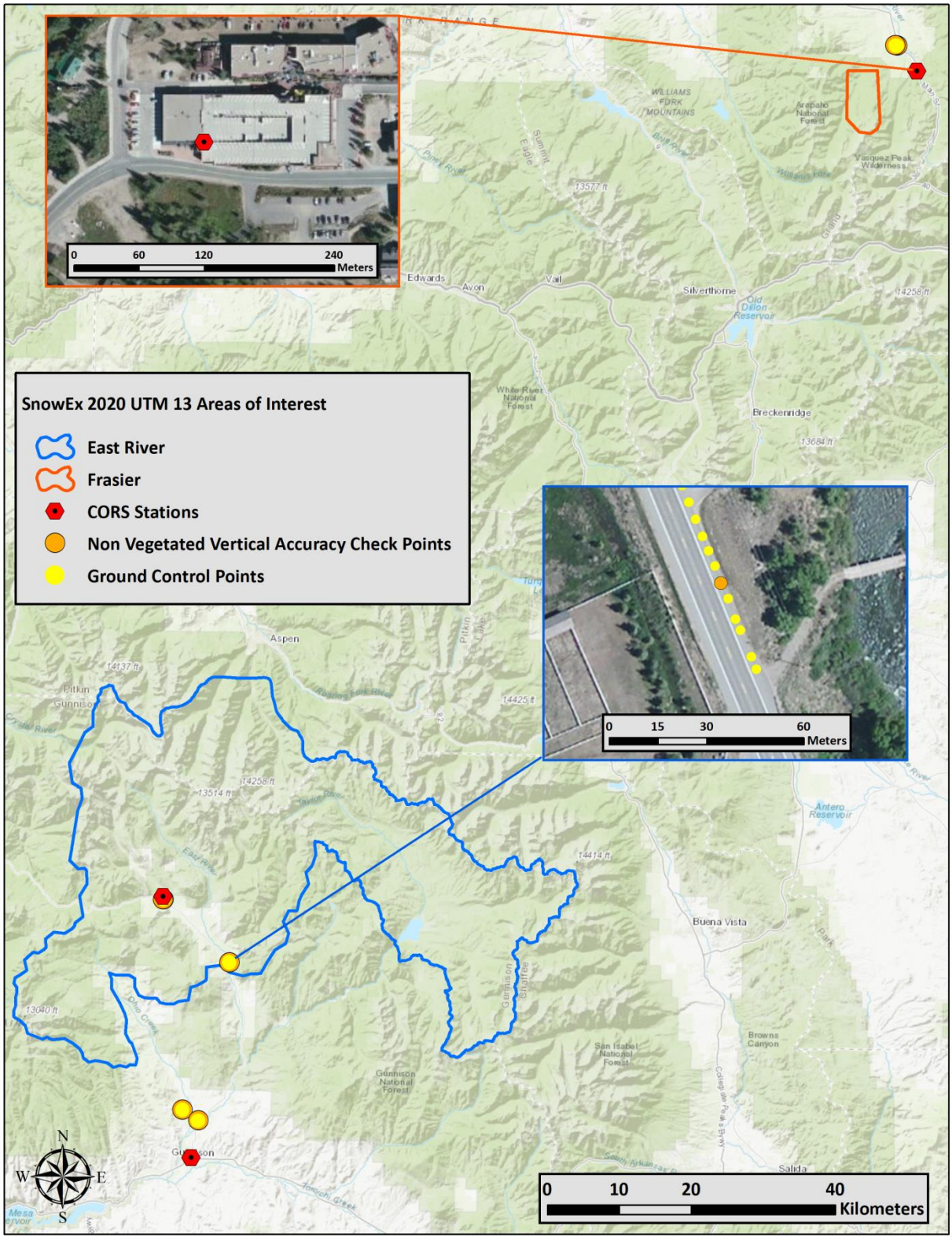

Figure 10: Ground survey location map, UTM 13

This image shows a view of the East River area of interest in Colorado. The image was created from the lidar bare earth model overlaid with the above ground point cloud and colored by orthoimagery.

Lidar Data

Upon completion of data acquisition, QSI processing staff initiated a suite of automated and manual techniques to process the data into the requested deliverables. Processing tasks included GPS control computations, smoothed best estimate trajectory (SBET) calculations, kinematic corrections, calculation of laser point position, sensor and data calibration for optimal relative and absolute accuracy, and lidar point classification (Table 8). Processing methodologies were tailored for the landscape. Brief descriptions of these tasks are shown in Table 9.

Table 8: ASPRS LAS classification standards applied to the SnowEx 2020 dataset

Classification Number	Classification Name	Classification Description
1	Default/Unclassified	Laser returns that are not included in the ground class, composed of vegetation and anthropogenic features
2	Ground	Laser returns that are determined to be ground using automated and manual cleaning algorithms
7	Noise	Laser returns that are often associated with birds, scattering from reflective surfaces, or artificial points below the ground surface
129	Edge Clip/Overlap	Laser returns at the outer edges of flight lines that are geometrically unreliable

Table 9: lidar processing workflow

Lidar Processing Step	Software Used
Resolve kinematic corrections for aircraft position data using kinematic aircraft GPS and static ground GPS data. Develop a smoothed best estimate of trajectory (SBET) file that blends post-processed aircraft position with sensor head position and attitude recorded throughout the survey.	PosPac MMS v.8.3
Calculate laser point position by associating SBET position to each laser point return time, scan angle, intensity, etc. Create raw laser point cloud data for the entire survey in *.las (ASPRS v. 1.2) format. Convert data to orthometric elevations by applying a geoid correction.	RiProcess v.1.8.5
Import raw laser points into manageable blocks to perform manual relative accuracy calibration and filter erroneous points. Classify ground points for individual flight lines.	TerraScan v.20
Using ground classified points per each flight line, test the relative accuracy. Perform automated line-to-line calibrations for system attitude parameters (pitch, roll, heading), mirror flex (scale) and GPS/IMU drift. Calculate calibrations on ground classified points from paired flight lines and apply results to all points in a flight line. Use every flight line for relative accuracy calibration.	TerraMatch v.20
Classify resulting data to ground and other client designated ASPRS classifications (Table 8). Assess statistical absolute accuracy via direct comparisons of ground classified points to ground control survey data.	TerraScan v.20 TerraModeler v.20
Generate bare earth models as triangulated surfaces. Generate highest hit models as a surface expression of all classified points. Export all surface models as ESRI GRIDs format at a 0.5 meter pixel resolution.	TerraScan v.20 ArcMap v. 10.3.1
Correct intensity values for variability and export intensity images as GeoTIFFs at a 0.5 meter pixel resolution.	LAS Product Creator 3.0 (QSI proprietary)

Hyperspectral Data

Hyperspectral imagery was also passed by QSI processing staff through a series of routines in order to convert from raw to orthorectified radiance images for delivery. A summary of these steps and the software used to perform them is provided in Table 10, and descriptions follow below.

Table 10: Hyperspectral data processing workflow

Hyperspectral Processing Step	Software Used
Convert Raw Imagery DNs to Radiance Values	ITRES RCX
Calculate Smoothed Best Estimate of Trajectory (SBET)	PosPac MMS v.8.3
Orthorectification	ITRES GeoCorrection Software

Raw to Radiance

To convert raw data collected by the sensor to a usable format, we used the Radiometric Correction Xpress (RCX) software from ITRES Research Ltd. This program output *.pix (radiance images) and *.att (timing synchronization/attitude data) files for each flight line to be used in down-stream geometric processing.

To produce calibrated radiance data, RCX uses calibration coefficients, unique to each sensor, that are generated during laboratory calibrations using tools (integrating spheres, blackbodies, lamps, etc.) that are traceable to known standards. These coefficients are applied to the raw data in a three-subroutine process. The first subroutine accounts for environmental effects (spectral shifting of the data due to temperature/pressure shifts – not atmospheric corrections) and adjusts for any low/non-responsive pixels in the sensor array. The second subroutine applies a dark correction to account for electronic noise inherent to the sensor itself and applies the coefficients to map raw digital number (DN) to radiance (µW/cm2/ micron/sr^{-1} * 1000). The internal noise can come from a variety of sources including electrical and thermal energy generated by the sensor, as well as the reflection and diffraction of light energy off internal sensor components. The final subroutine resamples the spectral data to the desired output.

The output from this process is a 16-bit data cube, where pixel units are µW/cm2/ micron/sr^{-1} scaled by 1000 so the data can be stored as integer type. The file format used is Band Interleaved by Pixel (BIP) in an ENVI Standard Type file (binary file + text header sidecar file).

Boresight Overview

We also performed a boresighting routine for the set of hyperspectral imagery acquisitions completed for this project. Boresighting is a process by which positional and angular offsets of the sensor from the IMU are calculated. Calculating these offsets allows the very precise measurements of the IMU/GPS to be mapped to the head of the sensor unit, making accurate orthorectification possible.

This process was completed using ITRES's PBSBUND (Push Broom Scanner BUNDLE adjustment) program. First a six flight-line cross hatch pattern was flown over an area with existing lidar data, so spatially accurate DEM's and Ground Control Points could be marked. The flight lines were flown in alternating, perpendicular cardinal directions. This allowed for a variety of sensor orientations to be used during positional and angular offset calculations. The location of the Ground Control Points was translated from a coordinate reference system to sensor geometry image array coordinates. The pairs of coordinates were then used to solve a set of linear equations that produce the angular and positional offsets of the sensor with reference to the GPS/IMU system. These angles and positional offsets were used during the orthorectification process to calculate spatially and angularly accurate positional information for each frame of each flight-line.

Orthorectification

The final step in processing the hyperspectral imagery for the SnowEx 2020 areas of interest was orthorectification of radiance images for each flight line. Orthorectification is the process of removing image perspective (angle of sensor with respect to imaging surface) and terrain effects in order to create a planimetrically correct image. This allows the user to accurately measure distances, angles and area of features in a given image.

To orthorectify data from the ITRES CASI 1500h sensor, a series of four proprietary executables was used. First, positional information was extracted from the SBET to create the location of the aircraft in 3-dimensional earth-centric space. Next, timing and angular orientation data was taken from the attitude files (*.att) and cross-referenced with the timestamps from the SBET to create a file with timestamp, positional location, and sensor orientation. Then, the angular offsets from the boresight calculation were applied at each timestamp, resulting in a file with the precise position and angular orientation of the sensor for every frame in a flight-line. Finally, this information was used to project each pixel to the location where it intersects the earth surface, accounting for terrain, to create an image that is free from perspective and terrain-based distortions. During the orthorectification process the nearest neighbor resampling algorithm was used to ensure radiometric fidelity of the data. The output of this process was georeferenced 16-bit radiance images in the projected coordinate system used to process the data. Figures 12-18 depict orthorectified flight lines over each area of interest.

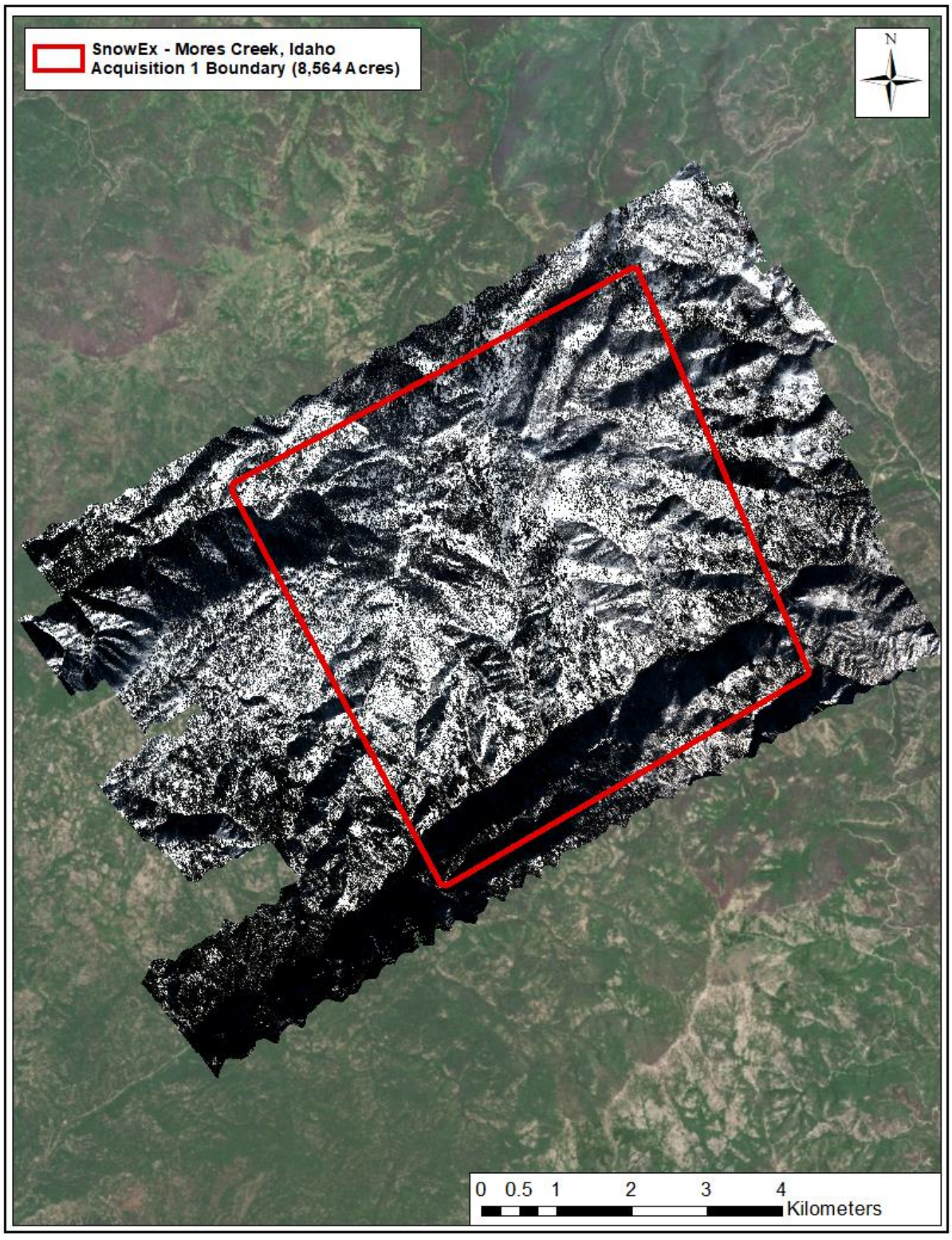

Figure 11: Orthorectified hyperspectral imagery (0.5 Meter) of Mores Creek, Idaho area, UTM 11

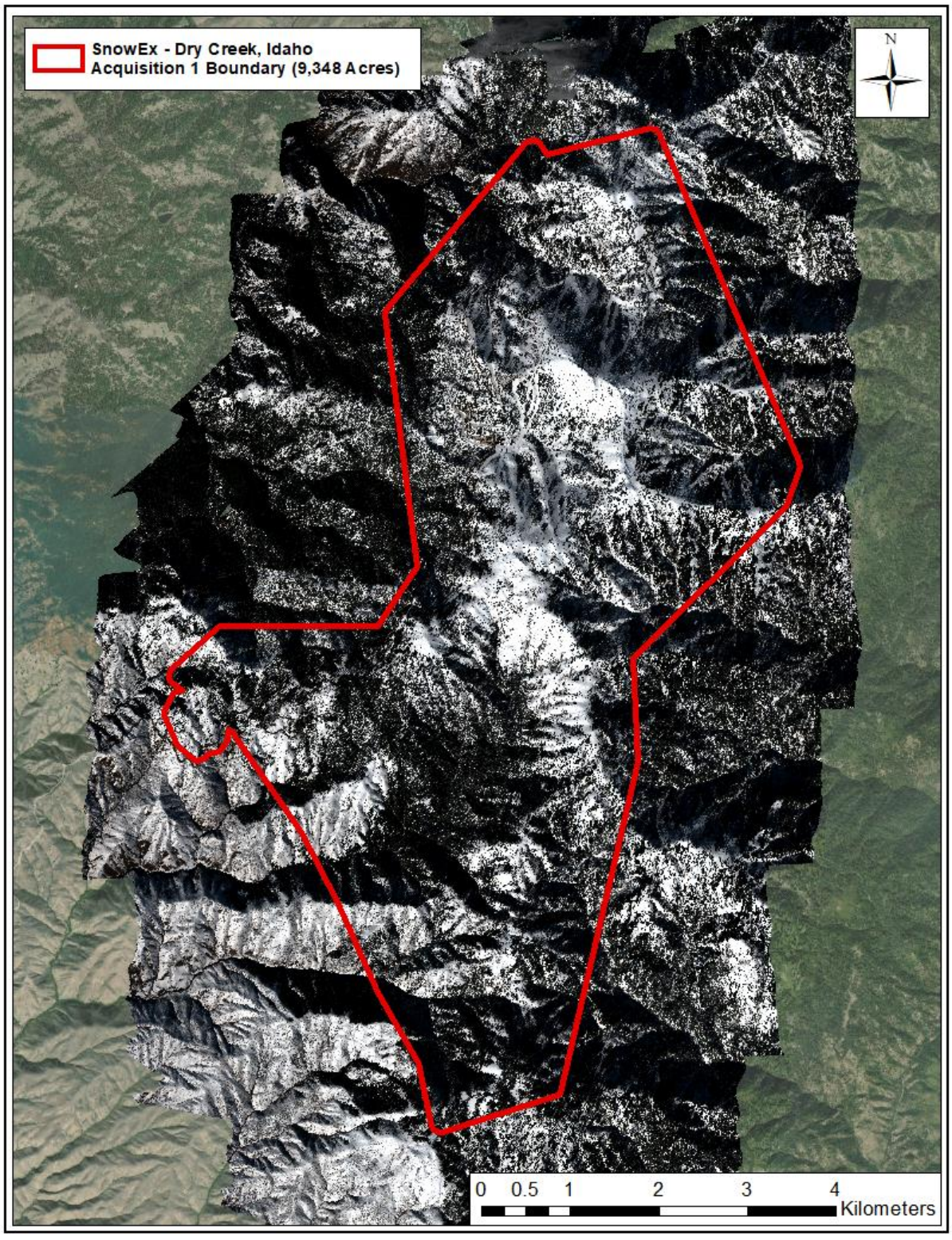

Figure 13: Orthorectified hyperspectral imagery (0.5 Meter) of Dry Creek, Idaho area, UTM 11

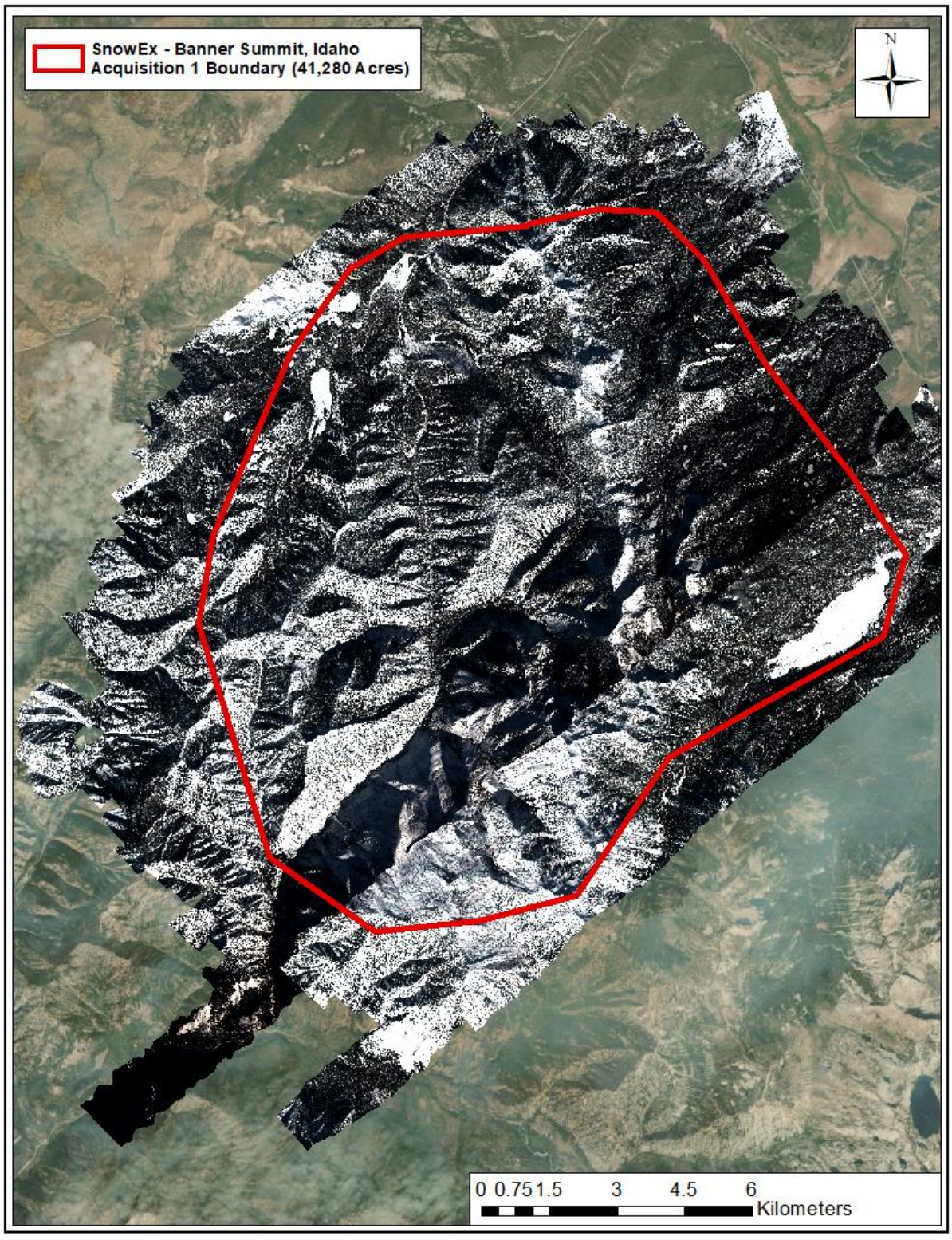

Figure 12: Orthorectified hyperspectral imagery (0.5 Meter) of Banner Summit, Idaho area, UTM 11

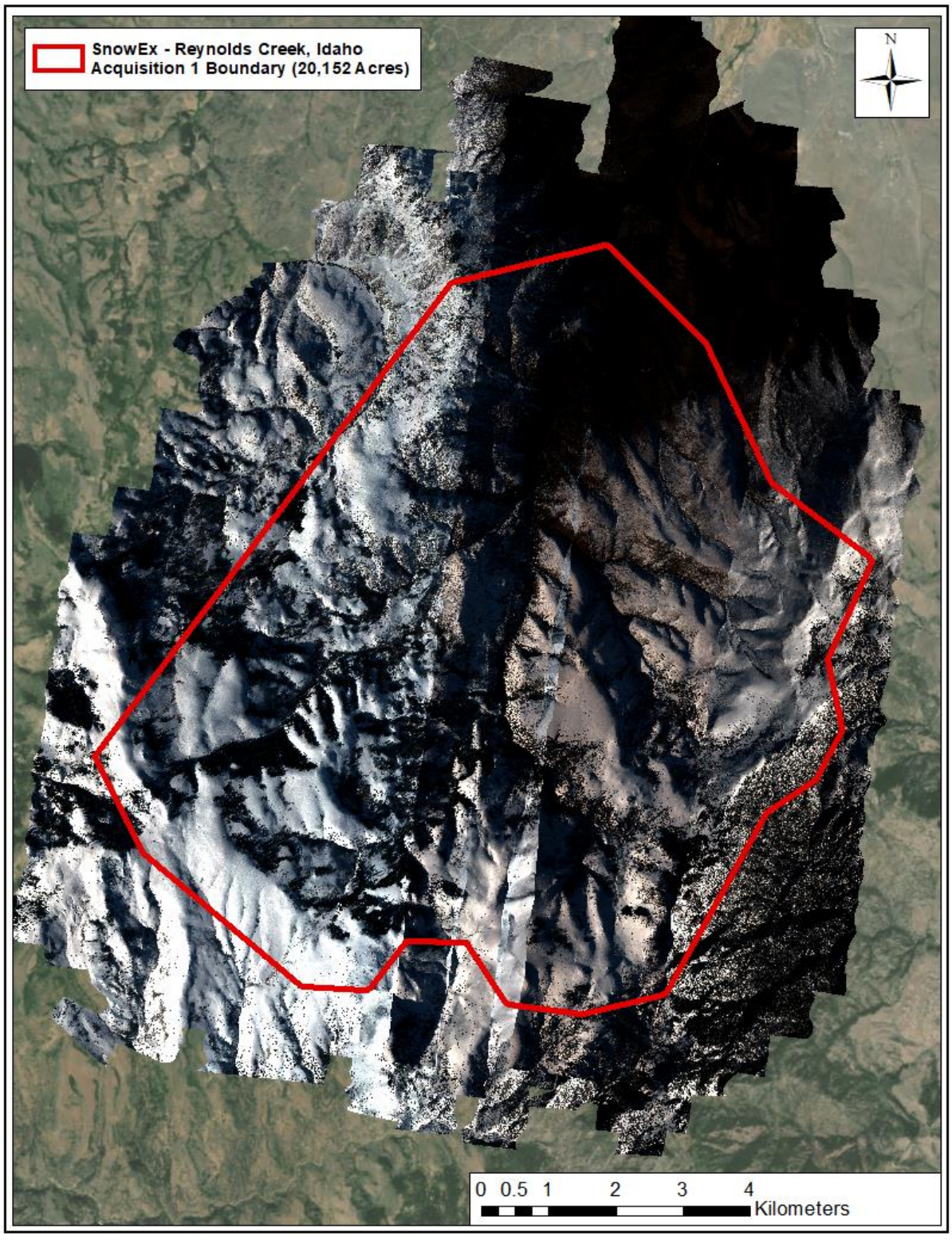

Figure 13: Orthorectified hyperspectral imagery (0.5 Meter) of Reynolds Creek, Idaho area, UTM 11

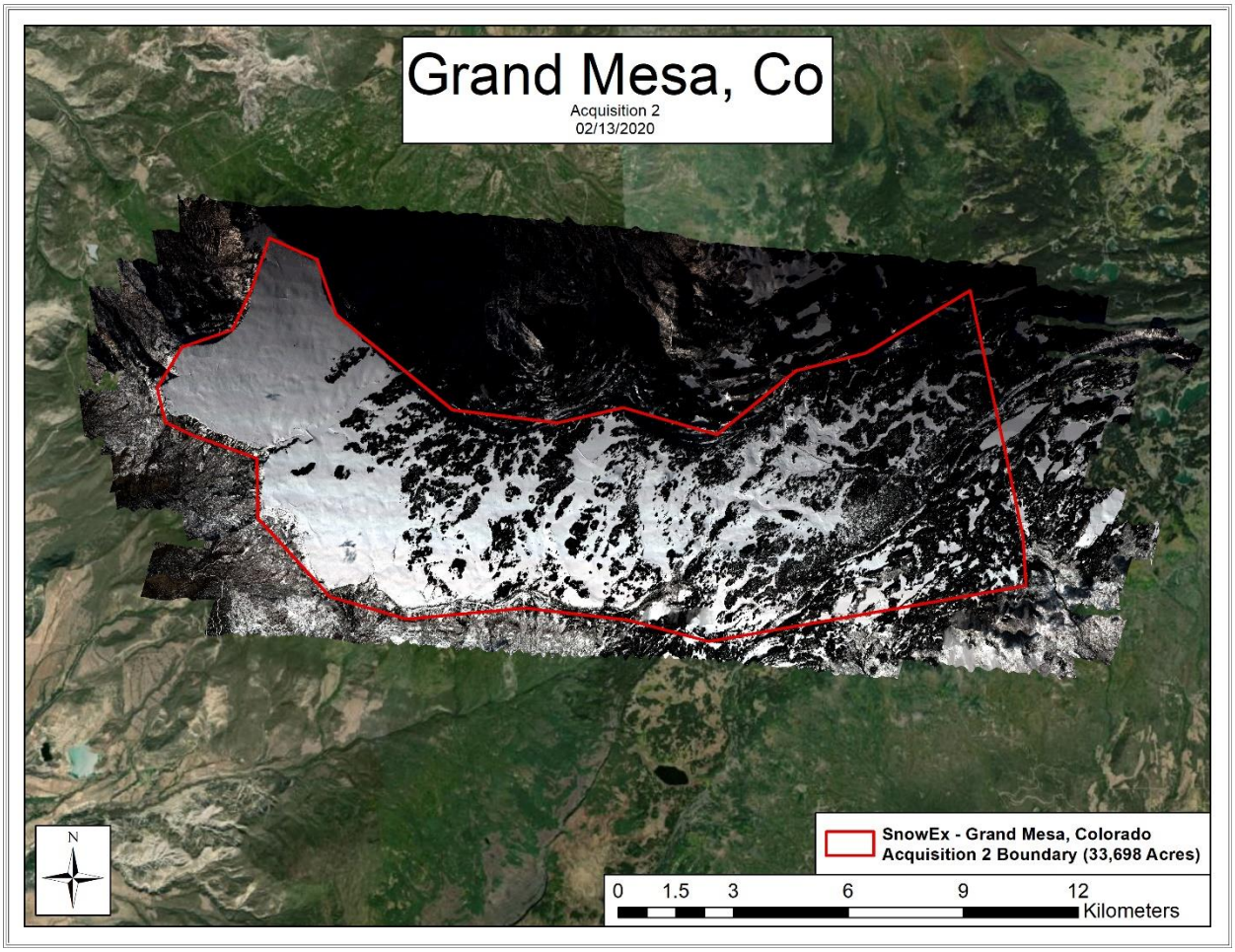

Figure 14: Orthorectified hyperspectral imagery (0.5 Meter) of Grand Mesa, Colorado area, UTM 12. Pictured imagery is from the second of two hyperspectral imagery acquisitions for this area.

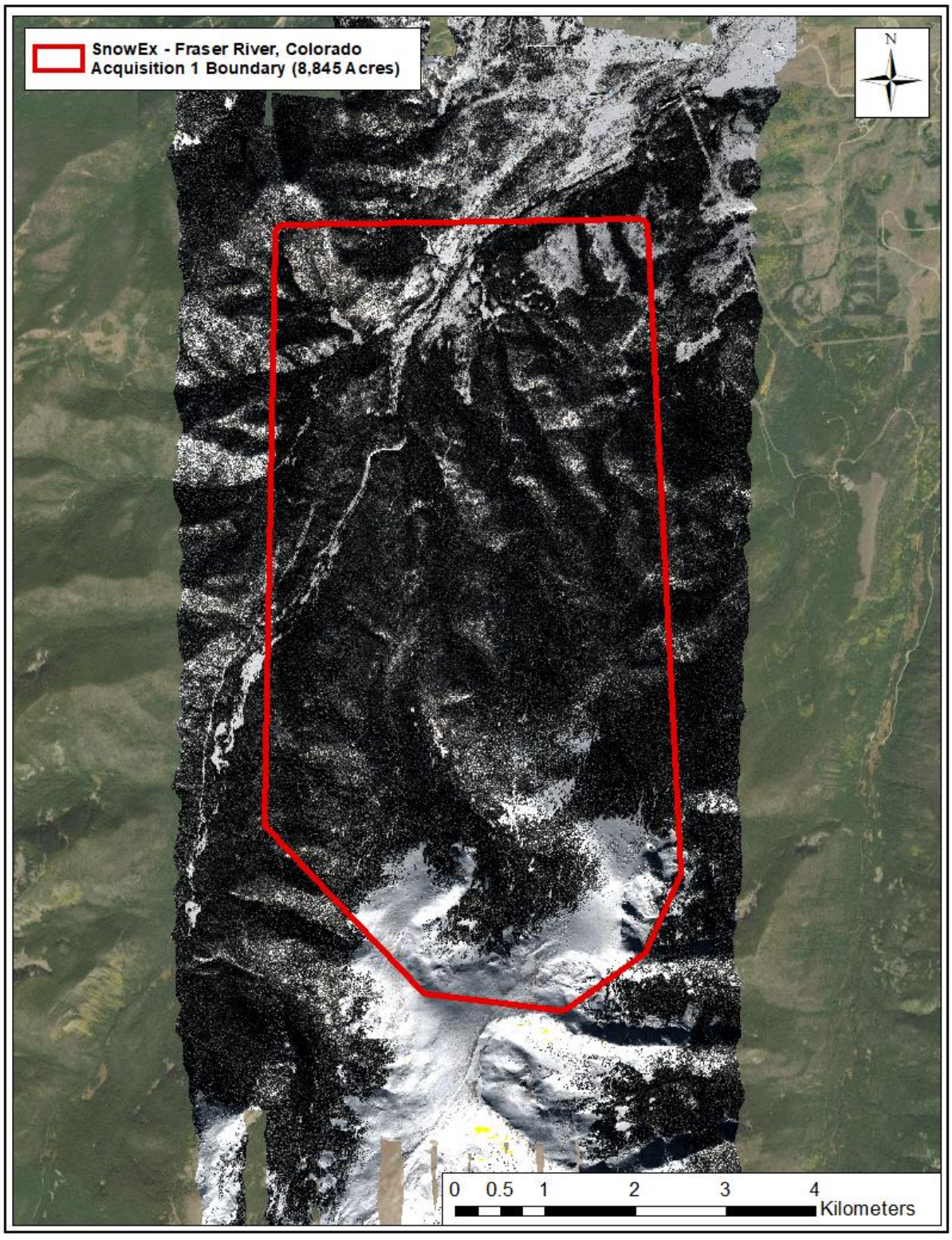

Figure 15: Orthorectified hyperspectral imagery (0.5 Meter) of Fraser River, Colorado area, UTM 13

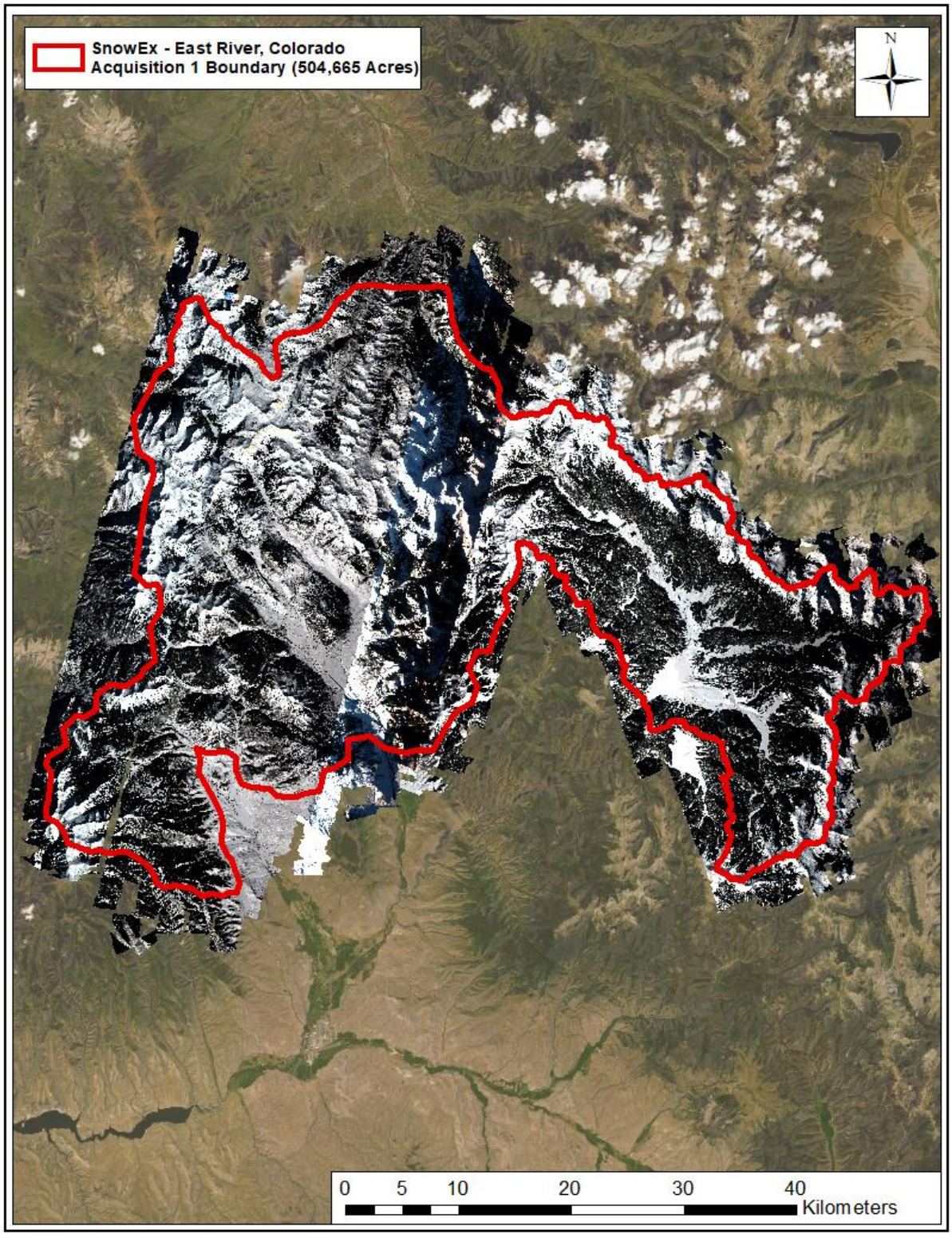

Figure 16: Orthorectified hyperspectral imagery (3 Meter) of East River, Colorado area, UTM 13

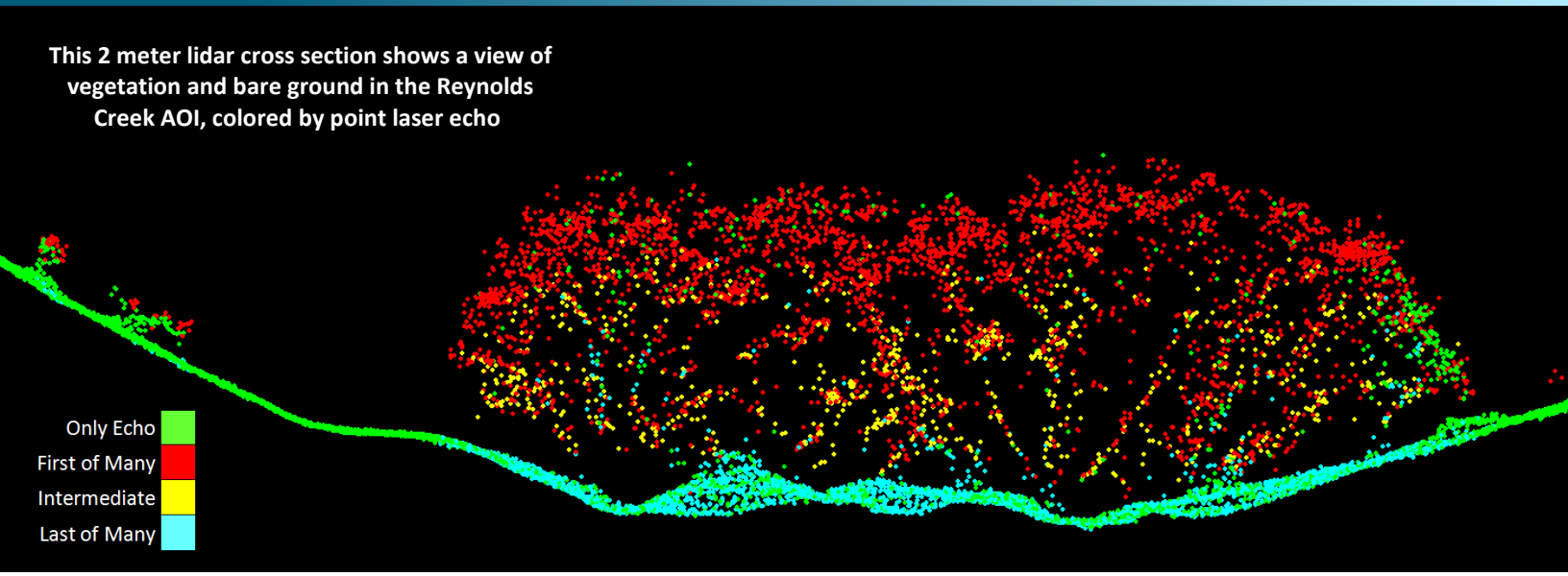

Lidar Density

The acquisition parameters were designed to acquire an average first-return density of 20 points/m^2 for the Grand Mesa, Fraser, Reynolds Creek, Banner Summit, Mores Creek and Dry Creek areas of interest. The East River area of interest acquisition parameters were designed to acquire and average first-return density of 1 point/m^2. First return density describes the density of pulses emitted from the laser that return at least one echo to the system. Multiple returns from a single pulse were not considered in first return density analysis. Some types of surfaces (e.g., breaks in terrain, water and steep slopes) may have returned fewer pulses than originally emitted by the laser. First returns typically reflect off the highest feature on the landscape within the footprint of the pulse. In forested or urban areas the highest feature could be a tree, building or power line, while in areas of unobstructed ground, the first return will be the only echo and represents the bare earth surface.

The density of ground-classified lidar returns was also analyzed for this project. Terrain character, land cover, and ground surface reflectivity all influenced the density of ground surface returns. In vegetated areas, fewer pulses may penetrate the canopy, resulting in lower ground density.

The average first-return and ground density of lidar data for the SnowEx 2020 project can be viewed in Table 11. The statistical and spatial distributions of first return densities and classified ground return densities per 100 m x 100 m cell are portrayed in Figure 17 through Figure 40.

Table 11: Average lidar point densities

Area of Interest	Classification	Point Density
Banner Summit	First-Return	53.99 points/m^2
	Ground Classified	11.51 points/m^2
Dry Creek	First-Return	41.57 points/m^2
	Ground Classified	9.80 points/m^2
Mores Creek	First-Return	36.54 points/m^2
	Ground Classified	9.90 points/m^2
Reynolds Creek	First-Return	41.29 points/m^2
	Ground Classified	9.96 points/m^2
Grand Mesa Acquisition 1	First-Return	34.77 points/m^2
	Ground Classified	9.48 points/m^2
Grand Mesa Acquisition 2	First-Return	34.74 points/m^2
	Ground Classified	13.40 points/m^2
Frasier	First-Return	63.69 points/m^2
	Ground Classified	10.22 points/m^2
East River	First-Return	1.76 points/m^2
	Ground Classified	1.13 points/m^2

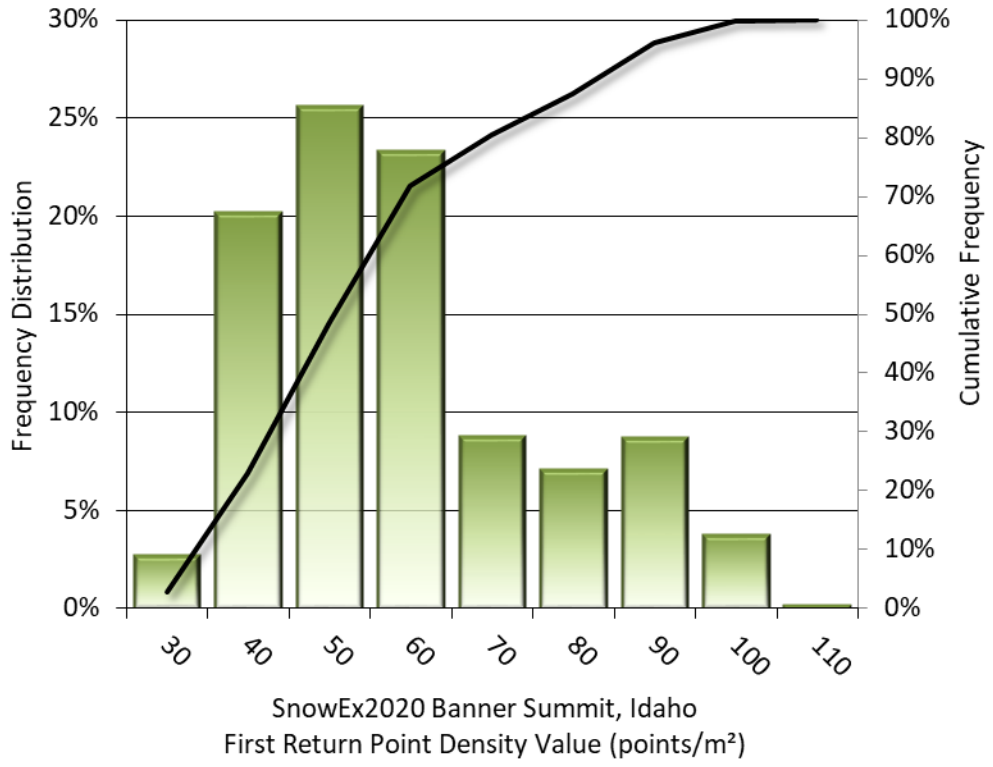

Figure 17: Frequency distribution of first return point density values per 100 x 100 m cell

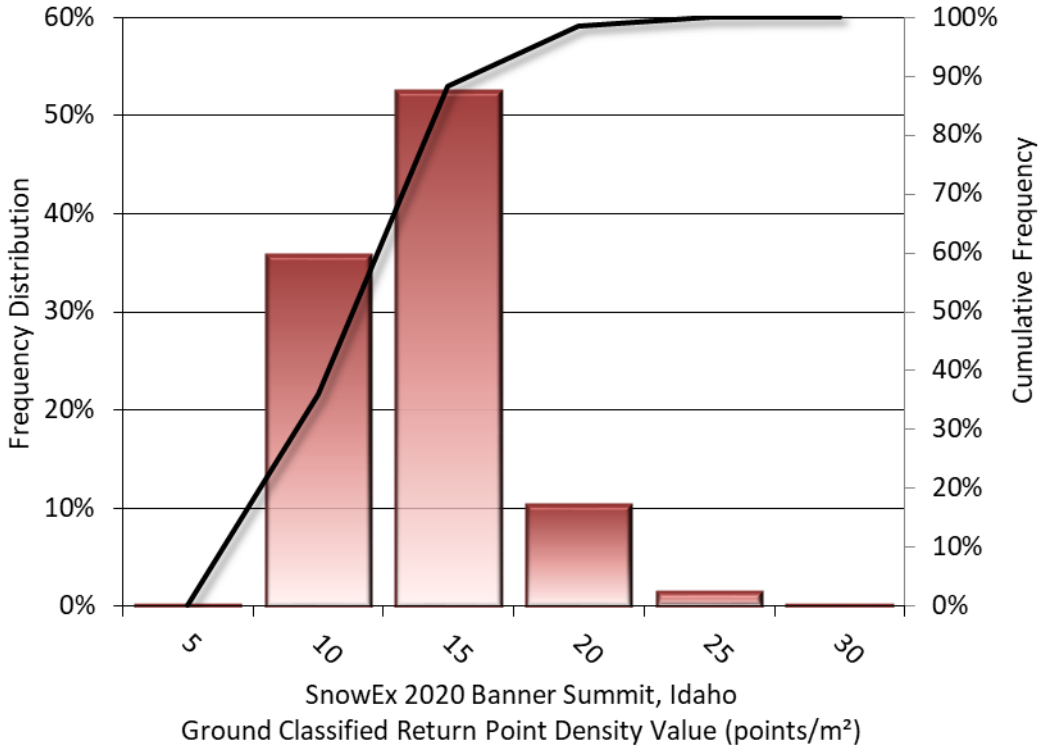

Figure 18: Frequency distribution of ground-classified return point density values per 100 x 100 m cell

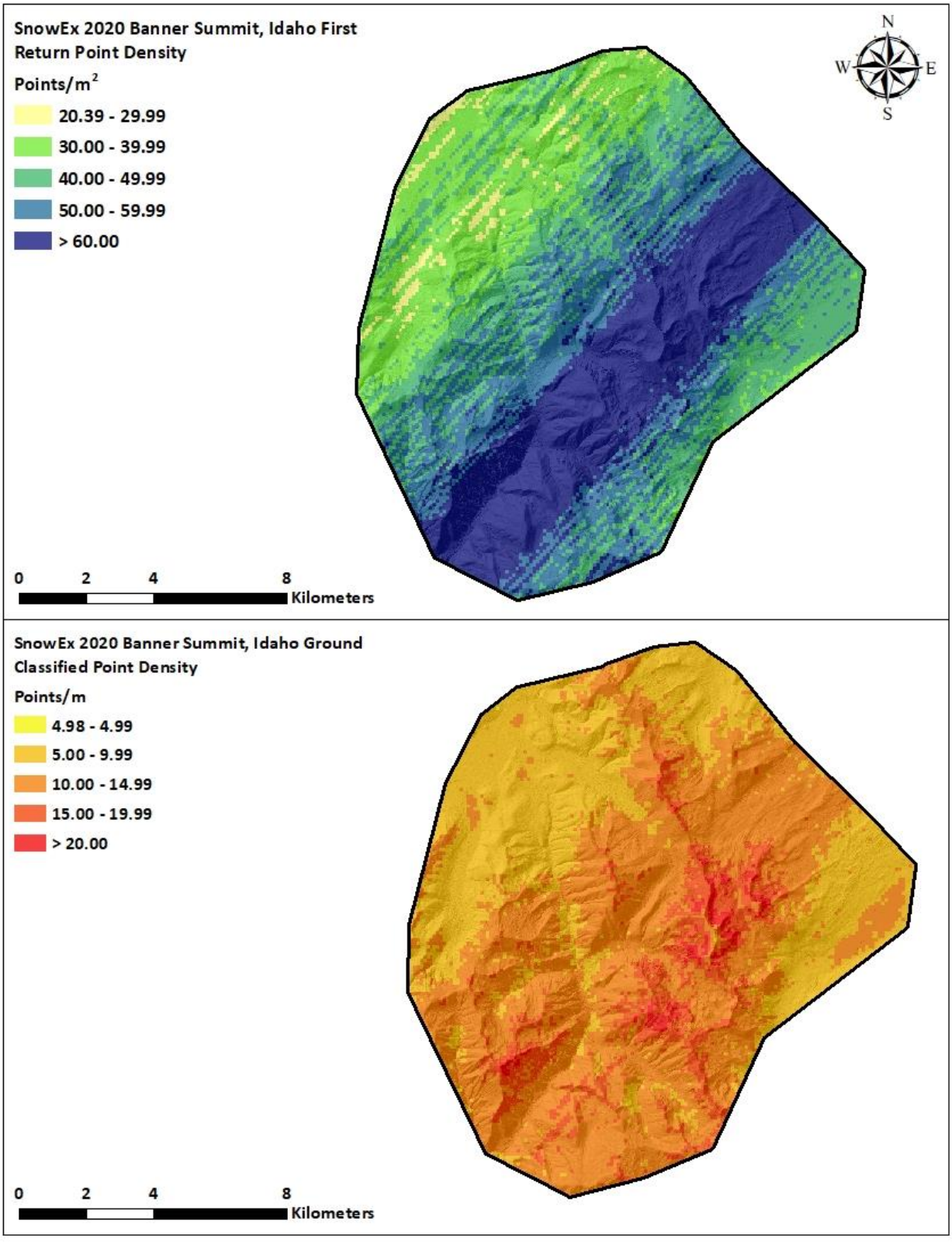

Figure 19: First return and ground-classified point density map for the SnowEx 2020 Banner Summit site (100 m x 100 m cells)

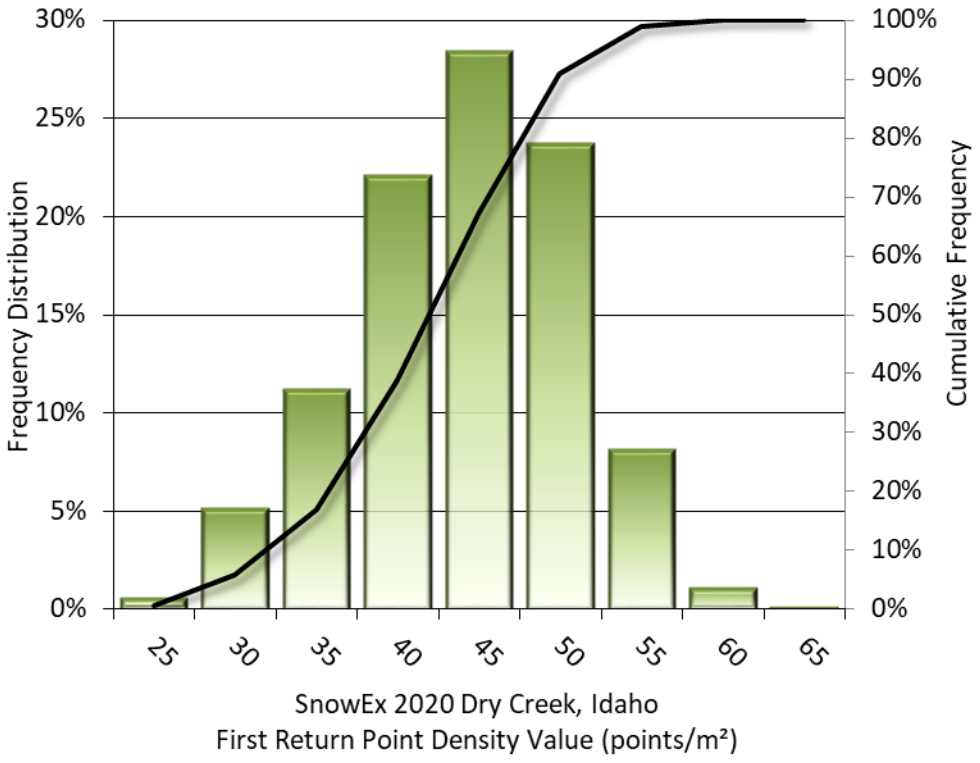

Figure 20: Frequency distribution of first return point density values per 100 x 100 m cell

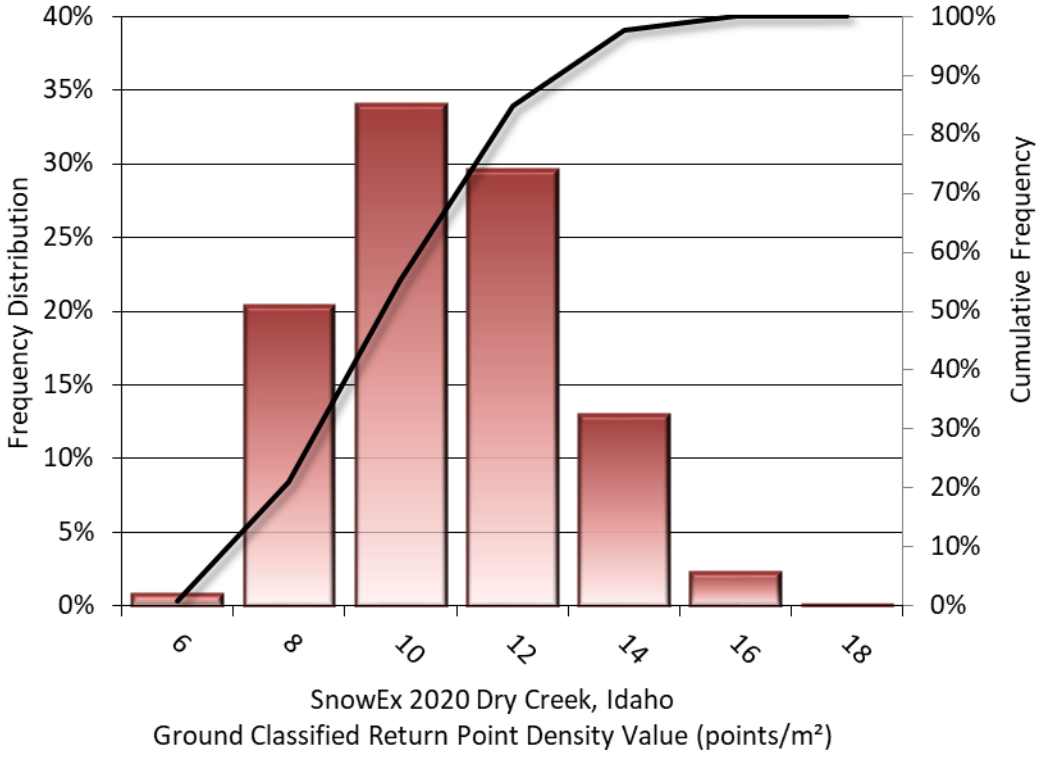

Figure 21: Frequency distribution of ground-classified return point density values per 100 x 100 m cell

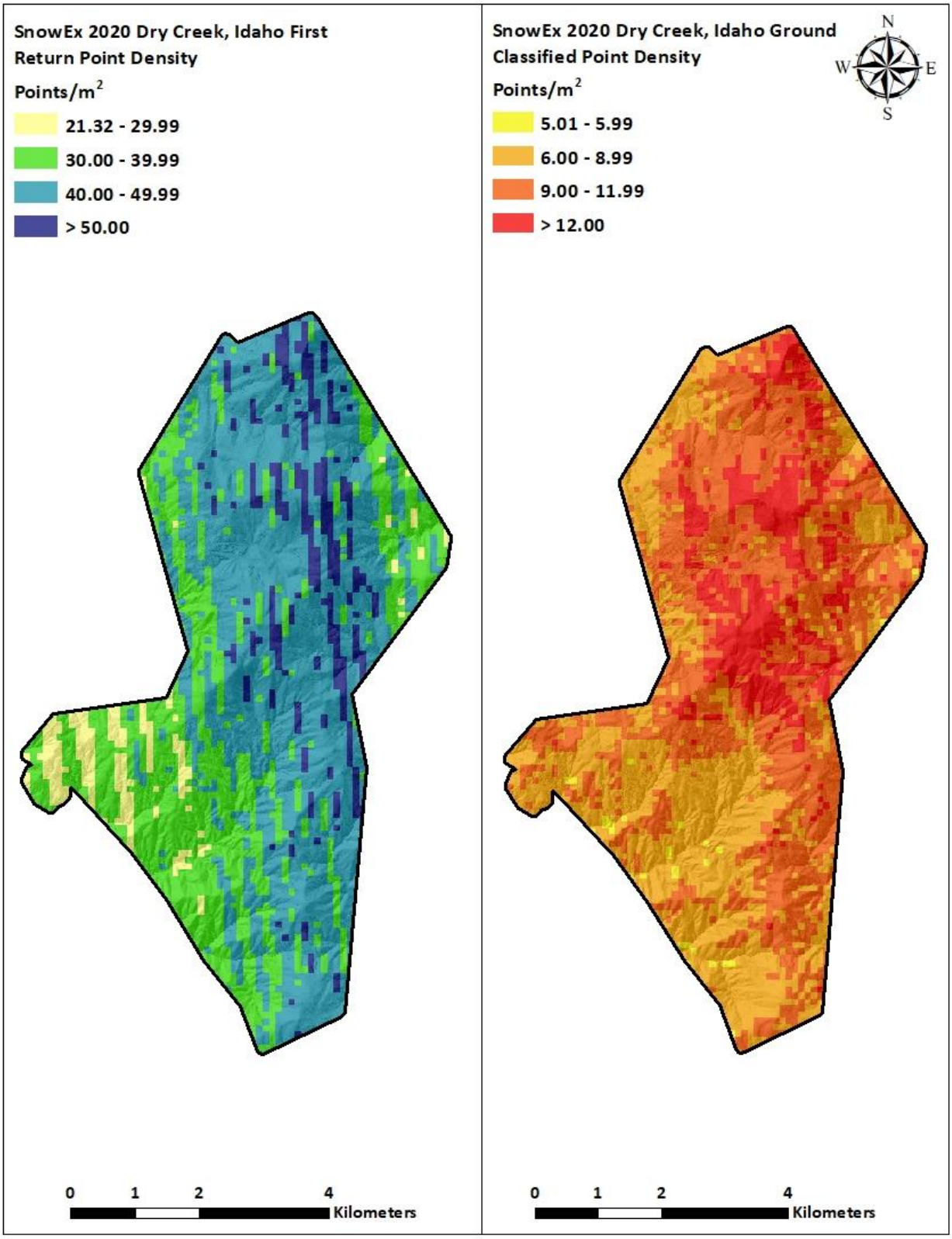

Figure 22: First return and ground-classified point density map for the SnowEx 2020 Dry Creek site (100 m x 100 m cells)

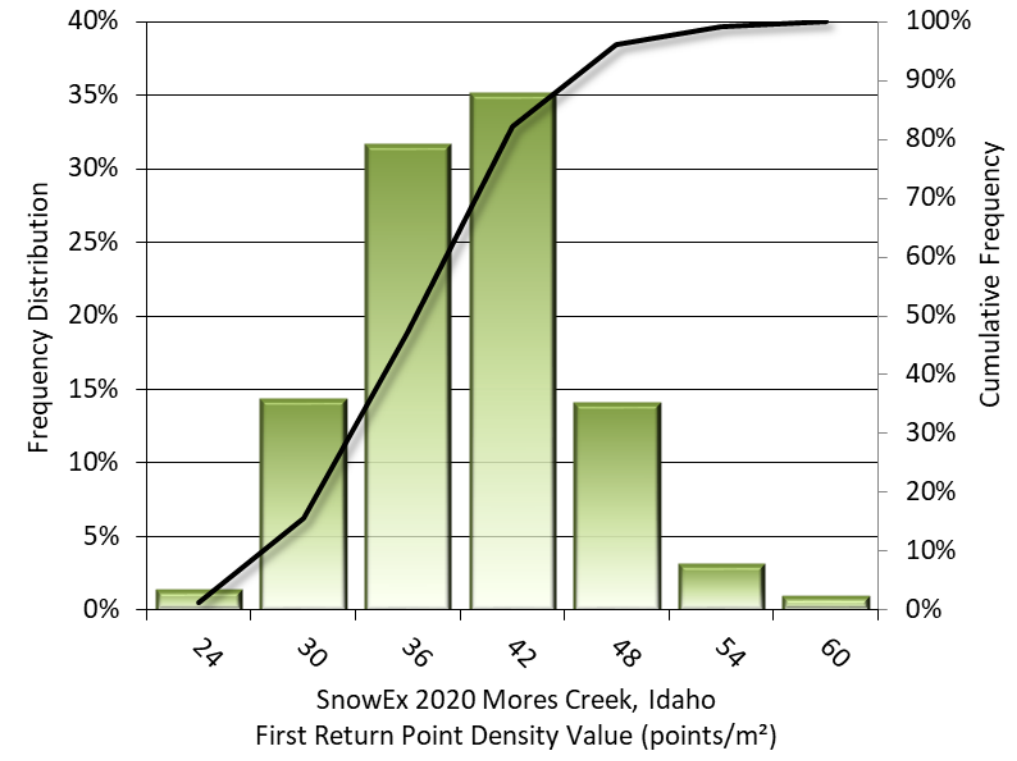

Figure 23: Frequency distribution of first return point density values per 100 x 100 m cell

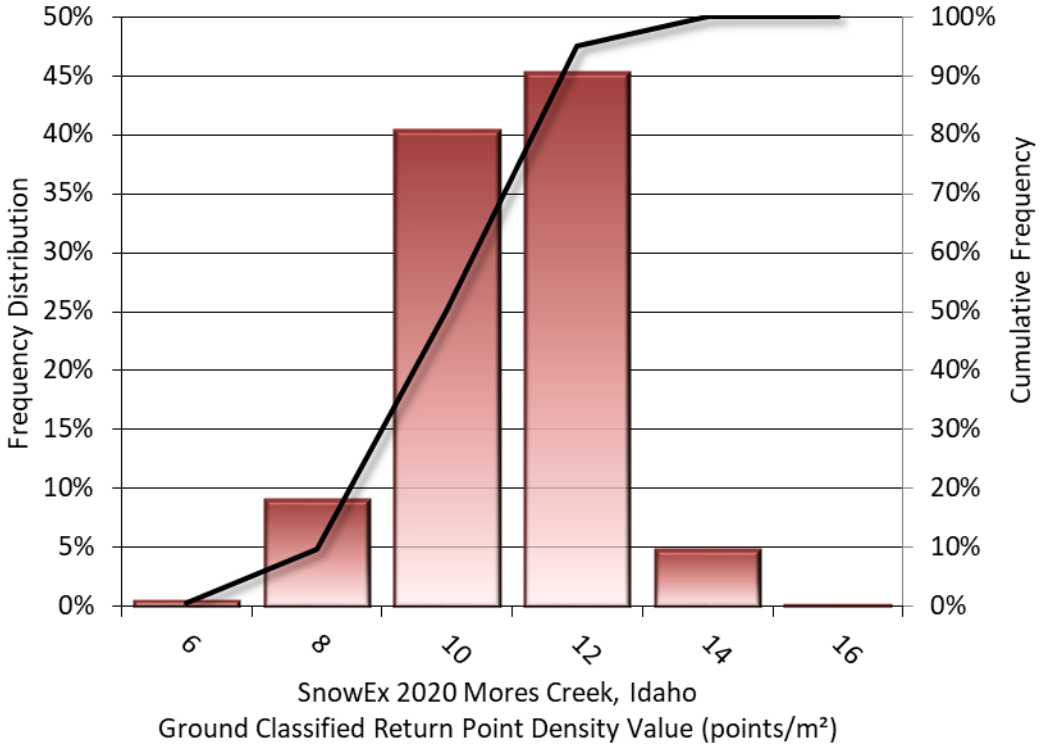

Figure 24: Frequency distribution of ground-classified return point density values per 100 x 100 m cell

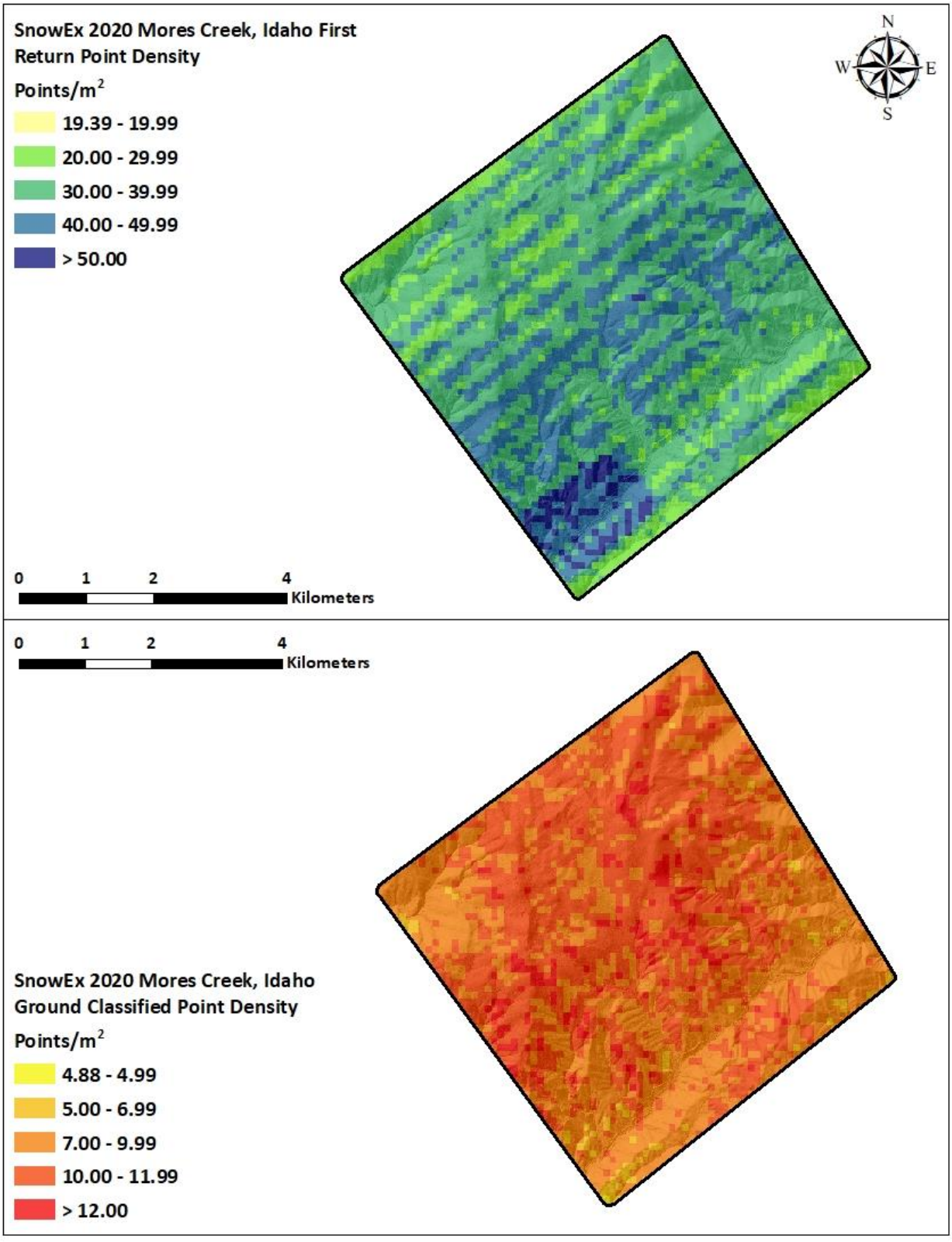

Figure 25: First return and ground-classified point density map for the SnowEx 2020 Mores Creek site (100 m x 100 m cells)

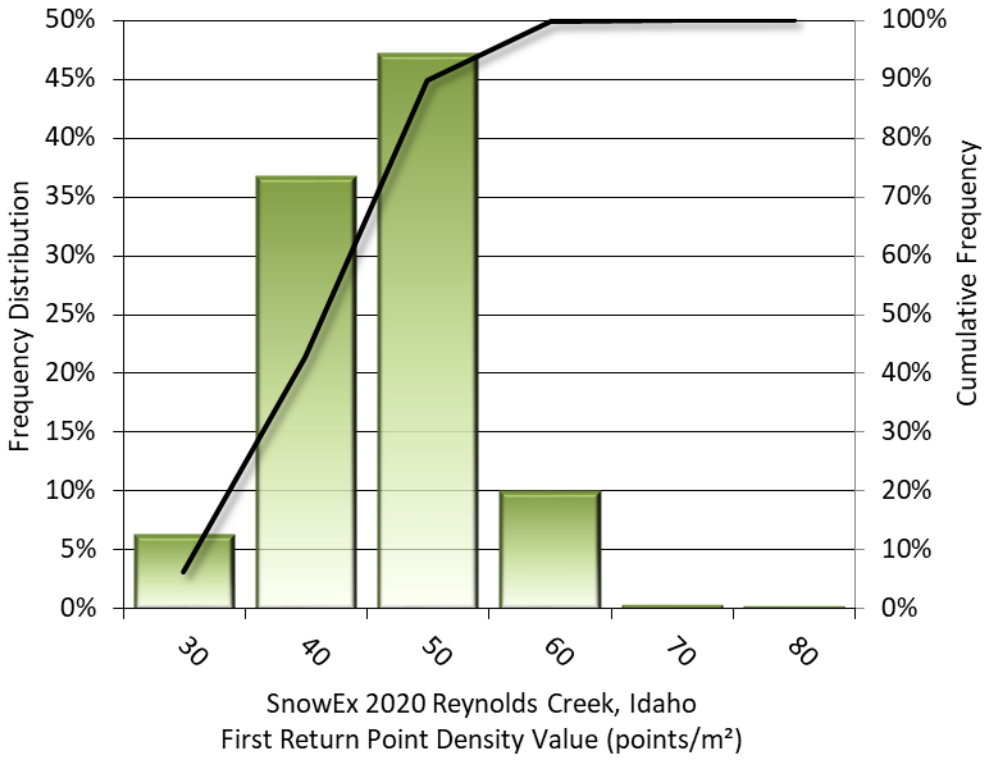

Figure 26: Frequency distribution of first return point density values per 100 x 100 m cell

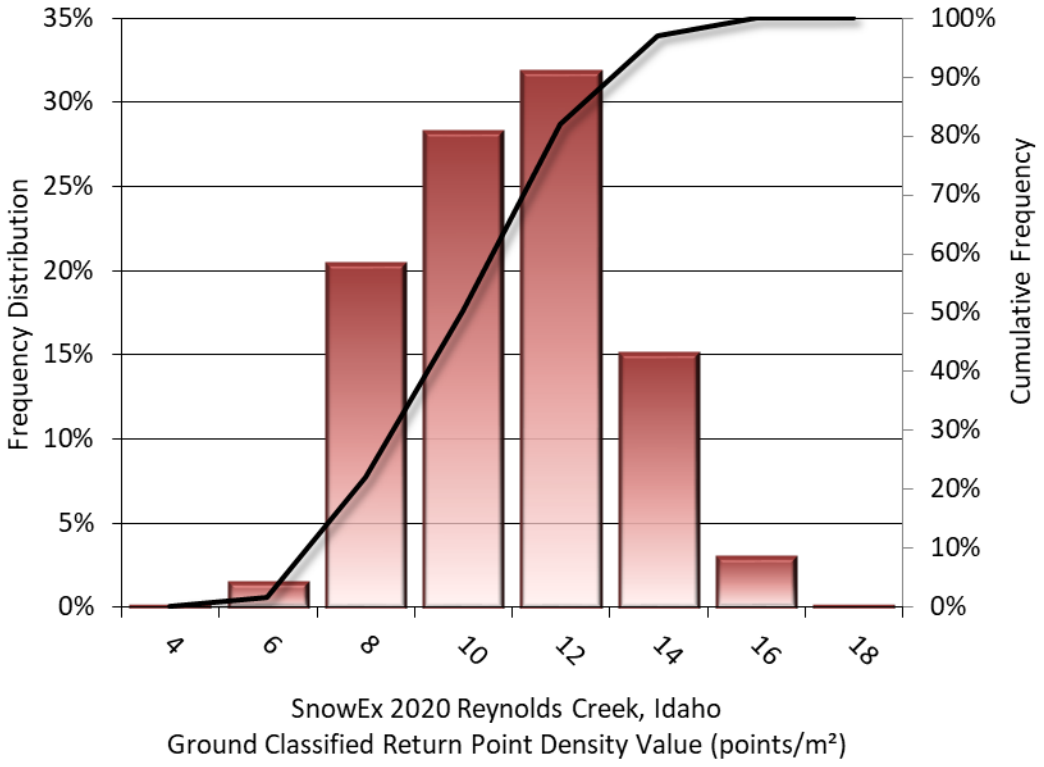

Figure 27: Frequency distribution of ground-classified return point density values per 100 x 100 m cell

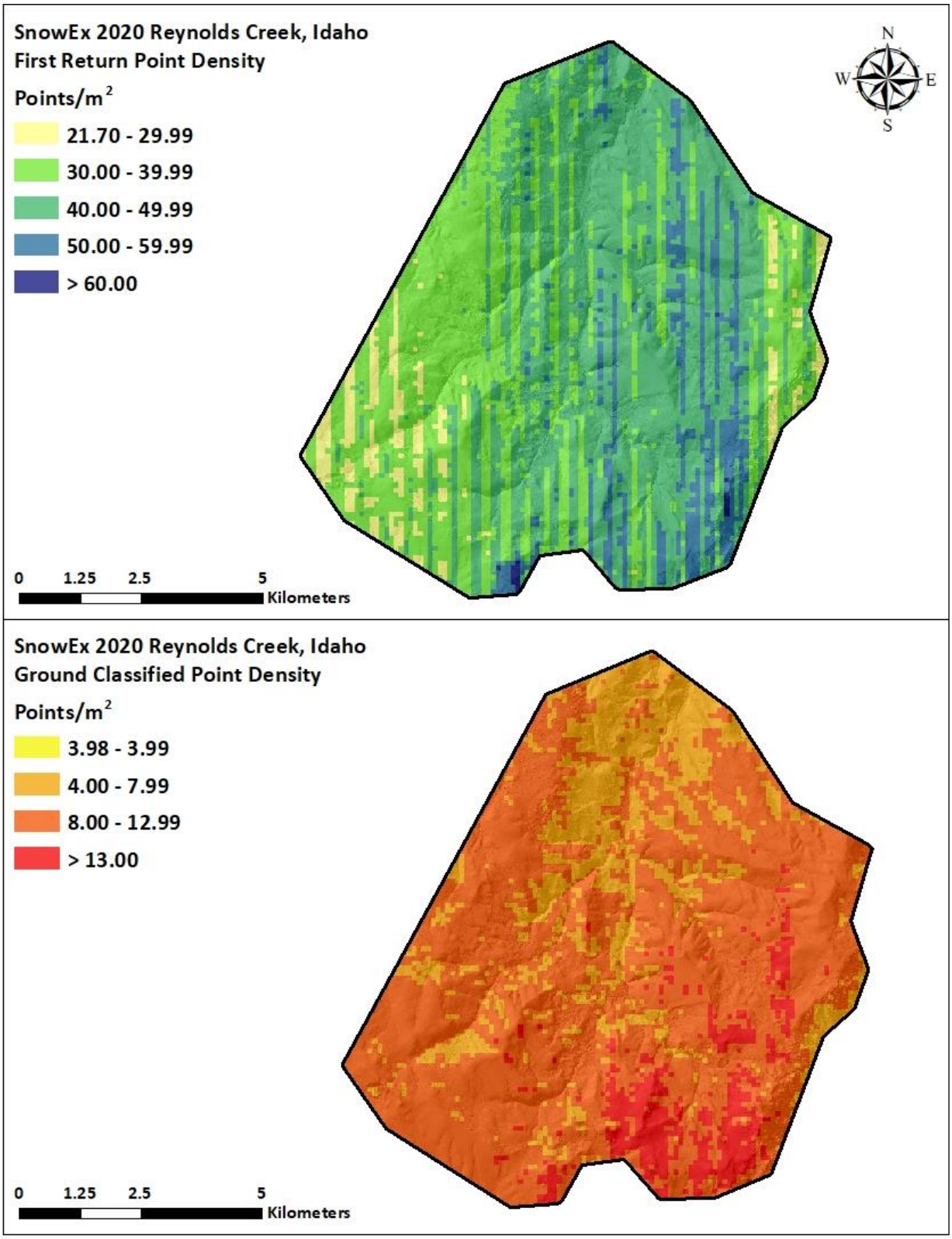

Figure 28: First return and ground-classified point density map for the SnowEx 2020 Reynolds Creek site (100 m x 100 m cells)

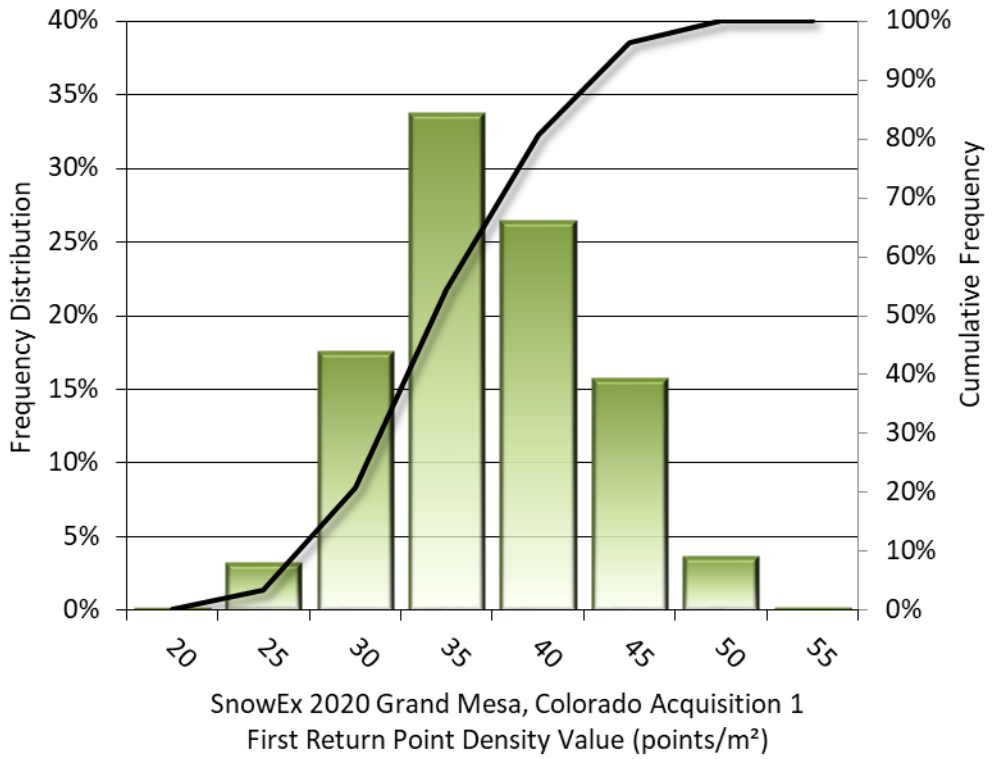

Figure 29: Frequency distribution of first return point density values per 100 x 100 m cell

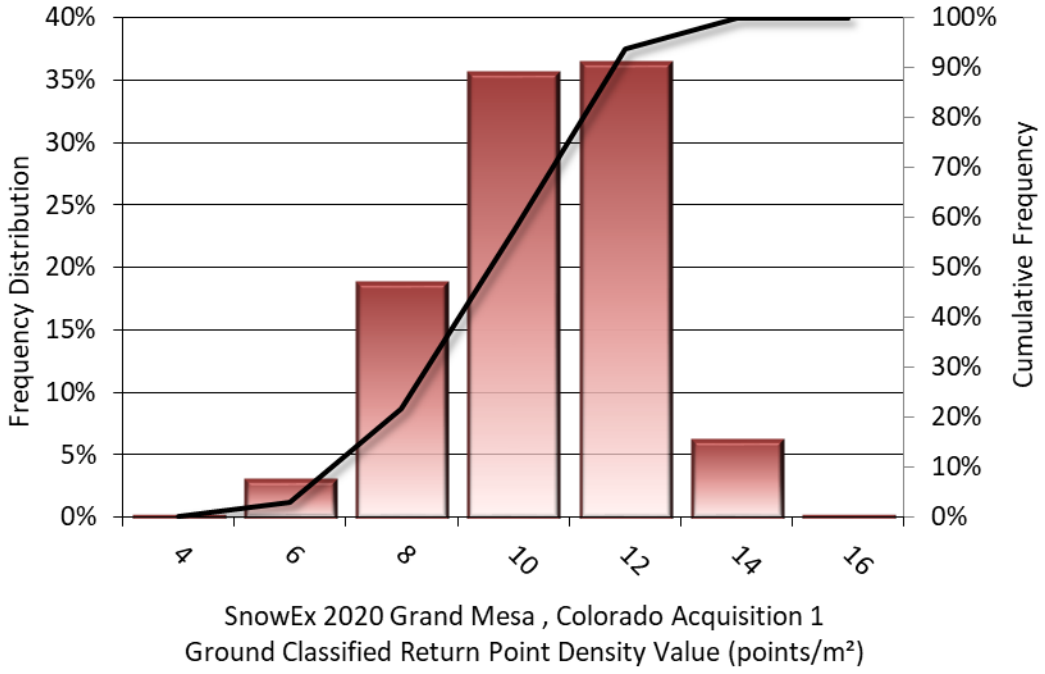

Figure 30: Frequency distribution of ground-classified return point density values per 100 x 100 m cell

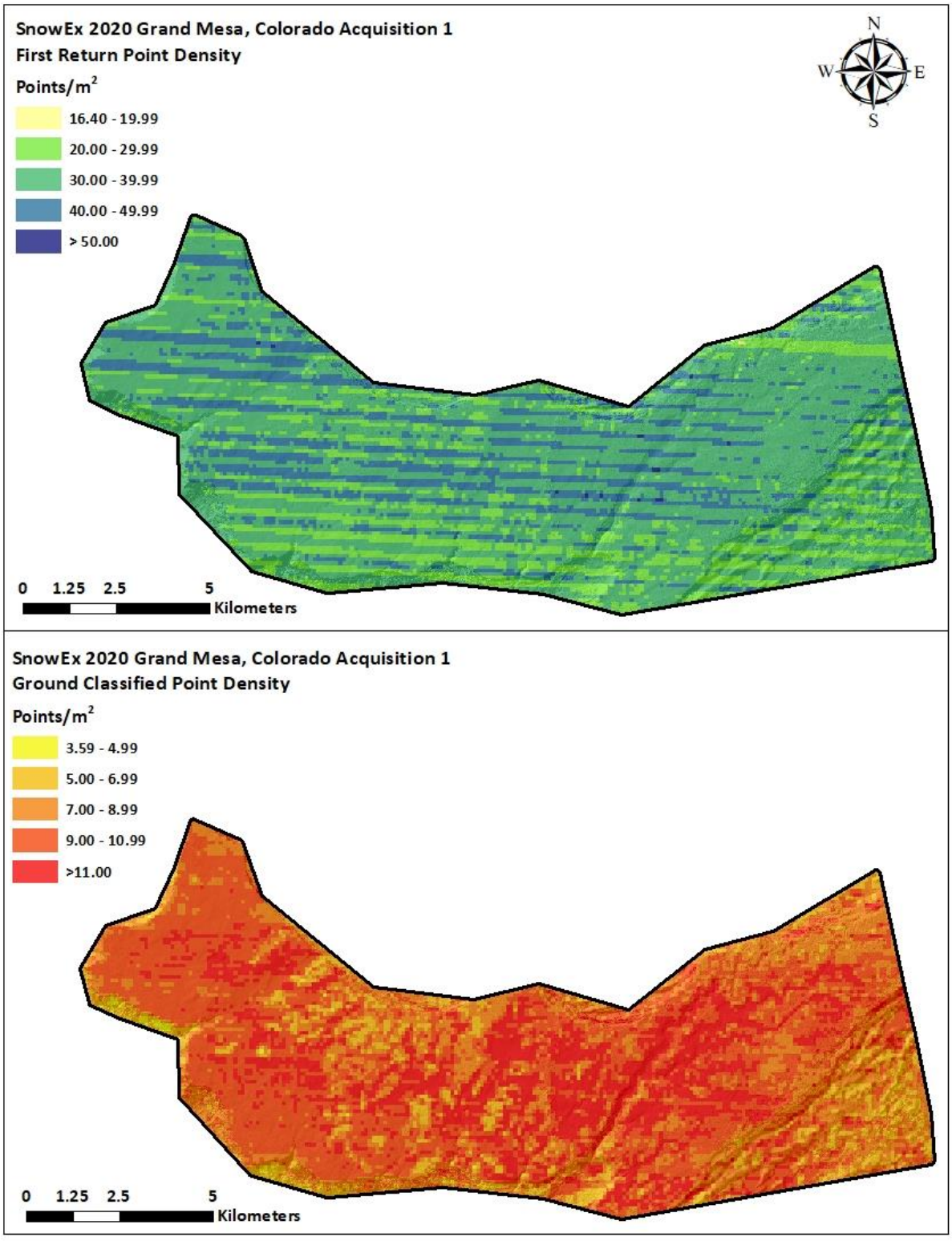

Figure 31: First return and ground-classified point density map for the SnowEx 2020 Grand Mesa Acquisition 1 site (100 m x 100 m cells)

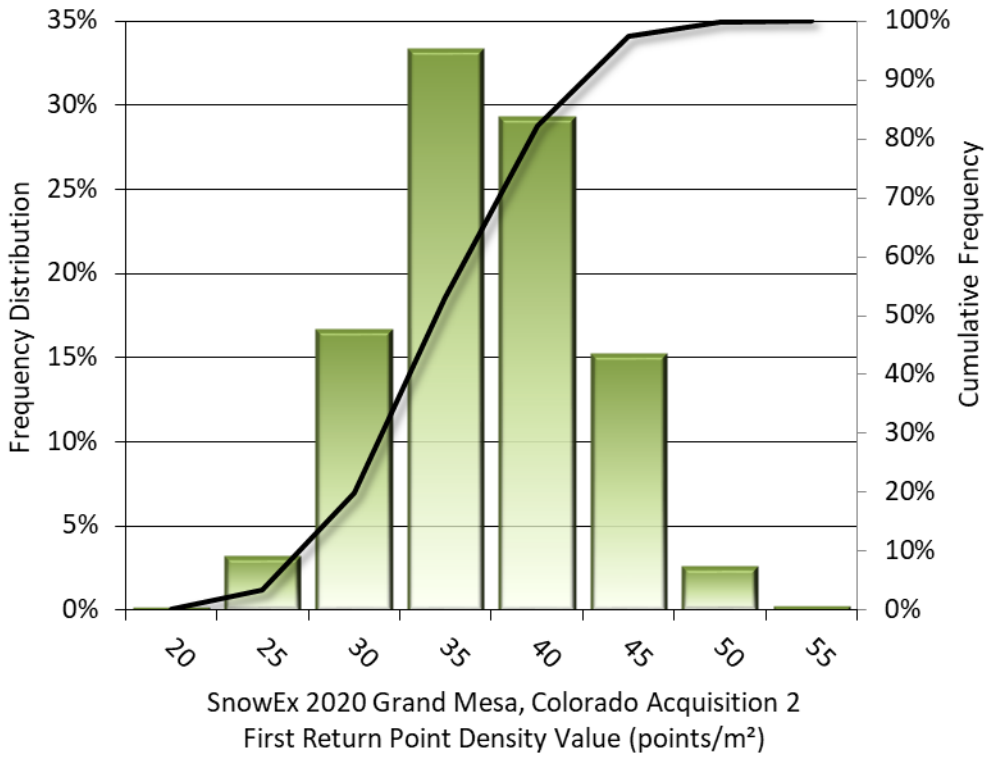

Figure 32: Frequency distribution of first return point density values per 100 x 100 m cell

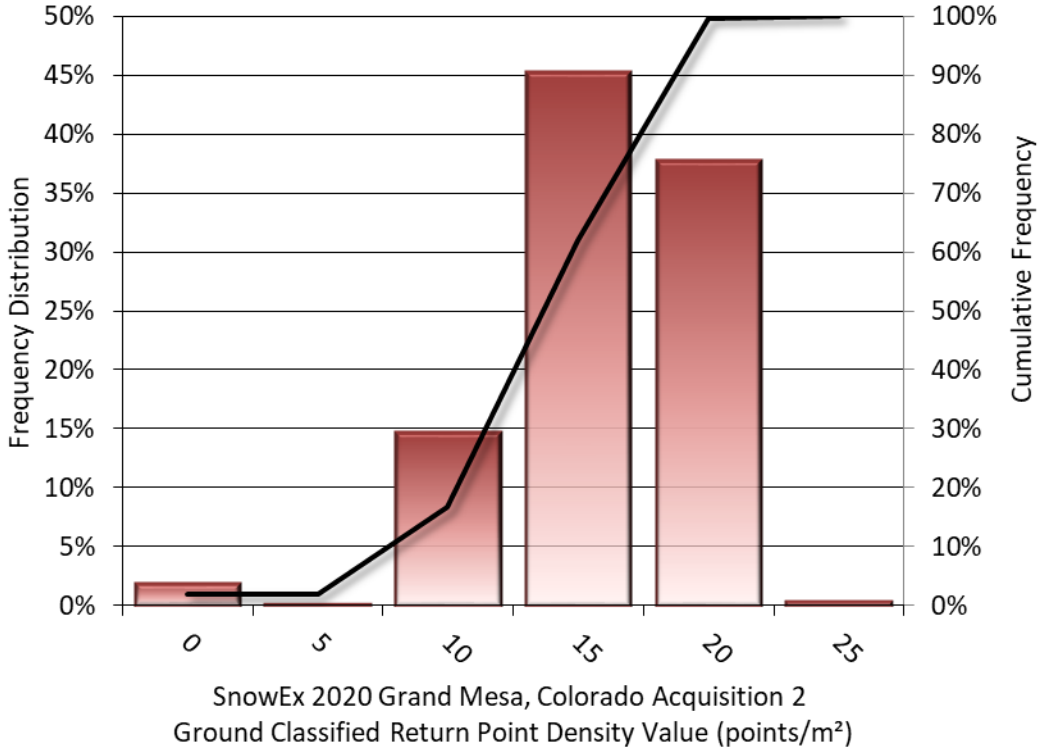

Figure 33: Frequency distribution of ground-classified return point density values per 100 x 100 m cell

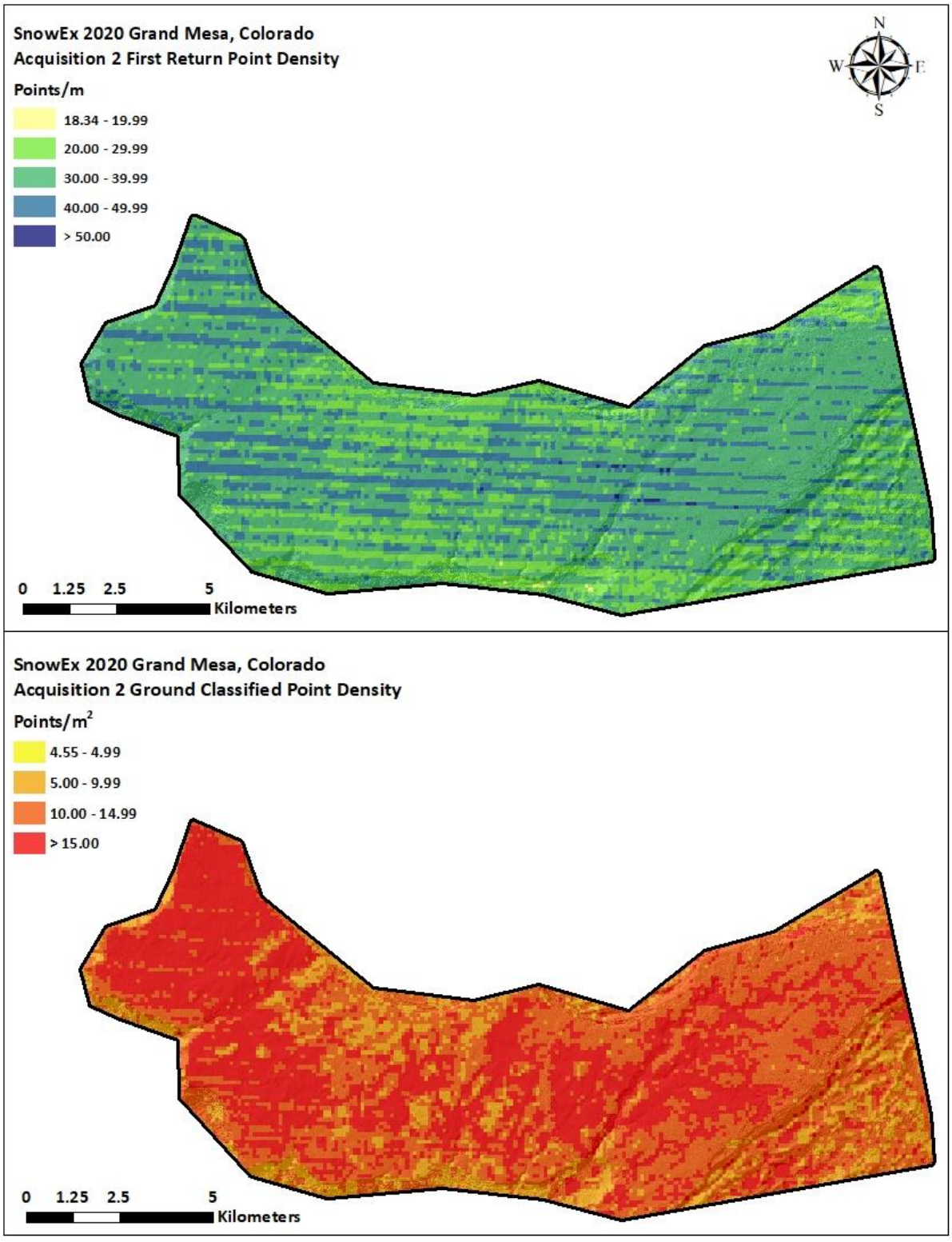

Figure 34: First return and ground-classified point density map for the SnowEx 2020 Grand Mesa Acquisition 2 site (100 m x 100 m cells)

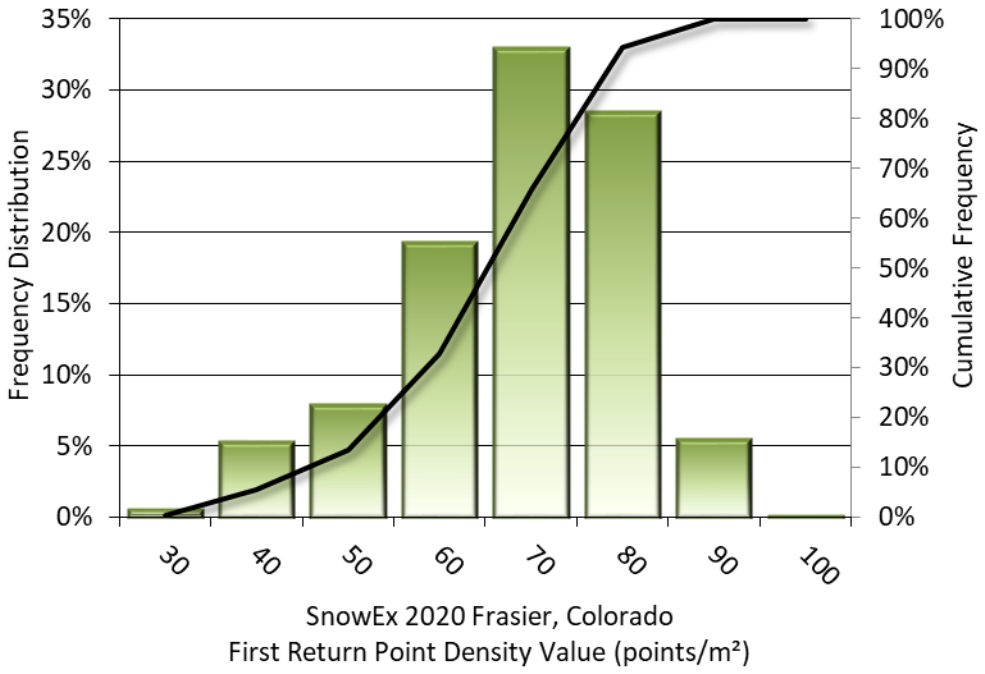

Figure 35: Frequency distribution of first return point density values per 100 x 100 m cell

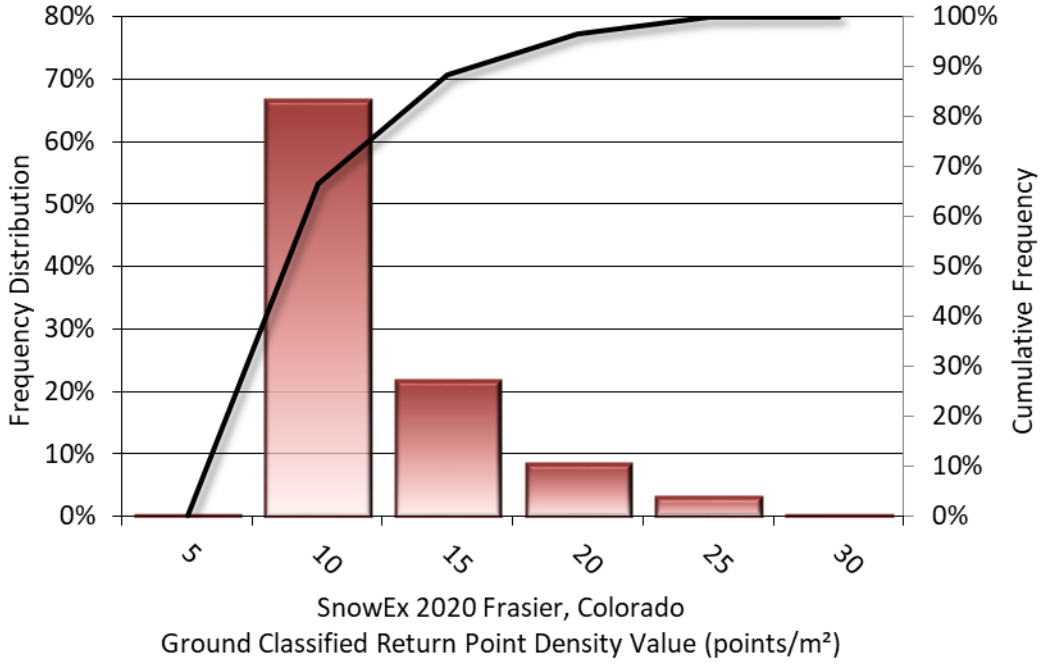

Figure 36: Frequency distribution of ground-classified return point density values per 100 x 100 m cell

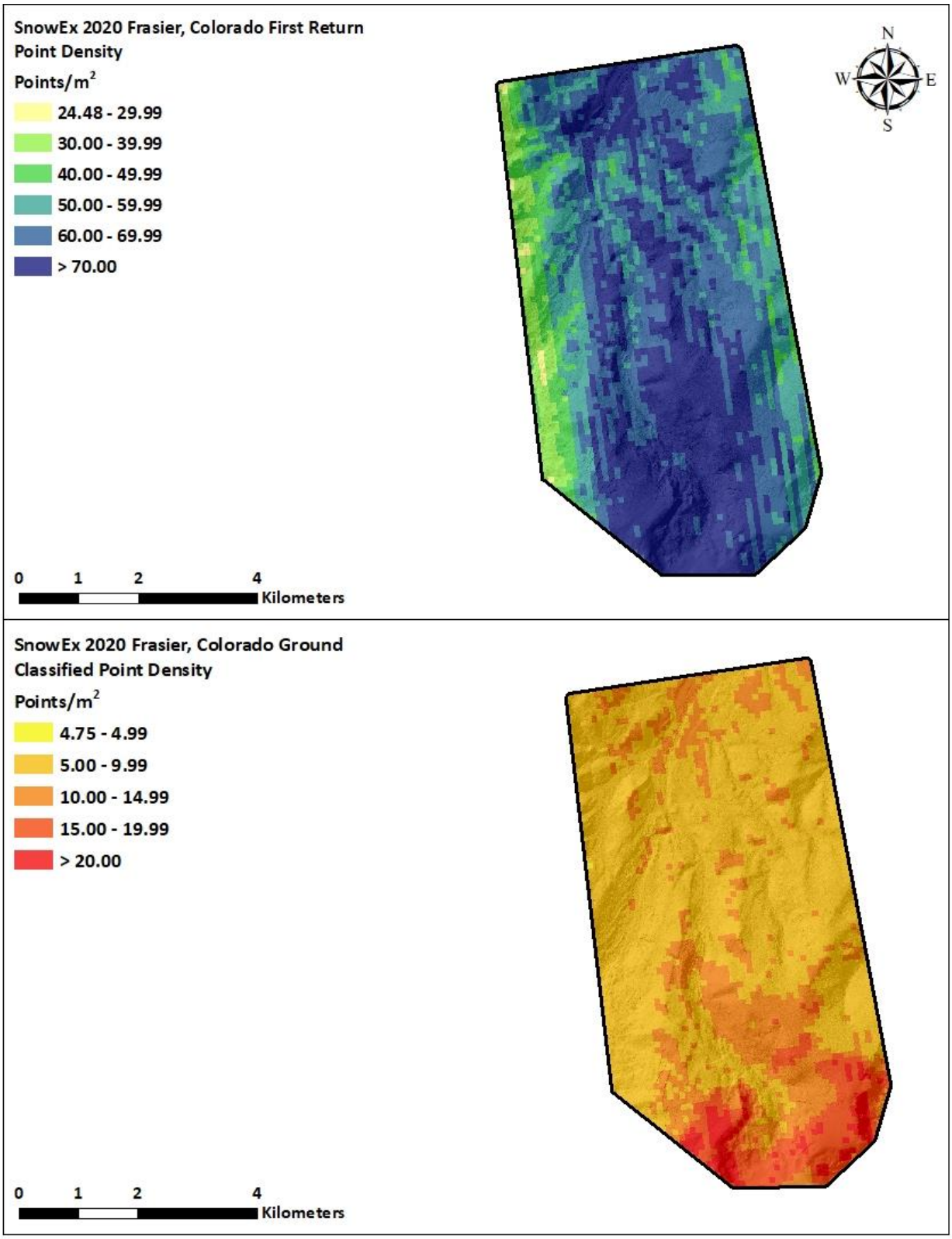

Figure 37: First return and ground-classified point density map for the SnowEx 2020 Frasier site (100 m x 100 m cells)

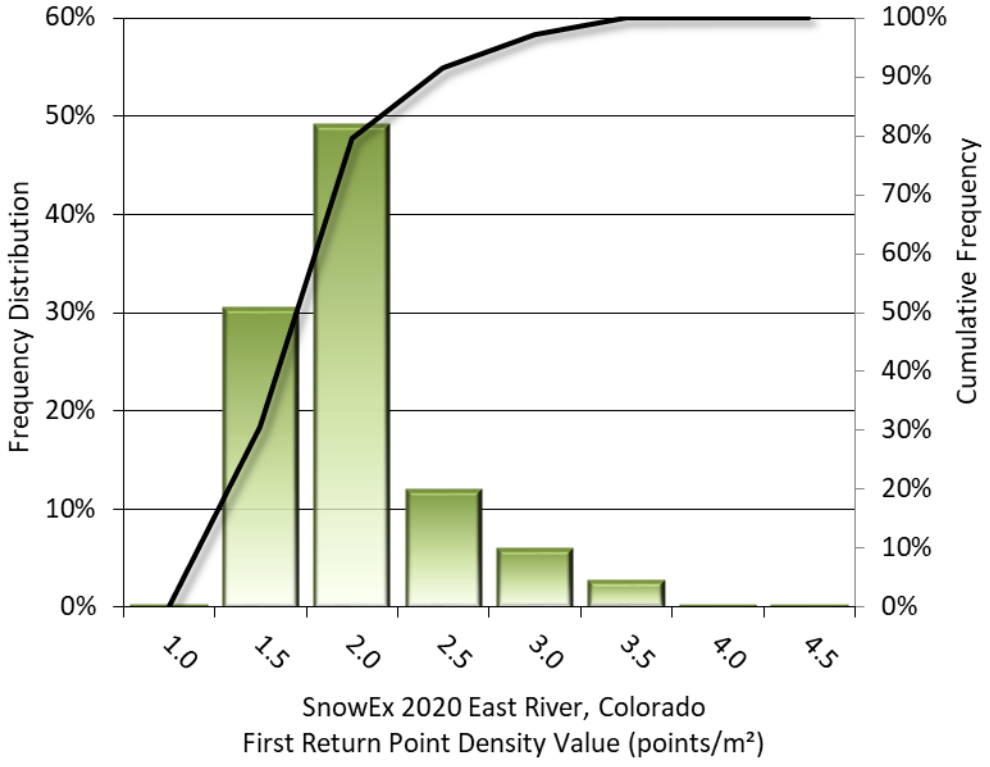

Figure 38: Frequency distribution of first return point density values per 100 x 100 m cell

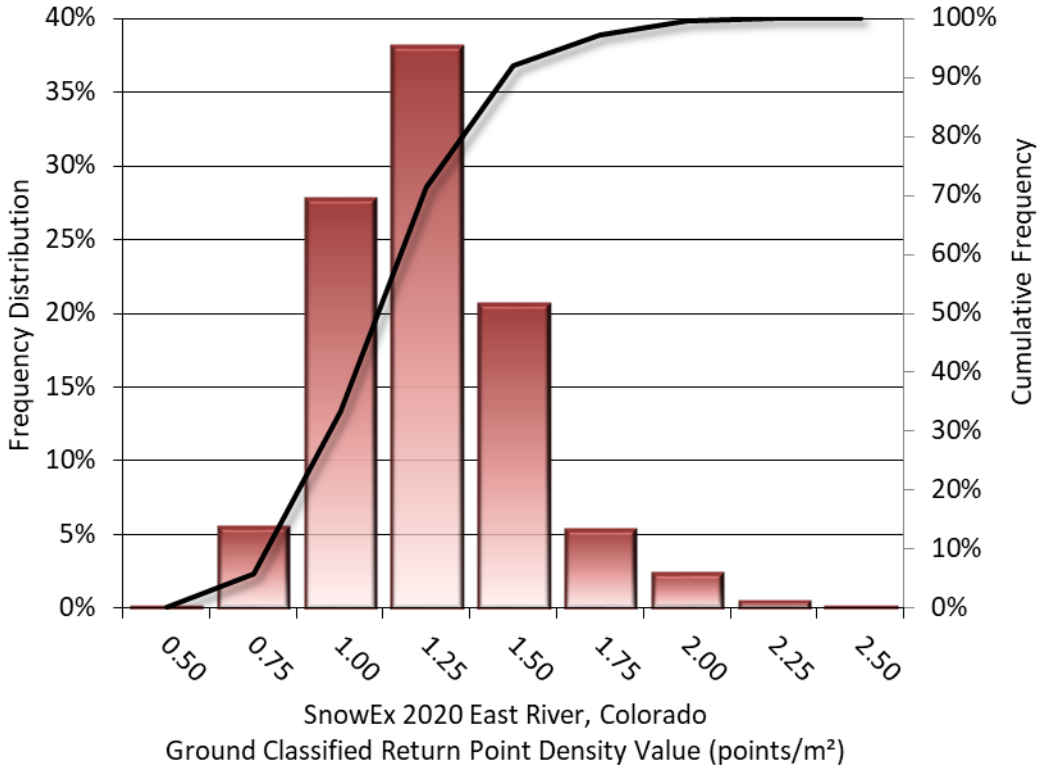

Figure 39: Frequency distribution of ground-classified return point density values per 100 x 100 m cell

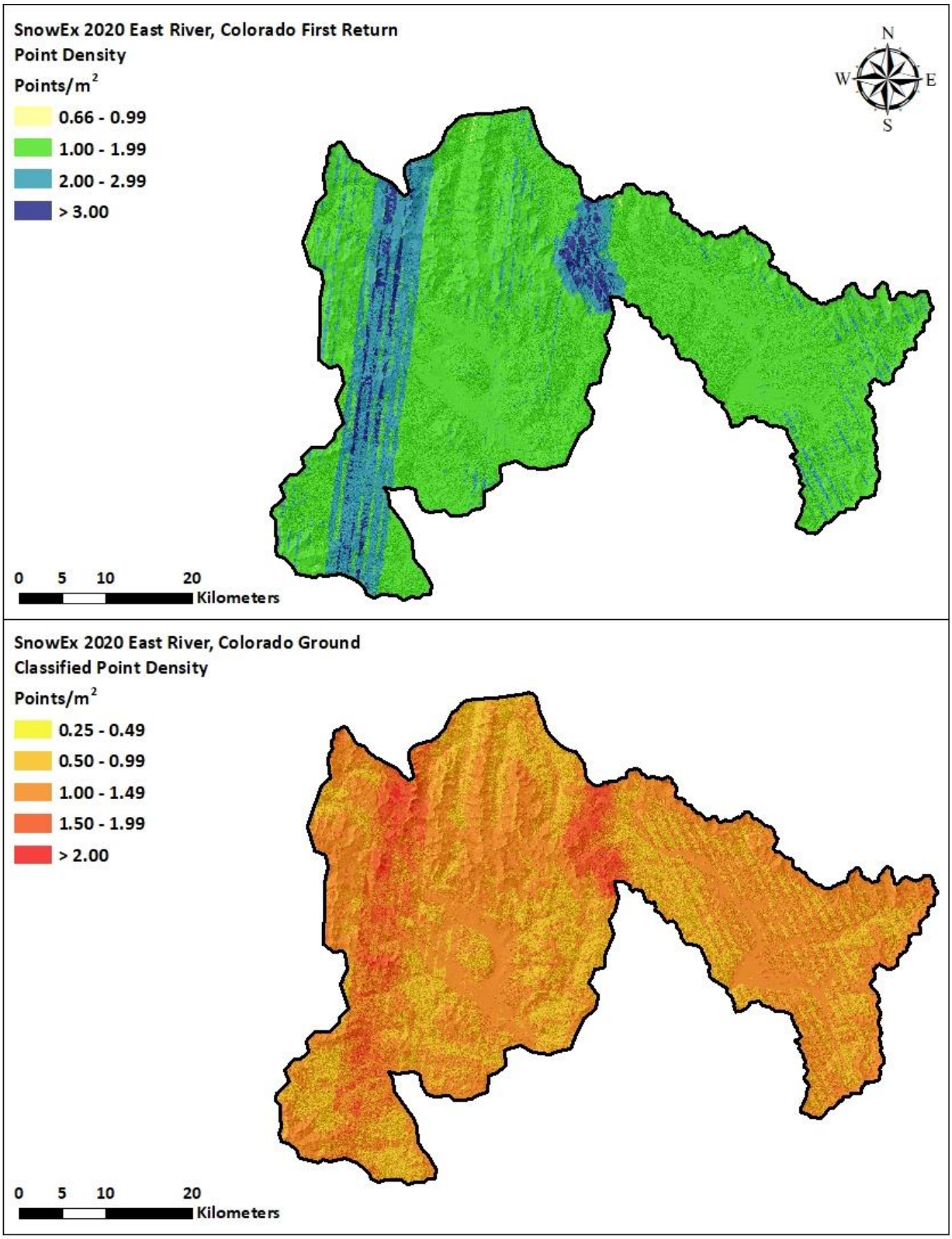

Figure 40: First return and ground-classified point density map for the SnowEx 2020 East River site (100 m x 100 m cells)

Lidar Accuracy Assessments

The accuracy of the lidar data collection can be described in terms of absolute accuracy (the consistency of the data with external data sources) and relative accuracy (the consistency of the dataset with itself). See Appendix A for further information on sources of error and operational measures used to improve relative accuracy.

Lidar Non-Vegetated Vertical Accuracy

Absolute accuracy was assessed using Non-Vegetated Vertical Accuracy (NVA) reporting designed to meet guidelines presented in the FGDC National Standard for Spatial Data Accuracy[3]. NVA compares known ground check point data that were withheld from the calibration and post-processing of the lidar point cloud to the triangulated surface generated by the unclassified lidar point cloud as well as the derived gridded bare earth DEM. NVA is a measure of the accuracy of lidar point data in open areas where the lidar system has a high probability of measuring the ground surface and is evaluated at the 95% confidence interval (1.96 * RMSE), as shown in Table 12.

The mean and standard deviation (sigma σ) of divergence of the ground surface model from quality assurance point coordinates are also considered during accuracy assessment. These statistics assume the error for x, y and z is normally distributed, and therefore the skew and kurtosis of distributions are also considered when evaluating error statistics. For the SnowEx 2020 survey, ground check points were withheld from the calibration and post processing of the lidar point cloud (Figure 41 through Figure 54 and Table 12 through Table 19).

QSI also assessed absolute accuracy using ground control points. Although these points were used in the calibration and post-processing of the lidar point cloud, they still provide a good indication of the overall accuracy of the lidar dataset, and therefore have been provided in (Figure 41 through Figure 54 and Table 12 through Table 19).

[3] Federal Geographic Data Committee, ASPRS POSITIONAL ACCURACY STANDARDS FOR DIGITAL GEOSPATIAL DATA EDITION 1, Version 1.0, NOVEMBER 2014. https://www.asprs.org/a/society/committees/standards/Positional_Accuracy_Standards.pdf.

Table 12: Banner Summit - Absolute accuracy results

Banner Summit - Absolute Vertical Accuracy			
	NVA, as compared to unclassified LAS	**NVA, as compared to bare earth DEM**	**Ground Control Points**
Sample	0 points	0 points	86 points
95% Confidence (1.96*RMSE)	n/a	n/a	0.039 m
Average	n/a	n/a	0.000 m
Median	n/a	n/a	0.000 m
RMSE	n/a	n/a	0.020 m
Standard Deviation (1σ)	n/a	n/a	0.020 m

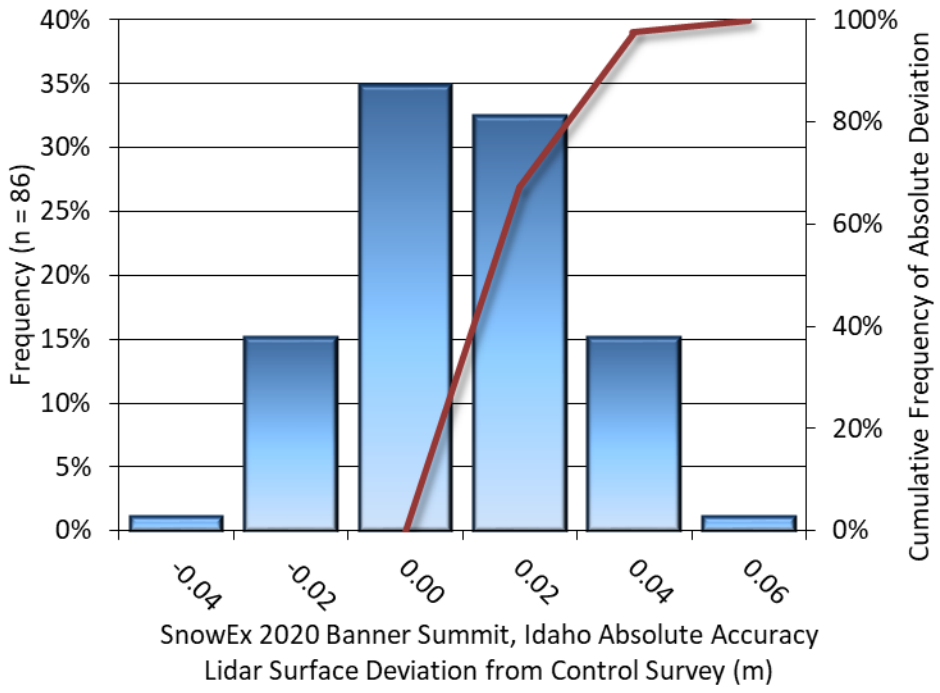

Figure 41: Frequency histogram for lidar surface deviation from ground control point values

Table 13: Dry Creek - Absolute accuracy results

Dry Creek - Absolute Vertical Accuracy			
	NVA, as compared to unclassified LAS	**NVA, as compared to bare earth DEM**	**Ground Control Points**
Sample	6 point	6 point	94 points
95% Confidence (1.96*RMSE)	0.050 m	0.053 m	0.034 m
Average	0.008 m	-0.006 m	-0.003 m
Median	0.003 m	-0.007 m	-0.002 m
RMSE	0.026 m	0.027 m	0.017 m
Standard Deviation (1σ)	0.027 m	0.029 m	0.017 m

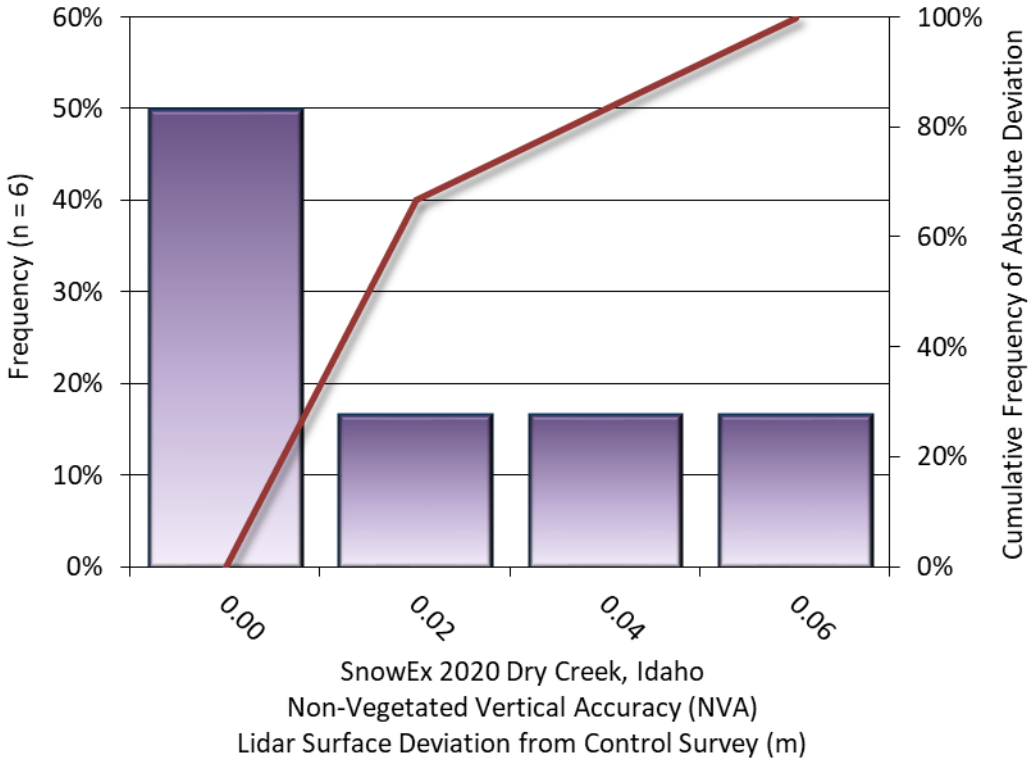

Figure 42: Frequency histogram for lidar unclassified LAS deviation from ground check point values (NVA)

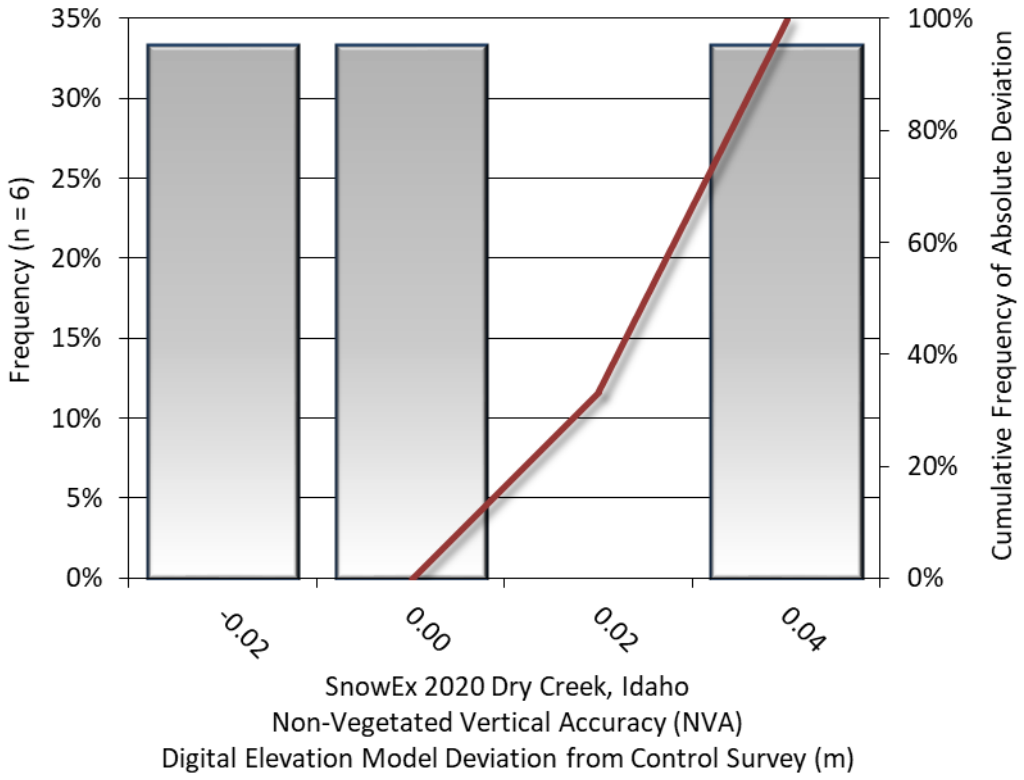

Figure 43: Frequency histogram for lidar bare earth DEM surface deviation from ground check point values (NVA)

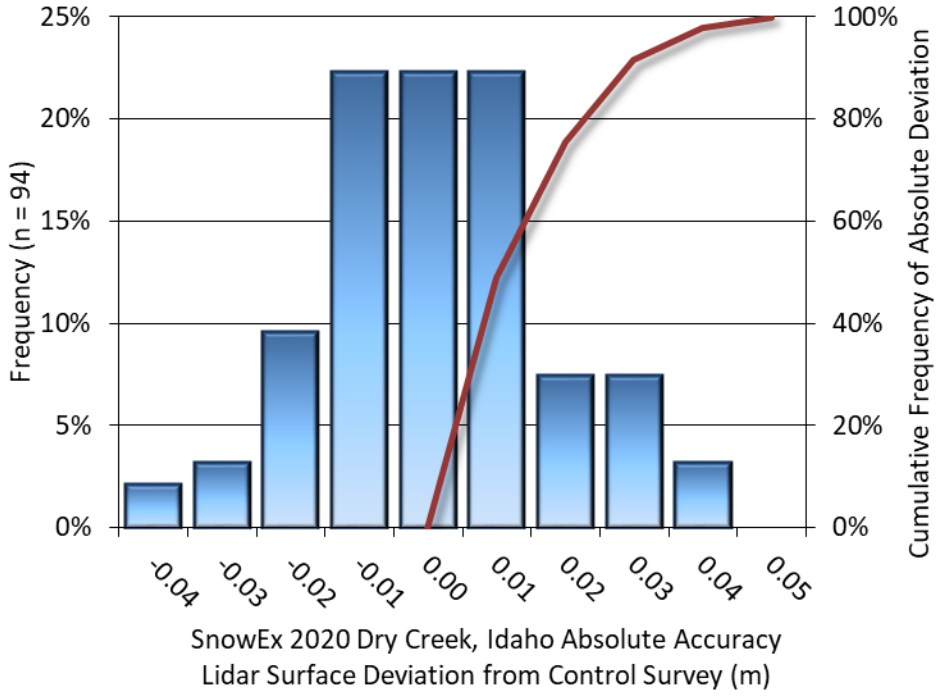

Figure 44: Frequency histogram for lidar surface deviation from ground control point values

Table 14: Mores Creek - Absolute accuracy results

Mores Creek - Absolute Vertical Accuracy			
	NVA, as compared to unclassified LAS	**NVA, as compared to bare earth DEM**	**Ground Control Points**
Sample	1 point	1 point	22 points
95% Confidence (1.96*RMSE)	0.039 m	0.000 m	0.040 m
Average	-0.020 m	0.000 m	0.001 m
Median	-0.020 m	0.000 m	-0.002 m
RMSE	0.020 m	0.000 m	0.021 m
Standard Deviation (1σ)	n/a	n/a	0.021 m

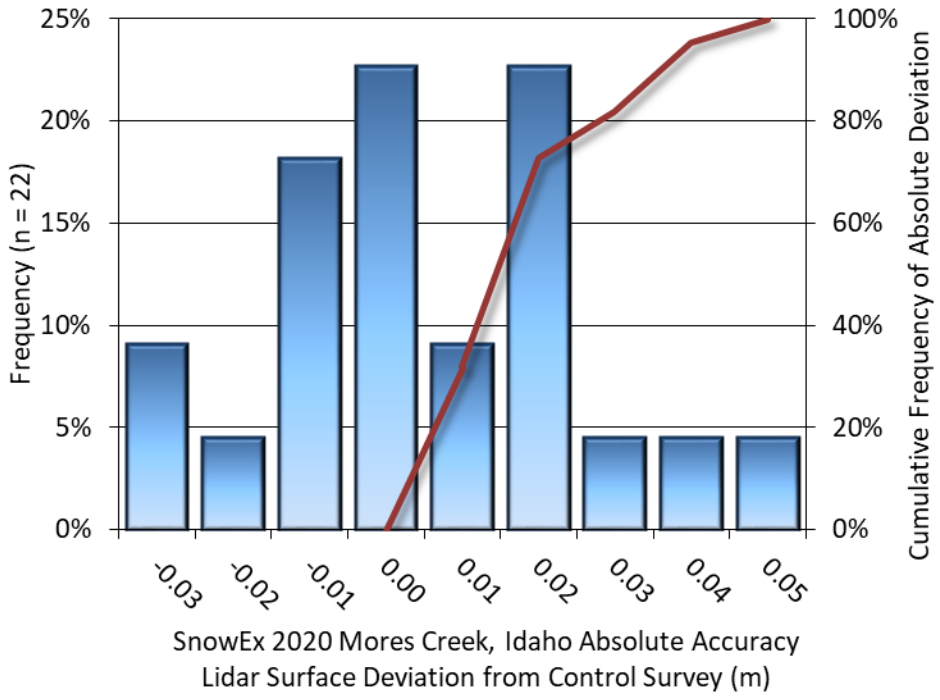

Figure 45: Frequency histogram for lidar surface deviation from ground control point values

Table 15: Reynolds Creek – Absolute accuracy results

Reynolds Creek - Absolute Vertical Accuracy			
	NVA, as compared to unclassified LAS	**NVA, as compared to bare earth DEM**	**Ground Control Points**
Sample	4 points	4 points	62 points
95% Confidence (1.96*RMSE)	0.057 m	0.051 m	0.049 m
Average	0.024 m	0.019 m	0.003 m
Median	0.029 m	0.028 m	0.004 m
RMSE	0.029 m	0.026 m	0.025 m
Standard Deviation (1σ)	0.019 m	0.021 m	0.025 m

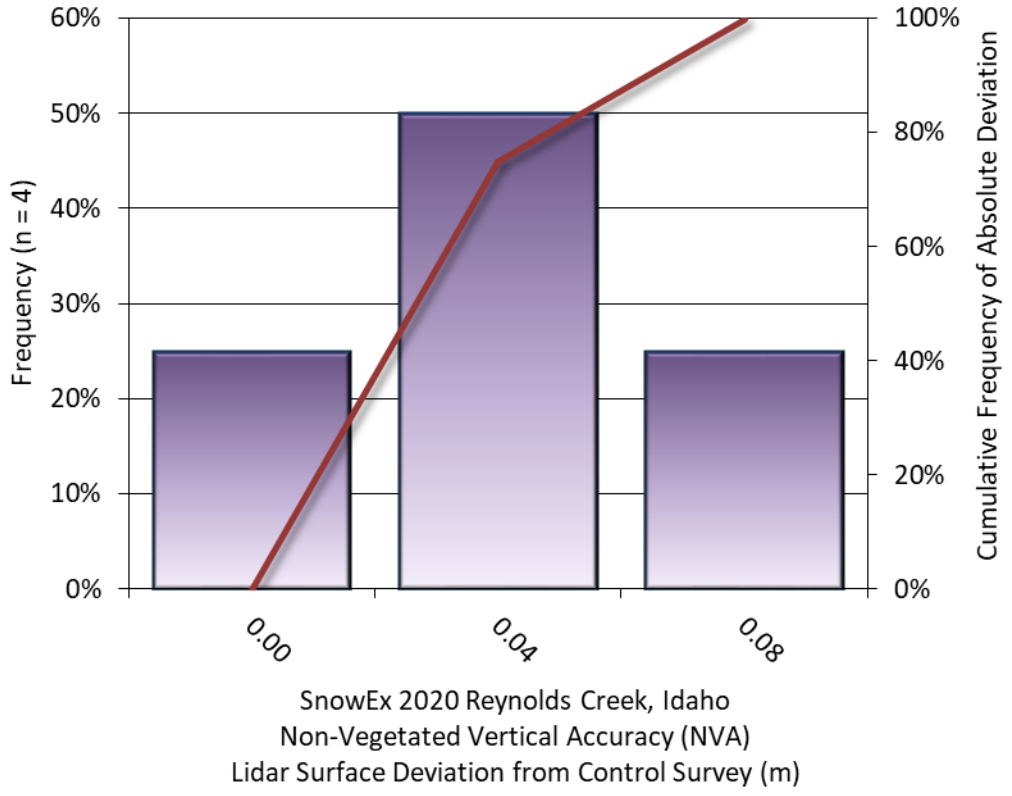

Figure 46: Frequency histogram for lidar unclassified LAS deviation from ground check point values (NVA)

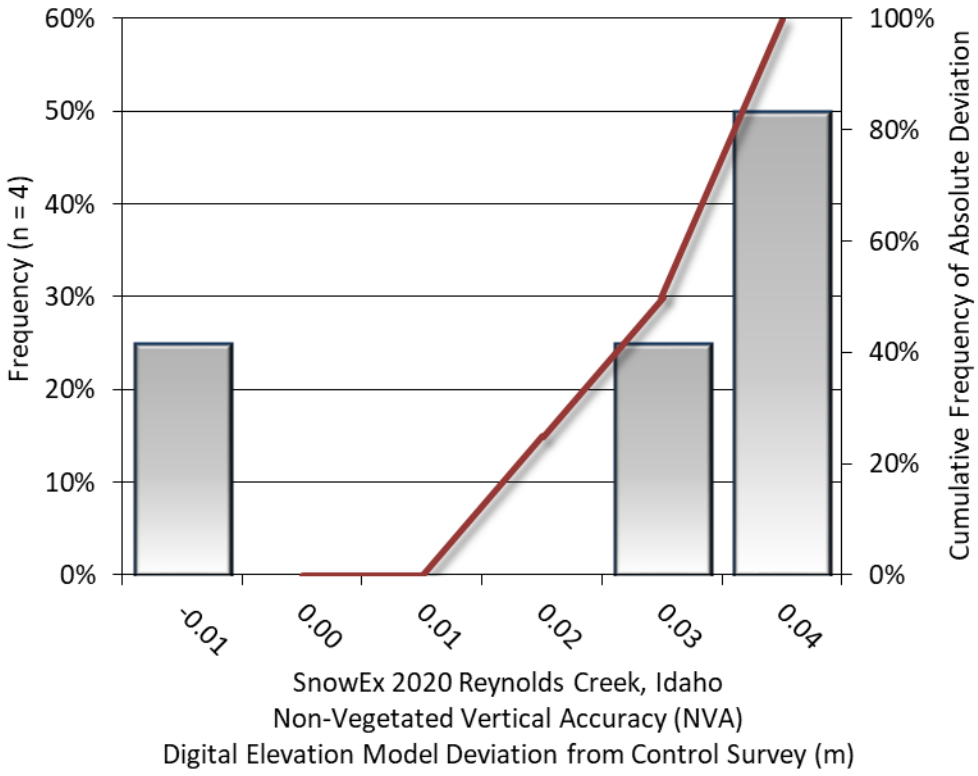

Figure 47: Frequency histogram for lidar bare earth DEM surface deviation from ground check point values (NVA)

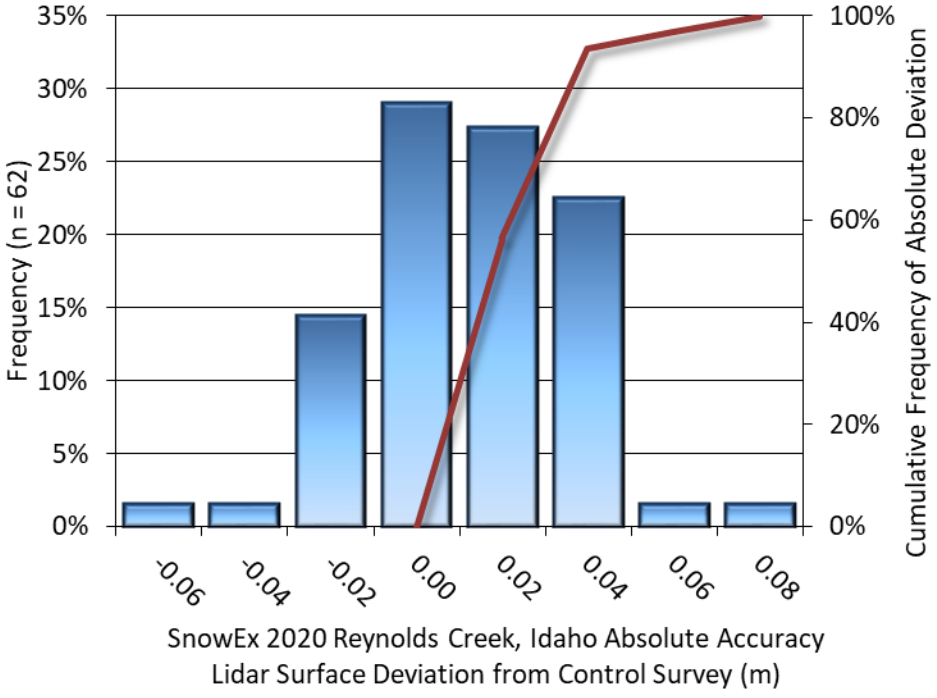

Figure 48: Frequency histogram for lidar surface deviation from ground control point values

Table 16: Grand Mesa Acquisition 1 – Absolute accuracy results

Grand Mesa Acquisition 1 - Absolute Vertical Accuracy			
	NVA, as compared to unclassified LAS	**NVA, as compared to bare earth DEM**	**Ground Control Points**
Sample	2 Points	2 Points	58 points
95% Confidence (1.96*RMSE)	0.083 m	0.029 m	0.056 m
Average	0.041 m	0.011 m	0.003 m
Median	0.041 m	0.011 m	0.008 m
RMSE	0.042 m	0.015 m	0.028 m
Standard Deviation (1σ)	0.014 m	0.015 m	0.028 m

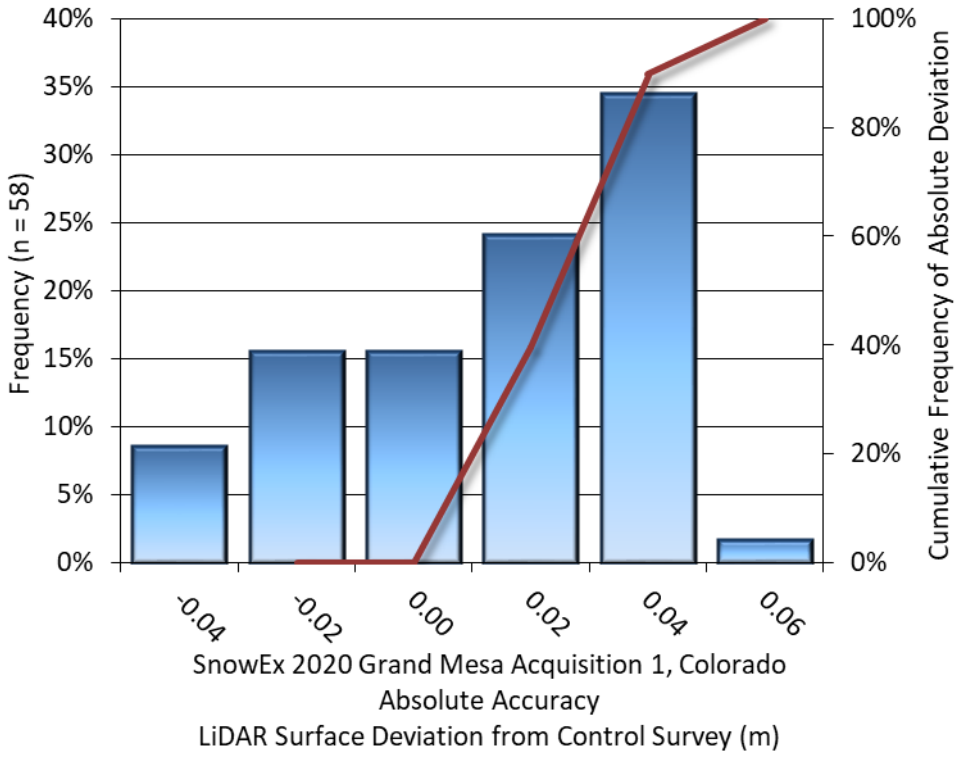

Figure 49: Frequency histogram for lidar surface deviation from ground control point values

Table 17: Grand Mesa Acquisition 2 – Absolute accuracy results

Grand Mesa Acquisition 2 - Absolute Vertical Accuracy			
	NVA, as compared to unclassified LAS	**NVA, as compared to bare earth DEM**	**Ground Control Points**
Sample	2 points	2 points	58 points
95% Confidence (1.96*RMSE)	0.146 m	0.098 m	0.068 m
Average	0.036 m	0.001 m	0.011 m
Median	0.036 m	0.001 m	0.004 m
RMSE	0.074 m	0.050 m	0.035 m
Standard Deviation (1σ)	0.092 m	0.071 m	0.033 m

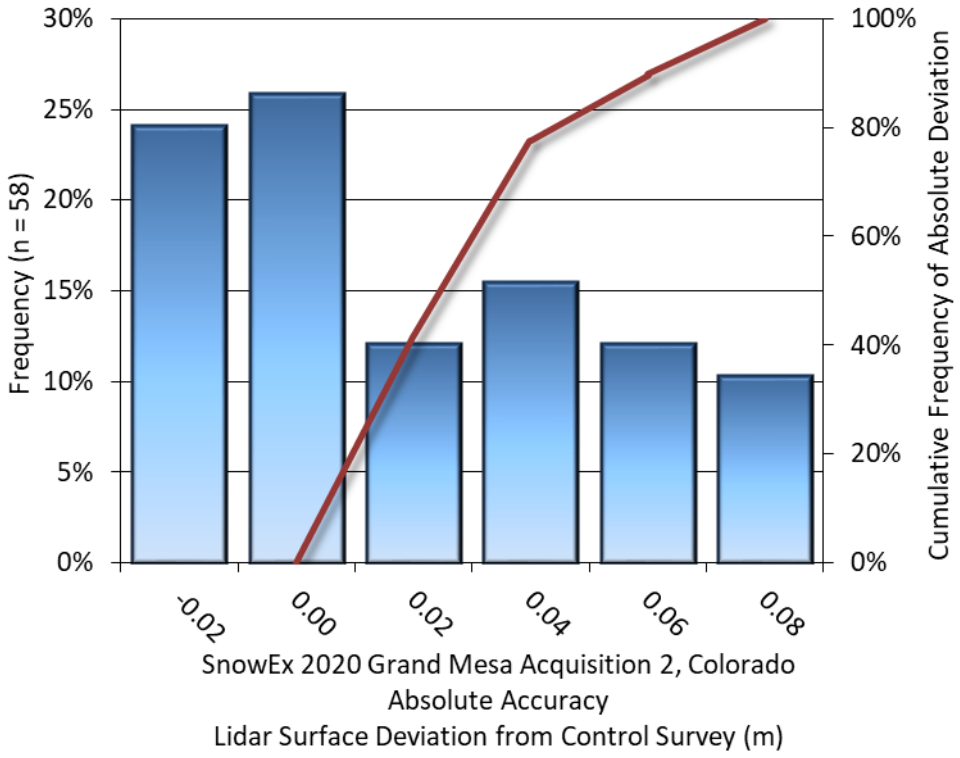

Figure 50: Frequency histogram for lidar surface deviation from ground control point values

Table 18: Frasier – Absolute accuracy results

Frasier - Absolute Vertical Accuracy			
	NVA, as compared to unclassified LAS	**NVA, as compared to bare earth DEM**	**Ground Control Points**
Sample	2 points	2 points	37 points
95% Confidence (1.96*RMSE)	0.046 m	0.047 m	0.033 m
Average	-0.015 m	-0.020 m	-0.008 m
Median	-0.015 m	-0.020 m	-0.007 m
RMSE	0.023 m	0.024 m	0.017 m
Standard Deviation (1σ)	0.025 m	0.018 m	0.015 m

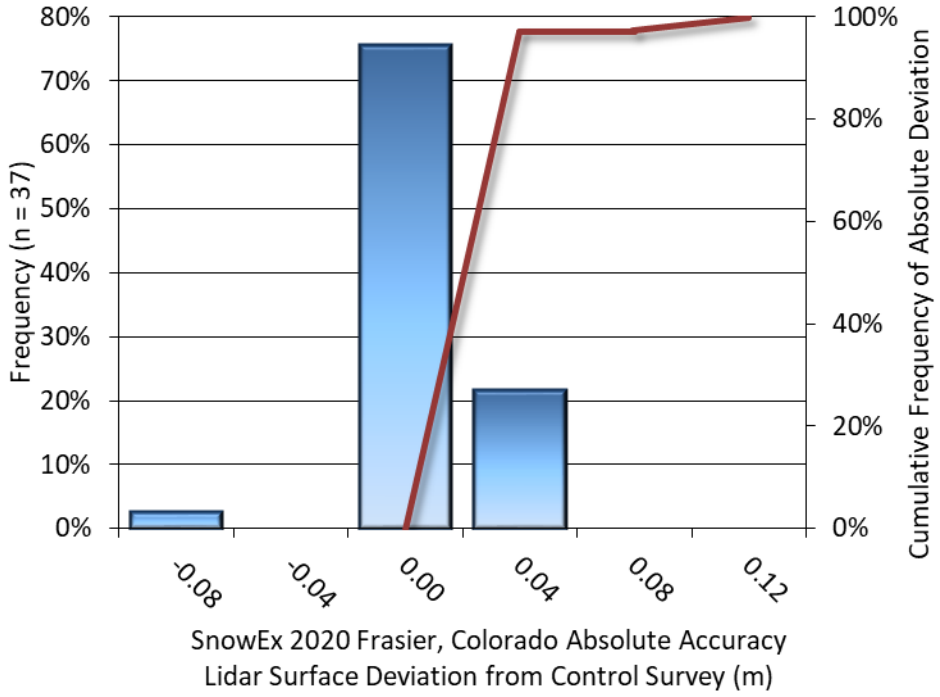

Figure 51: Frequency histogram for lidar surface deviation from ground control point values

Table 19: East River – Absolute accuracy results

East River - Absolute Vertical Accuracy			
	NVA, as compared to unclassified LAS	NVA, as compared to bare earth DEM	Ground Control Points
Sample	5 points	5 points	104 points
95% Confidence (1.96*RMSE)	0.057 m	0.050 m	0.059 m
Average	0.019 m	-0.009 m	0.002 m
Median	0.006 m	-0.004 m	0.005 m
RMSE	0.029 m	0.025 m	0.030 m
Standard Deviation (1σ)	0.025 m	0.027 m	0.030 m

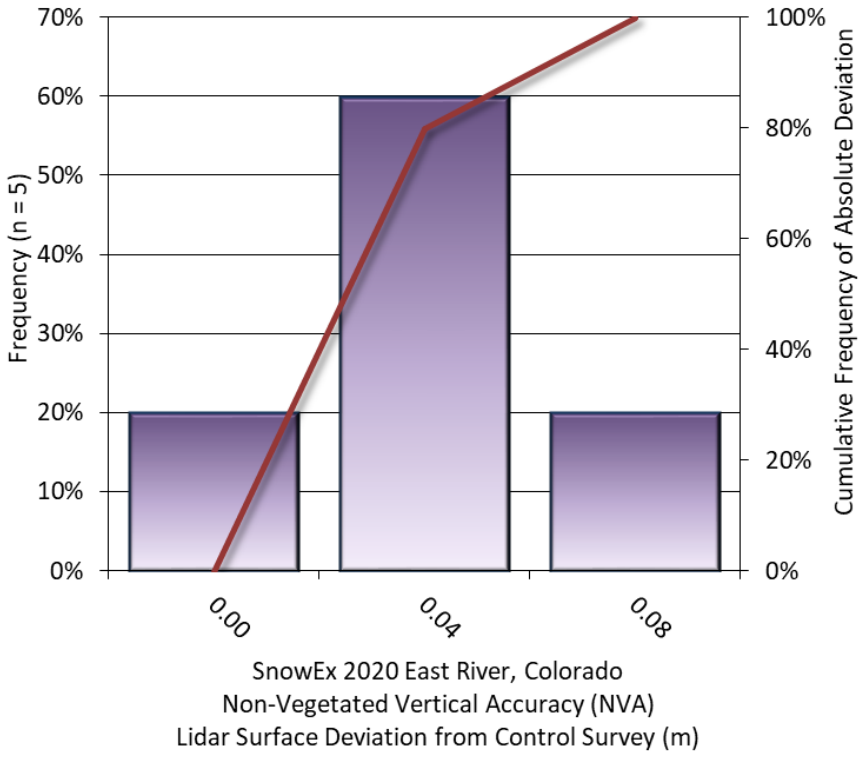

Figure 52: Frequency histogram for lidar unclassified LAS deviation from ground check point values (NVA)

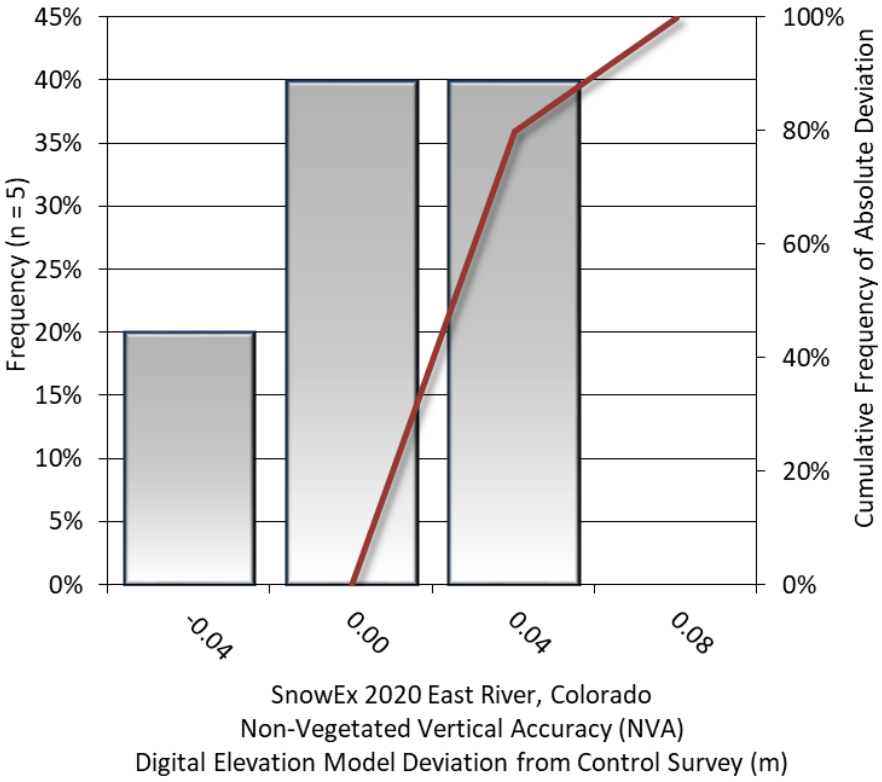

Figure 53: Frequency histogram for lidar bare earth DEM surface deviation from ground check point values (NVA)

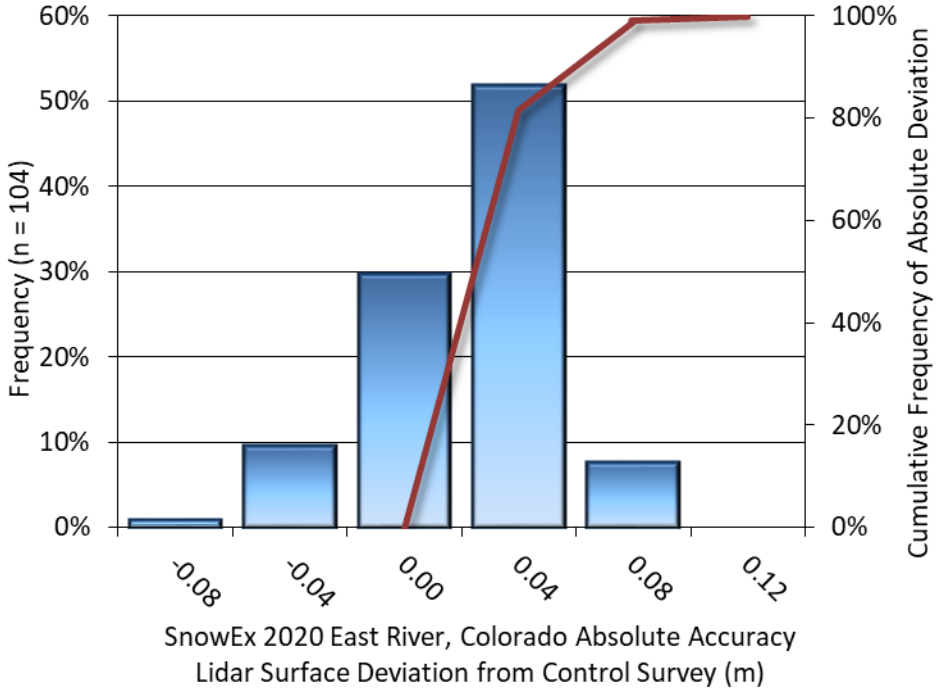

Figure 54: Frequency histogram for lidar surface deviation from ground control point values

Lidar Relative Vertical Accuracy

Relative vertical accuracy refers to the internal consistency of the data set as a whole: the ability to place an object in the same location given multiple flight lines, GPS conditions, and aircraft attitudes. When the lidar system is well calibrated, the swath-to-swath vertical divergence is low (<0.10 meters). The relative vertical accuracy was computed by comparing the ground surface model of each individual flight line with its neighbors in overlapping regions (Table 20 through Table 27 and Figure 55 through Figure 62).

Table 20: Relative accuracy results

Banner Summit - Relative Accuracy	
Sample	49 surfaces
Average	0.025 m
Median	0.026 m
RMSE	0.026 m
Standard Deviation (1σ)	0.001 m
1.96σ	0.003 m

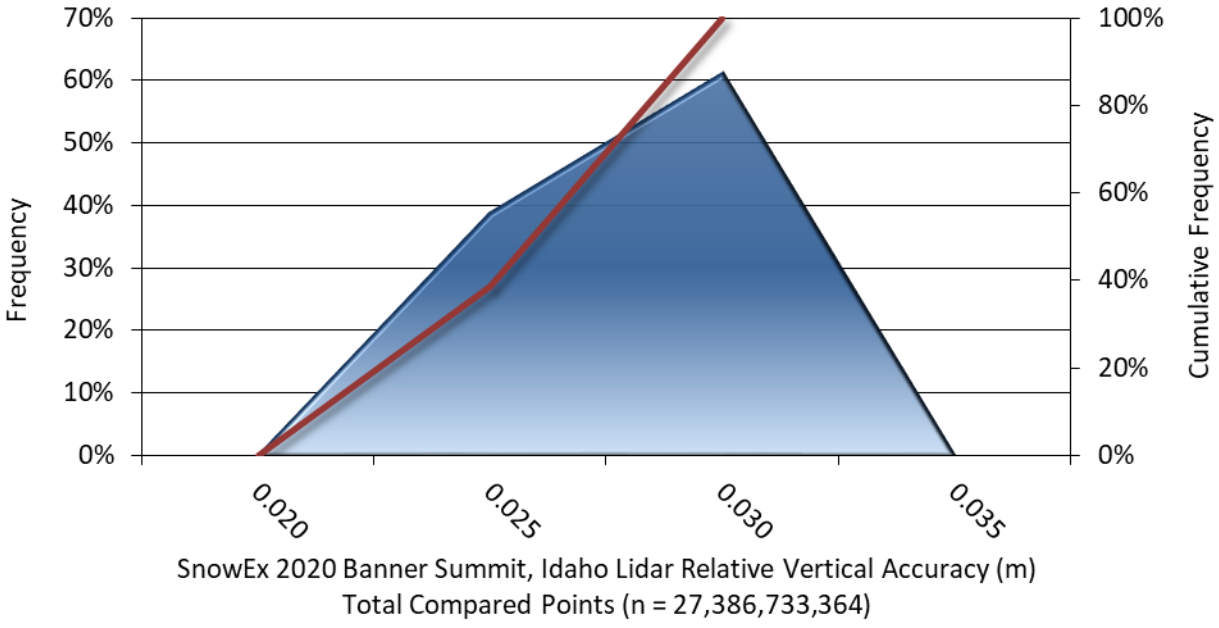

Figure 55: Frequency plot for relative vertical accuracy between flight lines

Table 21: Relative accuracy results

Dry Creek - Relative Accuracy	
Sample	19 surfaces
Average	0.015 m
Median	0.016 m
RMSE	0.015 m
Standard Deviation (1σ)	0.001 m
1.96σ	0.002 m

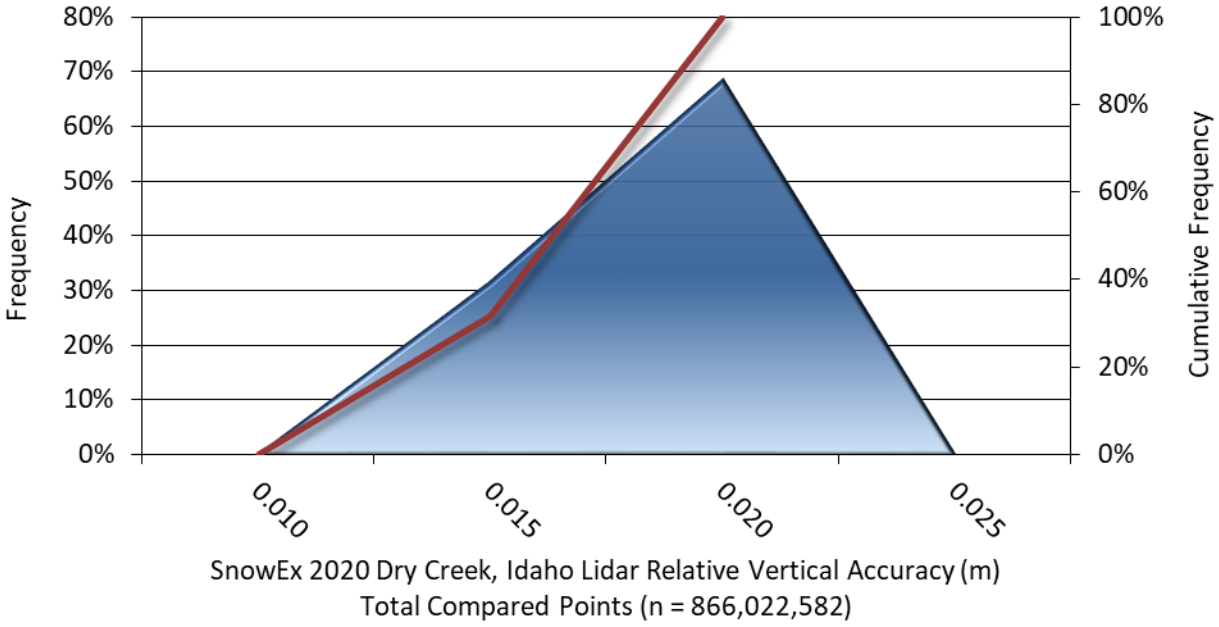

Figure 56: Frequency plot for relative vertical accuracy between flight lines

Table 22: Relative accuracy results

Mores Creek - Relative Accuracy	
Sample	16 surfaces
Average	0.025 m
Median	0.025 m
RMSE	0.025 m
Standard Deviation (1σ)	0.002 m
1.96σ	0.004 m

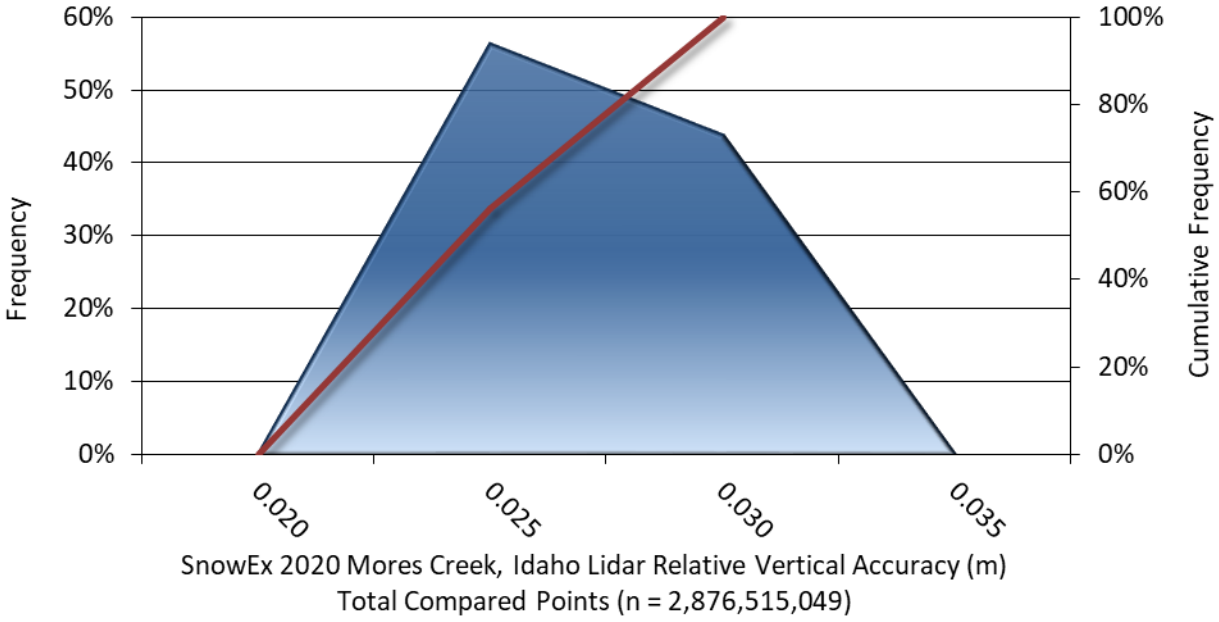

Figure 57: Frequency plot for relative vertical accuracy between flight lines

Table 23: Relative accuracy results

Reynolds Creek - Relative Accuracy	
Sample	29 surfaces
Average	0.022 m
Median	0.022 m
RMSE	0.021 m
Standard Deviation (1σ)	0.002 m
1.96σ	0.005 m

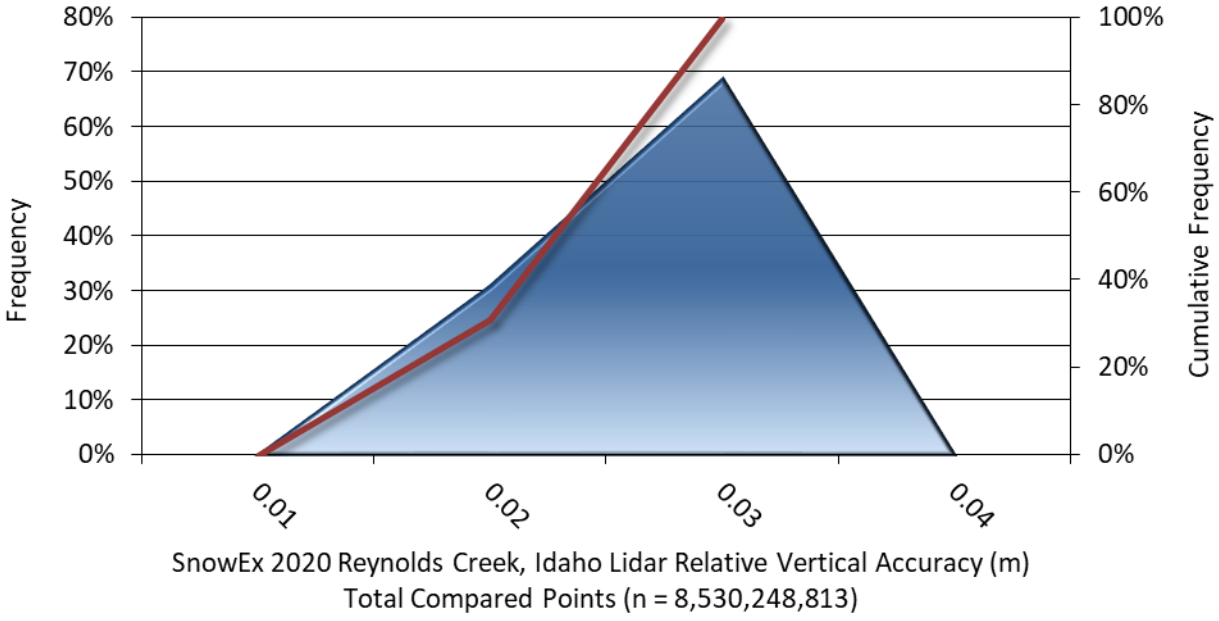

Figure 58: Frequency plot for relative vertical accuracy between flight lines

Table 24: Relative accuracy results

Grand Mesa Acquisition 1 - Relative Accuracy	
Sample	24 surfaces
Average	0.021 m
Median	0.020 m
RMSE	0.022 m
Standard Deviation (1σ)	0.003 m
1.96σ	0.006 m

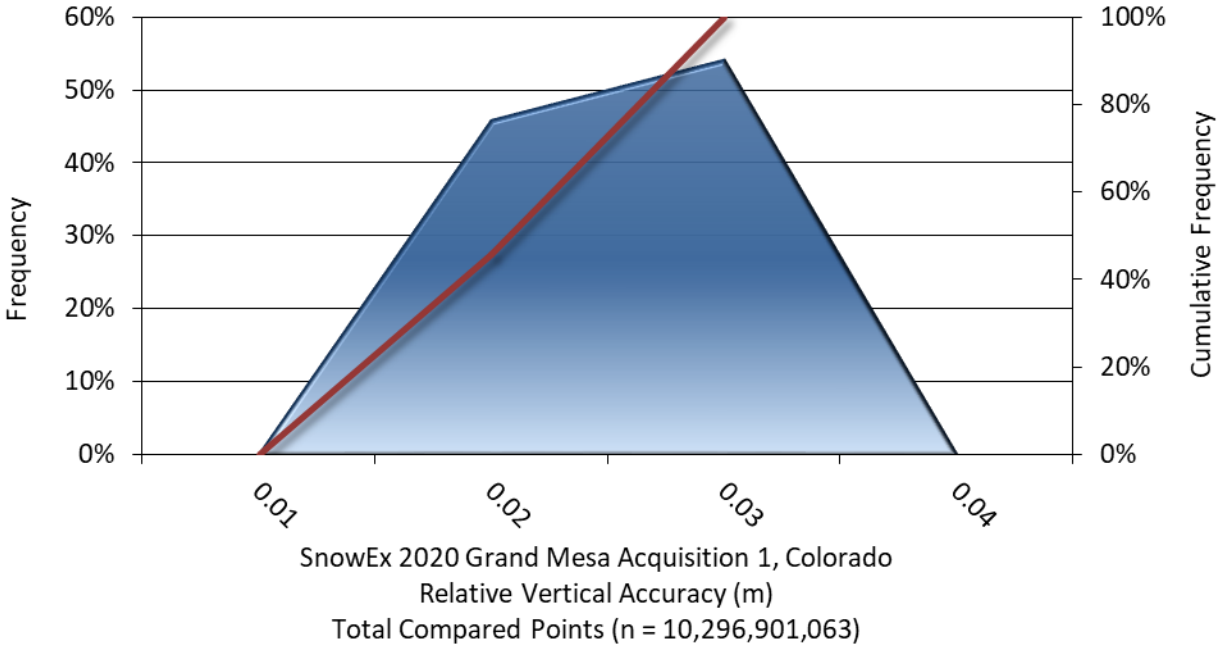

Figure 59: Frequency plot for relative vertical accuracy between flight lines

Table 25: Relative accuracy results

Grand Mesa Acquisition 2 - Relative Accuracy	
Sample	24 surfaces
Average	0.027 m
Median	0.027 m
RMSE	0.028 m
Standard Deviation (1σ)	0.004 m
1.96σ	0.007 m

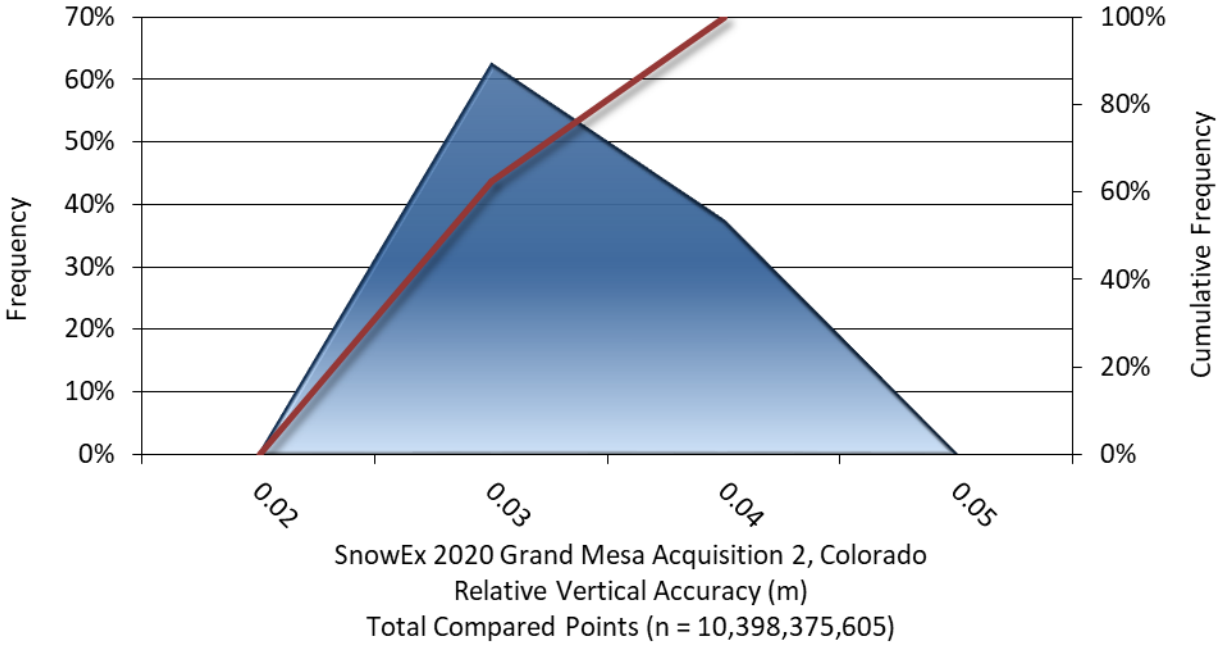

Figure 60: Frequency plot for relative vertical accuracy between flight lines

Table 26: Relative accuracy results

Frasier - Relative Accuracy	
Sample	24 surfaces
Average	0.023 m
Median	0.022 m
RMSE	0.024 m
Standard Deviation (1σ)	0.003 m
1.96σ	0.005 m

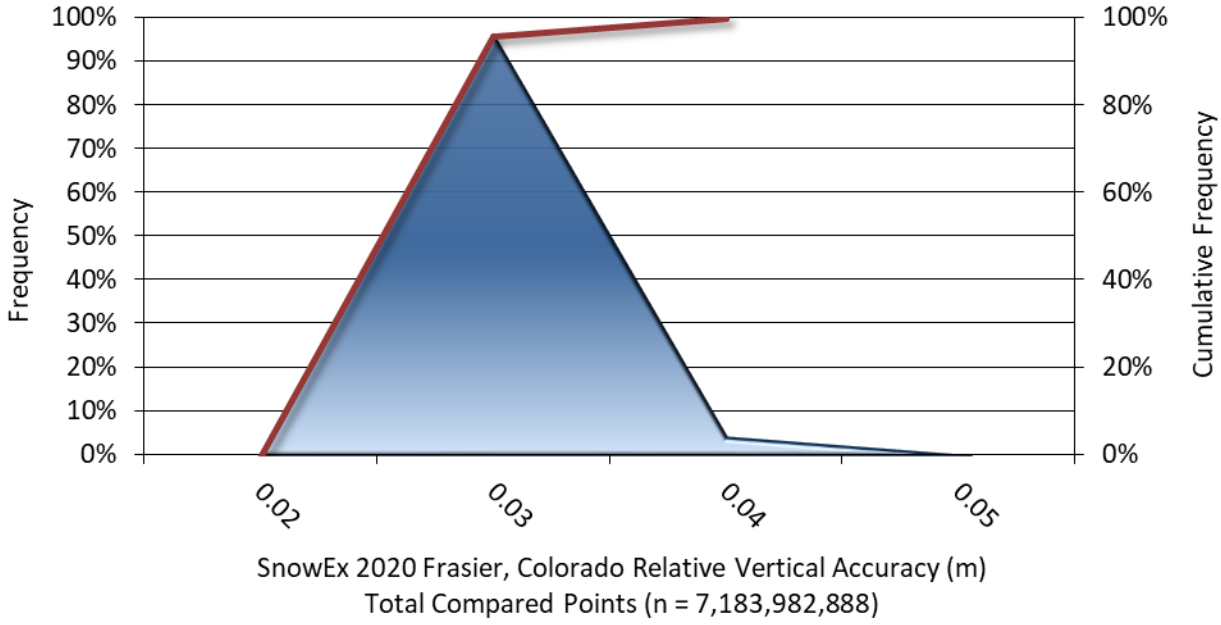

Figure 61: Frequency plot for relative vertical accuracy between flight lines

Table 27: Relative accuracy results

East River - Relative Accuracy	
Sample	66 surfaces
Average	0.062 m
Median	0.060 m
RMSE	0.062 m
Standard Deviation (1σ)	0.008 m
1.96σ	0.015 m

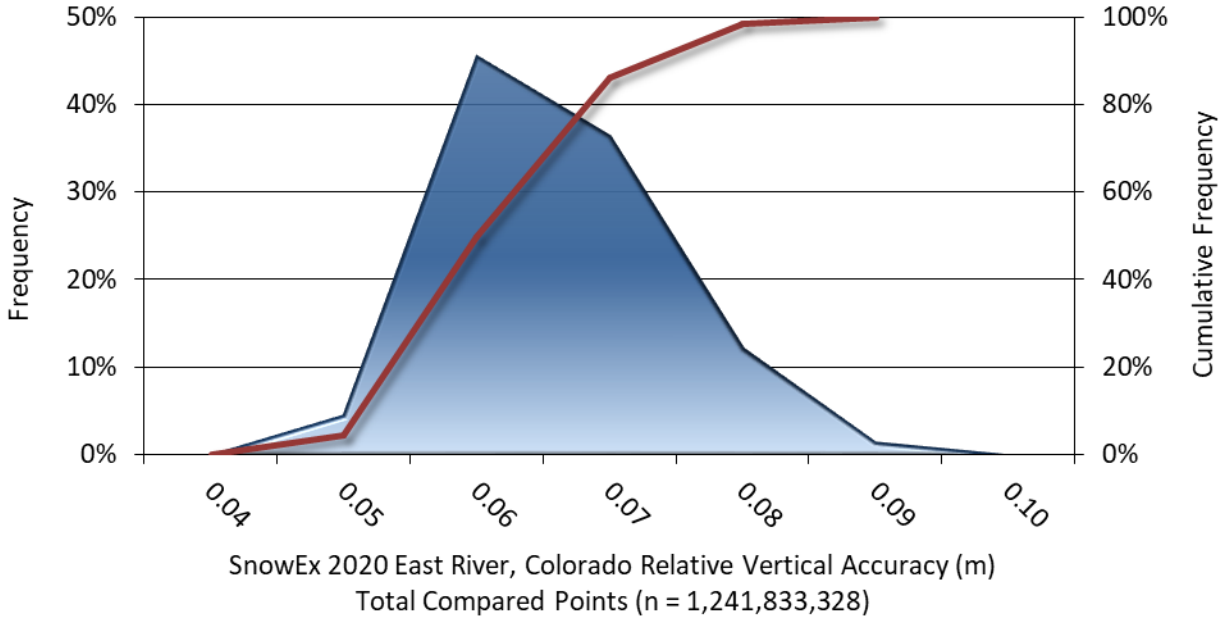

Figure 62: Frequency plot for relative vertical accuracy between flight lines

Lidar Horizontal Accuracy

Lidar horizontal accuracy is a function of Global Navigation Satellite System (GNSS) derived positional error, flying altitude, and INS derived attitude error. The obtained $RMSE_r$ value is multiplied by a conversion factor of 1.7308 to yield the horizontal component of the National Standards for Spatial Data Accuracy (NSSDA) reporting standard where a theoretical point will fall within the obtained radius 95 percent of the time. This project was compiled to meet 0.200 m horizontal accuracy at the 95% confidence level.

Table 28: Horizontal Accuracy

Area of Interest	Horizontal Accuracy	
Banner Summit	**$RMSE_r$**	0.09 m
	ACC_r	0.17 m
Dry Creek	**$RMSE_r$**	0.09 m
	ACC_r	0.17 m
Mores Creek	**$RMSE_r$**	0.09 m
	ACC_r	0.17 m
Reynolds Creek	**$RMSE_r$**	0.09 m
	ACC_r	0.17 m
Grand Mesa Acquisition 1	**$RMSE_r$**	0.09 m
	ACC_r	0.17 m
Grand Mesa Acquisition 2	**$RMSE_r$**	0.09 m
	ACC_r	0.17 m
Frasier	**$RMSE_r$**	0.09 m
	ACC_r	0.17 m
East River	**$RMSE_r$**	0.12 m
	ACC_r	0.22 m

Hyperspectral Imagery Accuracy Assessment

Due to the remote nature of the SnowEx Project's individual areas of interest (AOIs), and lack of remotely identifiable control point locations, the boresight location (Grand Junction Regional Airport - GJT) was chosen to perform accuracy assessment. The airport and its surrounding area are full of easily identifiable hard surface locations to assess accuracy, and due to the nature of direct georeferencing orthorectification used in the project, the accuracy assessed in this location is transferable to each AOI.

Image accuracy was measured using ground control points (GCPs), located on hard, permanent surfaces which were identified using LiDAR intensity images in areas of clear visibility. Once the GCPs were identified in the intensity images, the exact spot was identified in the orthorectified hyperspectral imagery, and the displacement was recorded for further statistical analysis. In order to support any and all desired user goals, Horizontal accuracy is reported based on Lidar-derived GCPs alone.

The NSSDA standard horizontal accuracy (ACCr) at 95% confidence level for the study area was 1.257 m. for the SnowEx Project measured by LiDAR derived GCPs.

Table 29: Hyperspectral accuracy statistics for SnowEx 2020

Hyperspectral Imagery Accuracy	
GCP Count	N = 24
Root Mean Square Error (RMSE); $RMSE_r = \sqrt{(RMSE_x^2 + RMSE_y^2)}$	
$RMSE_r$	0.726 meters
Circular Standard Error (CSE); $CSE = 0.5*(RMSE_x + RMSE_y)$	
CSE	0.514 meters
Horizontal Accuracy (ACC); $ACC_r = 2.4477*0.5*(RMSE_x + RMSE_y)$	
ACC_r	1.257 meters

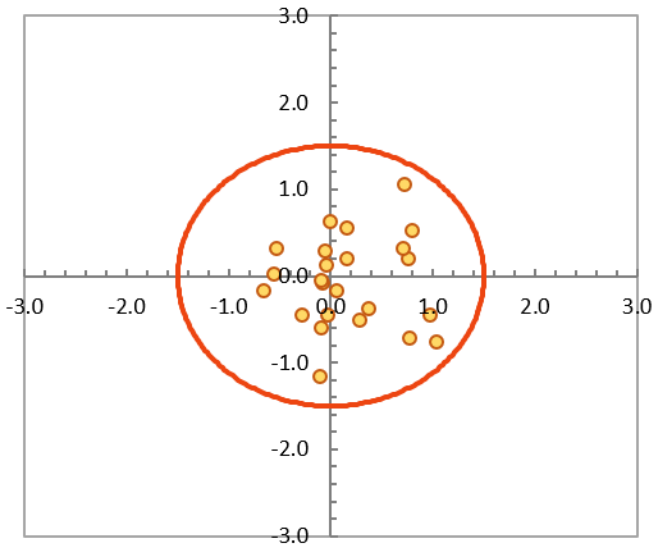

Figure 63: Scatterplot displaying XY deviation of ground control points in orthorectified hyperspectral imagery when compared against the lidar intensity images

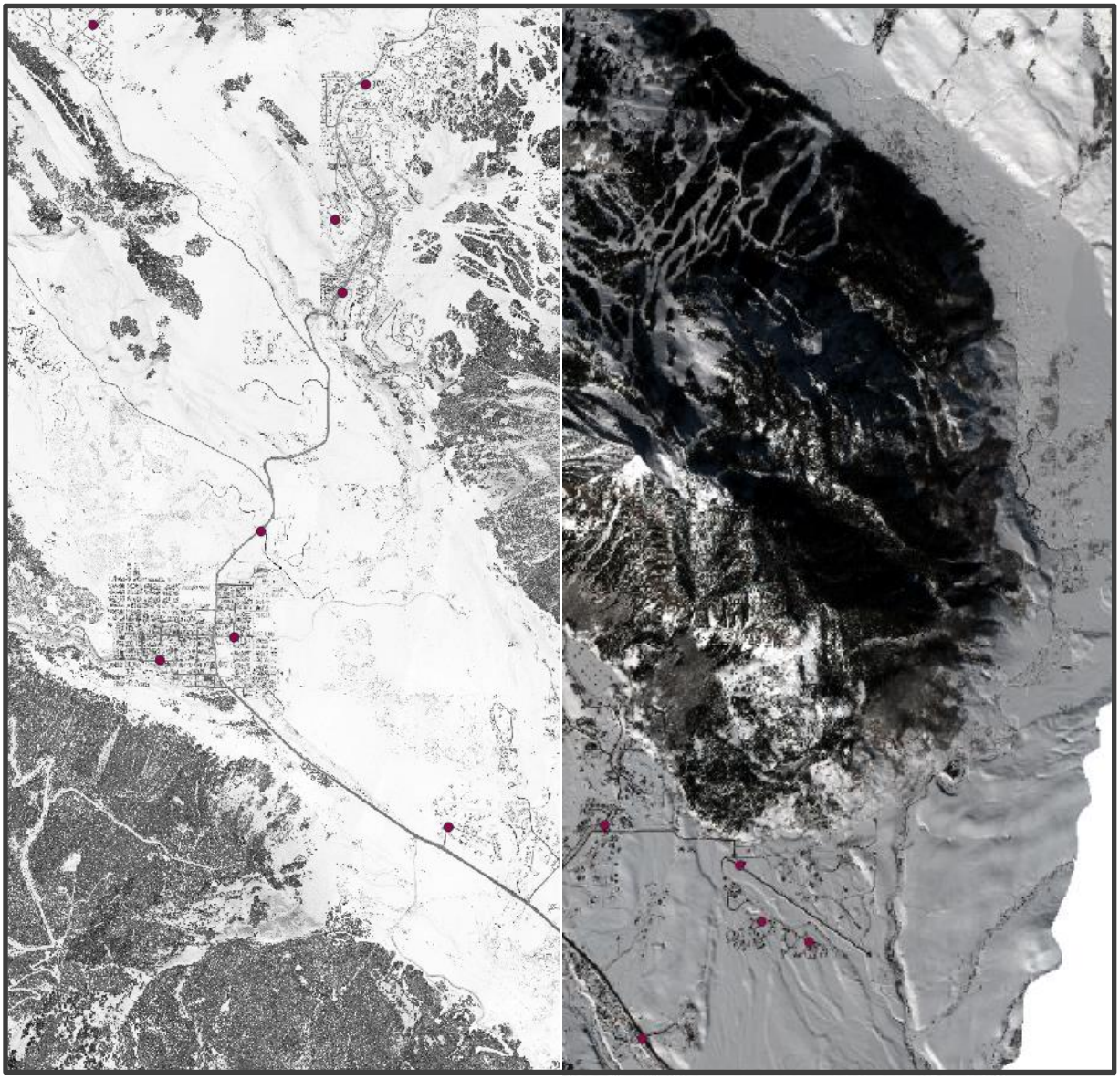

Figure 64: Example ground truth points displayed against lidar intensity image (Left) and hyperspectral imagery (Right) within the SnowEx 2020 East River, Colorado site.

CERTIFICATIONS

Quantum Spatial, Inc. provided lidar services for the SnowEx 2020 project as described in this report.

I, Ashley Daigle, have reviewed the attached report for completeness and hereby state that it is a complete and accurate report of this project.

Ashley Daigle 07/07/2020

Ashley Daigle
Project Manager
Quantum Spatial, Inc.

I, Steven J. Hyde, PLS, being duly registered as a Professional Land Surveyor in and by the states of Idaho and Colorado, hereby certify that the methodologies, static GNSS occupations used during airborne flights, and ground survey point collection were performed using commonly accepted Standard Practices. Field work conducted for this report was obtained between the dates of February 1, 2020 through February 20, 2020.

Accuracy statistics shown in the Accuracy Section of this Report have been reviewed by me and found to meet the "National Standard for Spatial Data Accuracy".

07/07/2020

Expires 12/31/20 Expires 10/31/21

Steven J. Hyde, PLS
Quantum Spatial, Inc.
St. Petersburg, FL

GLOSSARY

1-sigma (σ) Absolute Deviation: Value for which the data are within one standard deviation (approximately 68th percentile) of a normally distributed data set.

1.96 * RMSE Absolute Deviation: Value for which the data are within two standard deviations (approximately 95th percentile) of a normally distributed data set, based on the FGDC standards for Non-vegetated Vertical Accuracy (NVA) reporting.

Accuracy: The statistical comparison between known (surveyed) points and laser points. Typically measured as the standard deviation (sigma σ) and root mean square error (RMSE).

> **Absolute Accuracy:** The vertical accuracy of lidar data is described as the mean and standard deviation (sigma σ) of divergence of lidar point coordinates from ground survey point coordinates. To provide a sense of the model predictive power of the dataset, the root mean square error (RMSE) for vertical accuracy is also provided. These statistics assume the error distributions for x, y and z are normally distributed, and thus we also consider the skew and kurtosis of distributions when evaluating error statistics.
>
> **Relative Accuracy:** Relative accuracy refers to the internal consistency of the data set; i.e., the ability to place a laser point in the same location over multiple flight lines, GPS conditions and aircraft attitudes. Affected by system attitude offsets, scale and GPS/IMU drift, internal consistency is measured as the divergence between points from different flight lines within an overlapping area. Divergence is most apparent when flight lines are opposing. When the lidar system is well calibrated, the line-to-line divergence is low (<10 cm).
>
> **Root Mean Square Error (RMSE):** A statistic used to approximate the difference between real-world points and the lidar points. It is calculated by squaring all the values, then taking the average of the squares and taking the square root of the average.

Data Density: A common measure of lidar resolution, measured as points per square meter.

Digital Elevation Model (DEM): File or database made from surveyed points, containing elevation points over a contiguous area. Digital terrain models (DTM) and digital surface models (DSM) are types of DEMs. DTMs consist solely of the bare earth surface (ground points), while DSMs include information about all surfaces, including vegetation and man-made structures.

Intensity Values: The peak power ratio of the laser return to the emitted laser, calculated as a function of surface reflectivity.

Nadir: A single point or locus of points on the surface of the earth directly below a sensor as it progresses along its flight line.

Overlap: The area shared between flight lines, typically measured in percent. 100% overlap is essential to ensure complete coverage and reduce laser shadows.

Pulse Rate (PR): The rate at which laser pulses are emitted from the sensor; typically measured in thousands of pulses per second (kHz).

Pulse Returns: For every laser pulse emitted, the number of wave forms (i.e., echoes) reflected back to the sensor. Portions of the wave form that return first are the highest element in multi-tiered surfaces such as vegetation. Portions of the wave form that return last are the lowest element in multi-tiered surfaces.

Real-Time Kinematic (RTK) Survey: A type of surveying conducted with a GPS base station deployed over a known monument with a radio connection to a GPS rover. Both the base station and rover receive differential GPS data and the baseline correction is solved between the two. This type of ground survey is accurate to 1.5 cm or less.

Post-Processed Kinematic (PPK) Survey: GPS surveying is conducted with a GPS rover collecting concurrently with a GPS base station set up over a known monument. Differential corrections and precisions for the GNSS baselines are computed and applied after the fact during processing. This type of ground survey is accurate to 1.5 cm or less.

Scan Angle: The angle from nadir to the edge of the scan, measured in degrees. Laser point accuracy typically decreases as scan angles increase.

Native Lidar Density: The number of pulses emitted by the lidar system, commonly expressed as pulses per square meter.

Relative Accuracy Calibration Methodology:

Manual System Calibration: Calibration procedures for each mission require solving geometric relationships that relate measured swath-to-swath deviations to misalignments of system attitude parameters. Corrected scale, pitch, roll and heading offsets were calculated and applied to resolve misalignments. The raw divergence between lines was computed after the manual calibration was completed and reported for each survey area.

Automated Attitude Calibration: All data were tested and calibrated using TerraMatch automated sampling routines. Ground points were classified for each individual flight line and used for line-to-line testing. System misalignment offsets (pitch, roll and heading) and scale were solved for each individual mission and applied to respective mission datasets. The data from each mission were then blended when imported together to form the entire area of interest.

Automated Z Calibration: Ground points per line were used to calculate the vertical divergence between lines caused by vertical GPS drift. Automated Z calibration was the final step employed for relative accuracy calibration.

Lidar accuracy error sources and solutions:

Type of Error	Source	Post Processing Solution
GPS (Static/Kinematic)	Long Base Lines	None
	Poor Satellite Constellation	None
	Poor Antenna Visibility	Reduce Visibility Mask
Relative Accuracy	Poor System Calibration	Recalibrate IMU and sensor offsets/settings
	Inaccurate System	None
Laser Noise	Poor Laser Timing	None
	Poor Laser Reception	None
	Poor Laser Power	None
	Irregular Laser Shape	None

Operational measures taken to improve relative accuracy:

Low Flight Altitude: Terrain following was employed to maintain a constant above ground level (AGL). Laser horizontal errors are a function of flight altitude above ground (about 1/3000th AGL flight altitude).

Focus Laser Power at narrow beam footprint: A laser return must be received by the system above a power threshold to accurately record a measurement. The strength of the laser return (i.e., intensity) is a function of laser emission power, laser footprint, flight altitude and the reflectivity of the target. While surface reflectivity cannot be controlled, laser power can be increased and low flight altitudes can be maintained.

Reduced Scan Angle: Edge-of-scan data can become inaccurate. The scan angle was reduced to a maximum of ±29.25^{o} from nadir, creating a narrow swath width and greatly reducing laser shadows from trees and buildings.

Quality GPS: Flights took place during optimal GPS conditions (e.g., 6 or more satellites and PDOP [Position Dilution of Precision] less than 3.0). Before each flight, the PDOP was determined for the survey day. During all flight times, a dual frequency DGPS base station recording at 1 second epochs was utilized and a maximum baseline length between the aircraft and the control points was less than 13 nm at all times.

Ground Survey: Ground survey point accuracy (<1.5 cm RMSE) occurs during optimal PDOP ranges and targets a minimal baseline distance of 4 miles between GPS rover and base. Robust statistics are, in part, a function of sample size (n) and distribution. Ground survey points are distributed to the extent possible throughout multiple flight lines and across the survey area.

50% Side-Lap (100% Overlap): Overlapping areas are optimized for relative accuracy testing. Laser shadowing is minimized to help increase target acquisition from multiple scan angles. Ideally, with a 50% side-lap, the nadir portion of one flight line coincides with the swath edge portion of overlapping flight lines. A minimum of 50% side-lap with terrain-followed acquisition prevents data gaps.

Opposing Flight Lines: All overlapping flight lines have opposing directions. Pitch, roll and heading errors are amplified by a factor of two relative to the adjacent flight line(s), making misalignments easier to detect and resolve.